Application of multifocal electroretinogram in early detection of inner retinal changes in experimental glaucoma

---

By

Lakshmi Priya Rajagopalan

In partial satisfaction of the requirements for the degree of

DOCTOR OF PHILOSOPHY

In

PHYSIOLOGICAL OPTICS

Presented to the Graduate Faculty of the

College of Optometry

University of Houston

December 2016

Approved:

_____
Laura J. Frishman, PhD (Chair)

_____
Ronald S. Harwerth, OD, PhD

_____
Han Cheng, OD, PhD

_____
Nimesh B. Patel, OD, PhD

_____
Suresh Viswanathan, PhD

Acknowledgements

For the past seven years, the University of Houston, College of Optometry (UHCO) has been a second home for me. Houston has been the city in which I have spent the most time after my home city back in India. It has been a wonderful experience where I have grown a lot professionally through the incredible guidance of my mentors and made many friends who have given me memories to cherish for a long time.

Firstly, I would like to thank Dr. Laura Frishman for the tremendous support she has given me over the years and for being the guiding force during the doctoral program. She has spent hours of her valuable time with me, providing me with all the necessary insight I needed to carry out my research experiments and data analysis. I consider myself extremely lucky to have spent some of my most important professional years under her mentorship. She has been a great mentor to not only me but to every graduate student here at the UHCO in her position as the Associate Dean for Graduate Studies and her efforts in making sure the program attracts the best students from around the world and provides a nurturing and career-defining experience for every one of them is awe-inspiring.

I have to thank Dr. Ronald Harwerth for his valuable inputs throughout my research work. My discussions with him have yielded me tremendous insights that have eventually led to improved outcomes in my research. I would also like to thank Dr. Nimesh Patel for his role in making my doctoral program a professional success. He took me under his wing and taught me the ways of handling animals and conducting experiments on them. He was very generous in sharing the imaging data and his knowledge. We have had numerous discussions on our research work, which have all helped me in learning important aspects in my field of research.

I would also like to thank Dr. Suresh Viswanathan for his guidance and spending time with me every time we had a chance to meet at conferences over the years. The

learnings from these discussions have been of tremendous value in gaining technical expertise. I would also like to thank Dr. Han Cheng for her support and guidance in my work here at UHCO. She has been a great source for me to turn to at various times that I needed valuable input about my research experiments. I am also very thankful to Dr. Jason Porter for his support through the past few years, providing me with the resources I needed to successfully complete my dissertation. I am thankful to Dr. Julia Benoit who helped with some of the important statistical analysis in this dissertation.

I would also like to take this opportunity to the wonderful friends I have made during my doctoral program here – Divya, Ayeswarya, Amitabha, Arun, Nripun, Kevin Julie and so on. They have all helped me at various times in the past few years, both with the academic work and providing the lighter moments during the stressful journey of the PhD. These memories have made my stay here in Houston that much sweeter.

Finally, some of the most important people for who I am today are my family. My parents, Mala and Rajagopalan have always given their all to ensure that my brother and I had a great childhood and a solid upbringing that was based on values and were the source of inspiration for us to chase our dreams. They have stood by me during difficult times as the people I lean on for their able guidance. I consider myself very lucky to have been blessed with such supportive parents. I am also thankful to my husband Koushik who has been supportive of my career pursuits. He gave me both moral and technical support with his expertise. I am also thankful to our son Saaketh who has redefined the purpose of our life and careers. I am grateful to every one of these individuals and put my best foot forward in trying to emulate a piece of every one of them in my personal and professional career forward.

General abstract

Purpose: Glaucoma is a multifactorial disease that causes structural and functional damage to retinal ganglion cells (RGCs) and their axons (retinal nerve fiber layer, RNFL). Early diagnosis is critical to preserving vision. The electroretinogram (ERG) is a noninvasive technique of assessing retinal function. The goal of this dissertation was to explore the utility of two ERG techniques (multifocal, mfERG and full field) in detecting early functional changes and to compare the changes with early structural changes in retina and optic nerve head (ONH) in an experimental model of glaucoma.

Methods: All experiments were conducted on nonhuman primates *(Mucaca Mulatta).* In Experiment 1, using a slow sequence mfERG protocol, the stimulus consisted of a 19 hexagon array subtending angles of 35^{o} X 34^{o} on the retina. The protocol was modified by adding up to six initial focal flashes in a 30 frame sequence to increase the amplitude of the multifocal photopic negative response (mfPhNR). mfPhNR and multifocal oscillatory potentials (mfOPs) using the modified mfERG protocol were recorded in experimental (Exp) and fellow control (Con) eyes of seven monkeys with unilateral experimental glaucoma. Structural measures including RNFL thickness (RNFLT), macular ganglion cell inner plexiform layer thickness (m-GCIPLT) and deep ONH structures, minimum rim width (MRW) and anterior lamina cribrosa depth (ALCSD) were obtained concurrently. All parameters were measured globally (g) and locally (sectoral, s and macular, m). Time points of first significant changes in structural and functional measures were compared. In Experiment 2, mfPhNR was measured from a slow sequence protocol with a 103 hexagon array and a m-sequence of one focal flash followed by 14 dark frames (F14). Time points of change in the mfPhNR-F14 were compared with the corresponding structural changes and with mfPhNRs from Experiment 1. In Experiment 3, longitudinal changes in the full field PhNR (FF-PhNR)

were measured and the time point of change in the FF-PhNR amplitude was compared with the structural measures.

Results: Experiment 1: mfPhNR amplitude increased with increasing number of focal frames and saturated at 5 focal frames (F30-5), corresponding to an approximate duration of 53 ms. In Exp eyes, mfERG measures showed early reductions as cumulative IOP increased. g-mfPhNR amplitude was linearly related to MRW (R^2=0.66, *P*<0.01) and ALCSD (R^2=0.54, *P*<0.01) but showed an exponential relationship with g-RNFLT (R^2=0.58, *P*<0.01). ONH structural changes either preceded or coincided with functional losses (mfPhNR) and g-RNFLT was the last parameter to change (K-M survival, *P*<0.05, log rank test). Reductions in m-mfPhNR amplitude occurred prior to m-GCIPL thinning in half of the monkeys. s-RNFL showed thinning prior to g-RNFL (*P*<0.05, paired t-test).

Experiment 2: The coefficient of variation (CV) was significantly lower for the F30-5 (9.1%) protocol compared to the F14 (14.1 %) (*P*<0.05, paired t test). In Exp eyes, the mfPhNR-F14 amplitude changed early along with the ONH measures but prior to RNFL thinning. Time points for changes in the mfPhNR amplitudes from the two mfERG protocols were similar.

Experiment 3: Early reduction in FF-PhNR amplitude occurred concurrently with the ONH changes but prior to g-RNFL and m-GCIPL thinning (*P<0.05*, log rank test). Time points for changes in mfPhNR-F30 and FF-PhNR were similar.

Conclusion: Functional changes in mfPhNR and FF-PhNR amplitudes and changes in the ONH structures (MRW and ALCSD) occurred prior to structural changes in the inner retina (RNFLT and m-GCIPLT) in experimental glaucoma. Local RNFLT showed changes prior to global. While the FF-ERG can be used as a screening tool to detect

early functional changes, mfERG can used to track changes in function related to local structural changes in the inner retina in glaucoma.

Table of contents

Acknowledgements 2

General abstract 4

Table of contents 7

List of Tables 13

List of Figures 14

List of Abbreviations 17

Chapter 1 18

1.1 Introduction 19

1.2 Nonhuman primate (NHP) model of experimental glaucoma 20

1.3 Inner retinal contributions to the electroretinogram 22

1.4 Multifocal electroretinogram (mfERG) 25

1.5 Structural and functional changes in glaucoma 28

1.5.1 Structural changes 28

1.5.1.1 Peripapillary retinal nerve fiber layer (RNFL) changes 28

1.5.1.2 Macular ganglion cell inner plexiform layer (GCIPL) changes 29

1.5.1.3 Optic nerve head (ONH) changes 29

1.5.2 Functional changes 30

1.5.2.1 Early inner retinal functional changes 30

1.5.2.2 Visual sensitivity changes 31

1.6 Structure-function relationship in glaucoma 32

1.7 Potential mechanisms involved in RGC dysfunction and degeneration in glaucoma 33
1.7.1 Early biomechanical alterations 33
1.7.2 Reduced axonal transport 34
1.7.3 Vascular changes 35
1.7.4 Glial cell activation 36
1.7.5 Dendritic shrinkage and synaptic degeneration 38
1.8 Major Goal of the research in this dissertation 39
1.9 Specific aims 39
Chapter 2…… 41
Abstract 42
2.1 Introduction 44
2.2 Methods 46
2.2.1 Animals and animal preparation 46
2.2.2 Multifocal electroretinogram 47
2.2.3 mfERG offline processing and analysis 48
2.2.4 Intravitreal injections 49
2.2.5 Optical coherence tomography and data analysis 51
2.2.6 Comparison of mfPhNR and mfOPs with RNFLT and MRW 54
2.2.7 Comparison of mfPhNR amplitude with macular GCIPL thickness 55
2.2.8 Biometric measurements and scaling 55

2.2.9 Statistical Analysis 56

2.3 Results 57

2.3.1 Adjustment of the mfERG stimulus duration to maximize mfPhNR amplitude… 57

2.3.2 Reduction of mfPhNR amplitude after TTX injection and in experimental glaucoma 57

2.3.3 Relationship between intraocular pressure (IOP) and global structural and functional measures 60

2.3.4 Global structure-function and structure–structure relationships 63

2.3.5 Local structure-function relationship 64

2.3.6 Relationship between g-mfPhNR and temporal RNFLT 64

2.3.7 Longitudinal analysis of structural and functional changes 69

2.3.7.1 Global longitudinal analysis 69

2.3.7.2 Sectoral longitudinal analysis 71

2.3.8 Comparison of time points for the first significant change 73

2.4 Discussion 76

2.4.1 Early changes in ONH structure and inner retinal function in Exp eyes 76

2.4.2 Early changes in the sectoral RNFLT prior to the global RNFLT 78

2.4.3 Relationship between function (mfPhNR) and inner retinal structures (m-GCIPLT and g-RNFLT) 79

2.4.4 Comparison of the mfERG-F30 with the slow sequence F14 protocol 80

2.4.5 Time difference between mfPhNR and RNFL changes 81

2.5 Conclusions....82
Chapter 3……....83
Abstract 84
3.1 Introduction 86
3.2 Methods 88
3.2.1 Animals and preparation. 88
3.2.2 Multifocal electroretinogram 89
3.2.3 mfERG offline processing and analysis 92
3.2.4 Optical coherence tomography and data analysis 94
3.2.5 Comparison of mfPhNR-F14 amplitude with RNFLT and MRW....94
3.2.6 Comparison of mfPhNR amplitude with macular GCIPLT....96
3.2.7 Biometric measurements and scaling....96
3.2.8 Statistical Analysis 96
3.3 Results....97
3.3.1 mfPhNR coefficient of variability (CV) and intraclass coefficient (ICC)....98
3.3.2 Reduction of mfPhNR (F14) and mfPhNR (F30-5) amplitude in experimental glaucoma 98
3.3.3 Effect of cumulative IOP on the mfPhNR amplitude 102
3.3.4 Global structure–functional relationship....102
3.3.5 Local structure-function relationship....105
3.3.6 Relationship between g-mfPhNR-F14 and temporal RNFLT 105

3.3.7 Longitudinal analysis of structural and functional changes 108

3.3.7.1 Global longitudinal analysis 108

3.3.7.2 Sectoral longitudinal analysis 111

3.3.8 Comparisons of time points for the first significant change 113

3.4 Discussion 115

3.4.1 Early changes in mfPhNR-F14 and ONH in experimental glaucoma 115

3.4.2 F14 and F30-5 mfERG protocols 117

3.5 Conclusions 117

3.6 Supplemental tables and figures 119

Chapter 4…… 120

Abstract 121

4.1 Introduction 123

4.2 Methods 125

4.2.1 Animals and animal preparation 125

4.2.2 ERG experiments 125

4.2.3 ERG signal processing and analysis 126

4.2.4 Optical coherence tomography and data analysis 127

4.2.5 Statistical analysis 127

4.3 Results 128

4.3.1 Reduction of FF-PhNR amplitude at an early stage of IOP elevation 128

4.3.2 Effect of cumulative IOP on the full field PhNR amplitude 132

4.3.3 Relationship between PhNR and structural measures.....132
4.3.4 Longitudinal analysis of structural and functional measures.....136
4.3.5 Comparisons of time points for changes in structural and functional parameters.....140
4.4 Discussion.....142
4.4.1 Full Field PhNR as an early functional biomarker.....142
4.4.2 Glial modulation in the ONH and inner retina.....143
4.4.3 Comparison of full field ERG with focal, multifocal and pattern ERG.....144
4.4.4 Advantages and limitations of full field ERG.....145
4.5 Conclusions.....146
Chapter 5……..147
5.1 Overview of the findings from the chapters in the dissertation.....148
5.2 Origin of multifocal photopic negative response (mfPhNR).....150
5.3 mfOPs and mfPhNR- Effects of tetrodotoxin and experimental glaucoma.....151
5.4 Early changes in mfPhNR, FF-PhNR and ONH in experimental glaucoma prior to RNFL thinning.....156
5.5 Is there a common perspective for the early changes in inner retinal function and ONH?.....158
5.6 ERG as an early functional biomarker in glaucoma diagnosis.....160
5.7 Conclusion.....162
References.....163

List of Tables

Table 2-1: IOP data for the control and experimental glaucoma eyes from the time of first laser session.....61

Table 3-1: Comparison of coefficient of variation of global and sectoral mfERGs for the F14 versus the F30-5 protocol. 99

Table 3-2: Intraclass coefficient (ICC) for the global and sectoral mfPhNR amplitudes from F14 and F30-5 protocols 100

Table 3-3: Time point of the first significant change in global and local parameters 110

Table 3-4: Time point of the first significant change in the global functional parameters (all monkeys) 119

Table 4-1: Parameters of Naka-Rushton function fits to FF-PhNR amplitudes...131

Table 4-2: Time point of first significant change in global and local structural and functional parameters.....139

List of Figures

Figure 1-1: ERG responses to a series of flash strengths of short duration red stimuli on a blue background from a monkey with experimental glaucoma.....24

Figure 1-2: mfERG stimulus array and a slow sequence protocol.. ……27

Figure 2-1: mfERG stimulus display showing the m-sequence and the mfERG responses from the 19 hexagons.....50

Figure 2-2: OCT segmentation and structure-function comparisons 52

Figure 2-3: Plot of the mfPhNR amplitude (mean ± SEM) vs time of stimulus onset from five normal monkey eyes. 59

Figure 2-4: Effect of pharmacological blockade of inner retinal spiking activity by TTX and of experimental glaucoma on mfERG.....59

Figure 2-5: Relationship between structural and functional measures and IOP…….. 62

Figure 2-6: Global structure-function and structure-structure relationships in experimental glaucoma.....66

Figure 2-7: Relationship of mfPhNR vs local structure in control and experimental glaucoma eyes.. 67

Figure 2-8: Comparison of global mfPhNR amplitude with the temporal RNFLT. …….. 68

Figure 2-9: Longitudinal analysis of global structure-function measures in experimental glaucoma (OHT- 70).....70

Figure 2-10: Longitudinal analysis of sectoral structure-function measures in experimental glaucoma (OHT- 71).....72

Figure 2-11: Kaplan-Meier survival analysis comparing time points for the first significant change in structural and functional parameters in experimental glaucoma eyes…….. 75

Figure 3-1: mfERG stimulus display with 103 hexagons and slow sequence mfERG F14 protocol. 91

Figure 3-2: mfERG F14 responses from 103 hexagons. Inset: Low pass (55 Hz) filtered mfERG signal showing the mfPhNR. 93

Figure 3-3: Structure function mapping for the mfERG measures and the structural parameters (RNFL, MRW and m-GCIPLT). 95

Figure 3-4: Effect of experimental glaucoma on mfERG for one monkey (OHT- 66) with advanced experimental glaucoma 101

Figure 3-5: Relationship between structural and functional measures and IOP……103

Figure 3-6: Global structure-function relationship in experimental glaucoma…….....104

Figure 3-7: Local structure vs mfPhNR-F14 in control and experimental eyes…….. 106

Figure 3-8: Comparison of global mfPhNR- F14 amplitude with the temporal RNFLT…….....107

Figure 3-9: Longitudinal analysis of global structure-function measures in experimental glaucoma (OHT-70).,.....109

Figure 3-10: Longitudinal analysis of sectoral structure- function measures in experimental glaucoma (OHT- 71).....112

Figure 3-11: Kaplan-Meier survival analysis comparing time points for the first significant change in the experimental glaucoma eyes. 114

Figure 3-12: Supplemental figure m- mfPhNR-F30-5 amplitude as a function of m-GCIPLT……..…..119

Figure 4-1: ERG traces in response to a 2.84 cd.s/ m^2 flash strength from one monkey (OHT- 72) with early unilateral experimental glaucoma.. 130

Figure 4-2: Amplitude of FF-PhNR as a function of stimulus strength.....131

Figure 4-3: Relationship between structural and functional measures and IOP…… 134

Figure 4-4: Structure-function relationship in experimental glaucoma……135

Figure 4-5: Longitudinal analysis of global structural and functional measures in experimental glaucoma (OHT-70).....138

Figure 4-6: Kaplan-Meier survival analysis comparing the time points for the first significant change in the experimental glaucoma eyes. 141

Figure 5-1: Nasal temporal asymmetry in mfOPs and mfPhNR; Effect of TTX and experimental glaucoma.....154

Figure 5-2: Relative time points of significant change in the structural and functional parameters. 157

List of Abbreviations

Functional measures

ERG	Electroretinogram
FF-ERG	Full field electroretinogram
mfERG	Multifocal electroretinogram
mfOPs	Multifocal oscillatory potentials
mfPhNR	Multifocal photopic negative response
PhNR	Photopic negative response

Structural measures

ALCSD	Anterior lamina cribrosa depth
GCIPLT	Ganglion cell inner plexiform layer thickness
MRW	Minimum rim width
RNFLT	Retinal nerve fiber layer thickness

Regional designations

g	Global
m	Macular
s	Sectoral
temp	Temporal

CHAPTER 1

General introduction

1.1 Introduction

Glaucoma is a multifactorial group of eye diseases that results in vision loss due to the death of retinal ganglion cells (RGCs) and their axons that form the retinal nerve fiber layer (RNFL) and the optic nerve. Statistics reported by the world health organization (WHO), show that glaucoma is the second leading cause of blindness globally. However, it is the leading cause of irreversible blindness (Quigley and Broman 2006) and recent studies predict that the prevalence of glaucoma in the age group of 40 to 80 years of age will increase from 64 million in 2013 to 112 million in the year 2040 (Tham et al. 2014). Therefore, it is extremely important to develop strategies for early diagnosis and treatment of the disease. Of the many risk factors for glaucoma, ocular hypertension is the only factor that can be modulated, and reducing intraocular pressure (IOP) helps to delay the onset and progression of glaucoma (Kass et al. 2002). Extensive previous research suggested that the optic nerve head (ONH) is the initial site of glaucomatous damage (Quigley and Green 1979; Quigley et al. 1981; Quigley 1982; Bellezza et al. 2003). Simultaneously, different studies in various animal experimental models of elevated IOP have reported that loss of RGC function assessed using electrophysiology also occurs early in glaucoma (Marx et al. 1986; Marx et al. 1988; Fortune et al. 2004; Saleh et al. 2007). The primary focus of this dissertation is to explore the use of the electroretinogram (ERG) in assessing early functional changes in the inner retina due to ocular hypertension in an animal model (nonhuman primate [NHP] model of experimental glaucoma) whose retina and optic nerve are similar in structure and function to those in humans. In pursuit of this goal, measurements of inner retinal function were made using full field flash electroretinogram (ERG) and two protocols for slow sequence multifocal electroretinogram (mfERG). Concurrent structural measures were obtained using

spectral domain optical coherence tomography (SD OCT) to quantify RNFL thickness, thickness of the ganglion cell + inner plexiform layer (GCIPL) and ONH parameters.

1.2 Nonhuman primate (NHP) model of experimental glaucoma

A variety of animal models used in biological research have increased our understanding of the nature and time course of various diseases in humans, and facilitated improvements in the process of therapeutic care and drug development. The animal models used for glaucoma include but are not limited to mice (Chang et al. 1999; Anderson et al. 2002; Aihara et al. 2003; Libby et al. 2005; Senatorov et al. 2006), rats (Morrison et al. 1997), rabbits (Bonomi et al. 1978), dogs (Gelatt et al. 1981), cats (Hampson et al. 2002), pigs (Ruiz-Ederra et al. 2005) and monkeys (Gaasterland and Kupfer 1974; Quigley and Addicks 1980b, a; Weber and Zelenak 2001). Although many of these animal models have contributed to different aspects of our understanding of the pathophysiology of glaucoma, the NHP model of glaucoma is the most closely comparable model to human glaucoma. Striking similarities in the genetics and anatomical structures and their function between humans and macaque monkeys, specifically the ocular structures such as retina and ONH, make the NHP model of glaucoma most informative of the pathophysiology of the disease in humans.

The model of chronic experimental glaucoma that was used in this dissertation was first developed by Gaasterland and Kupfer (Gaasterland and Kupfer 1974). It is a chronic unilateral experimental glaucoma model in which IOP is increased by laser photocoagulation of the trabecular meshwork (TM). Multiple laser treatments may be required to produce sustained ocular hypertension (OHT). Specimens from eyes with elevated IOP showed loss of RGCs and thinning of RNFL which are the classic signs of glaucomatous damage (Gaasterland and Kupfer 1974). The greatest advantages of this model are that it helps us to systematically study, in an eye similar to that of

humans, the chronic changes that take place as the disease progresses and that the fellow eye can be used as an internal control. IOP elevations achieved in this model range from low (mid 20s mm Hg) to high (50s and 60s mm Hg). Various labs have used this model to study structural and functional changes in glaucoma. To enumerate, Harwerth and collaborators established testing of visual sensitivity in NHPs using standard automated perimetry (SAP) (a longstanding gold standard for diagnosis and staging of the disease in humans (Johnson 1996)), and related visual field losses to ganglion cell losses (Harwerth et al. 1993; Harwerth et al. 1999a; Harwerth et al. 1999b; Harwerth et al. 2004; Harwerth et al. 2007; Harwerth et al. 2010). Other studies demonstrated that sustained IOP elevation leads to structural changes in the ONH (Burgoyne et al. 1995; Strouthidis et al. 2011; Patel et al. 2014), RNFL (Quigley et al. 1982; Harwerth et al. 2007), RGCs and GCIPL (Harwerth et al. 1999a; Luo et al. 2014), and in the lamina cribrosa (LC) (Vilupuru et al. 2007; Sredar et al. 2013; Ivers et al. 2015). In addition to this, functional changes in the inner retina have been measured objectively using flash, pattern and multifocal ERG (Marx et al. 1986; Frishman et al. 1996; Hood et al. 1999; Viswanathan et al. 1999; Frishman et al. 2000; Rangaswamy et al. 2003; Luo and Frishman 2011; Luo et al. 2011; Fortune et al. 2012; Luo et al. 2014).

Despite the advantages of the NHP model, a few disadvantages of this model exist as well. These are firstly, that experimental glaucoma in most instances is achieved at high levels of IOP (Gardiner et al. 2012) in this model which is in contrast with human glaucoma where damage can occur even at normal to low levels of IOP. Secondly, this model has less scope for genetic manipulations than the mouse (Chang et al. 1999; Zhou et al. 2008; Fujikawa et al. 2010) model that provides various genetic mutations to study different types of glaucoma. Nevertheless, this model is currently

the only well-established model to study chronic glaucomatous changes with close proximity to the human disease.

1.3 Inner retinal contributions to the electroretinogram

The electroretinogram (ERG) is a noninvasive objective technique to measure the electrical activity of the retina. Application of ERG to assessing the function of RGCs was first reported in 1981 in a study of the effects of unilateral optic nerve section in cat (Mafei and Fiorentini 1981). A progressive reduction of ERG responses to pattern reversal was observed in the experimental eye with preservation of the standard flash ERG that reflects the activity of outer retinal neurons. Reduction in the amplitude of the pattern ERG was correlated with histological evidence showing a loss of RGCs. From time to time, different laboratories have investigated various components of the ERG originating from the proximal retina using different techniques in the NHP model of experimental glaucoma. Some of the different components of the full field flash ERG sensitive to inner retinal dysfunction and glaucomatous damage are the scotopic threshold response (STR) (Frishman et al. 1996), the light-adapted photopic negative response (PhNR) (Viswanathan et al. 1999; Viswanathan et al. 2000) and oscillatory potentials (OPs) (Ogden 1973). In addition, responses have been recorded to pattern reversal stimuli, i.e. the pattern ERG (PERG) (Marx et al. 1986; Marx et al. 1988; Johnson et al. 1989) and focal stimuli producing a focal ERG which includes a PhNR (Kondo et al. 2008; Kurimoto et al. 2009) and multifocal ERG which includes PhNR, OPs, and an optic nerve head component (ONHC) (Hood et al. 1999; Frishman et al. 2000; Rangaswamy et al. 2003; Luo et al. 2011; Fortune et al. 2012; Luo et al. 2014).

Of these, the PhNR, a negative wave following the b-wave, has advantages in recording RGC function compared to the STR which requires complete dark adaptation

or the PERG which requires fixation and accurate refractive correction (Viswanathan et al. 1999). PhNR was found, initially, to be greatly reduced both in experimental glaucoma (Viswanathan et al. 1999) and in human glaucoma patients (Colotto et al. 2000; Viswanathan et al. 2001). In addition, the PhNR amplitude was reduced by tetrodotoxin (TTX) which blocks the sodium dependent action potentials generated by neurons in the inner retina. Figure 1-1 shows a full field flash ERG of a monkey with unilateral experimental glaucoma. PhNR amplitude was measured from baseline to the trough of the negative potential.

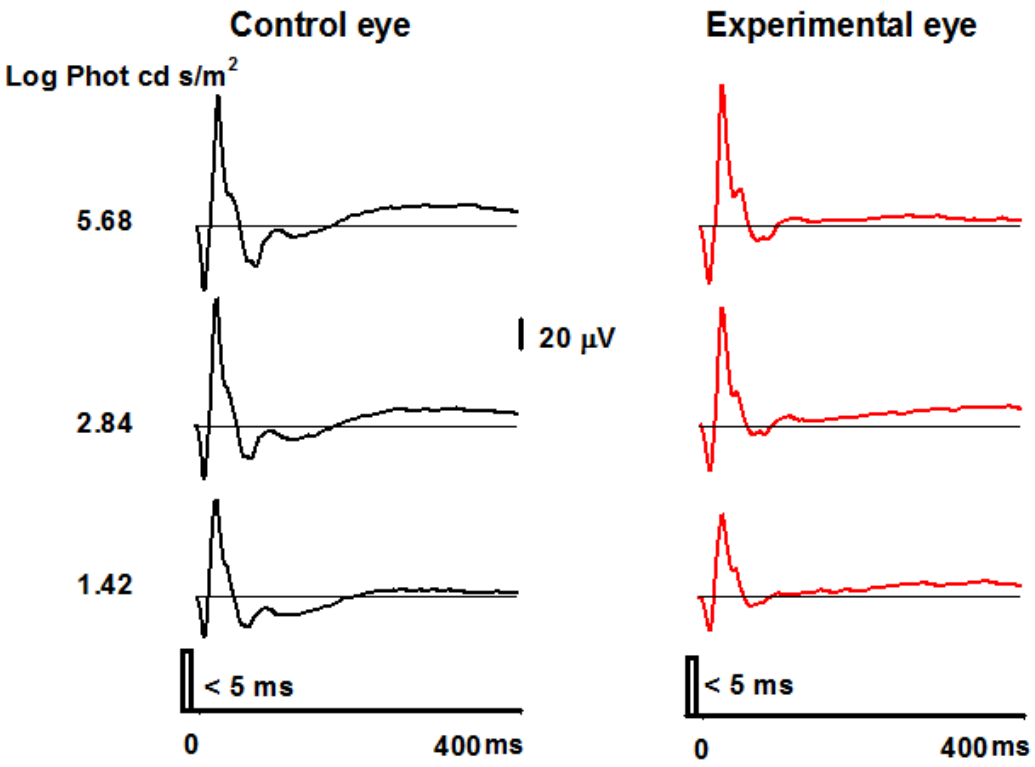

Figure 1-1: ERG responses to a series of flash strengths of short duration red stimuli on a blue background from a monkey with experimental glaucoma (OHT-71). ***(Left):*** Control eye, ***(Right):*** Experimental eye

1.4 Multifocal electroretinogram (mfERG)

Although the PhNR in the full field ERG can reflect inner retinal dysfunction, the full field test gives the mass response of the retina and does not provide information about local damage. To alleviate this limitation of the full field ERG, focal ERG (Miyake et al. 1981) was developed to assess local function in the retina. Recent studies have shown that focal PhNR is reduced in glaucoma (Machida et al. 2010; Nakamura et al. 2011). Furthermore, Tamada et al reported that focal macular PhNR was reduced in eyes with optic nerve atrophy and central scotomas while there was no significant reduction in full field PhNR (Tamada et al. 2009). However, the disadvantage of focal ERG techniques currently used is that, it is not possible to simultaneously record from multiple regions of the retina. Focal ERG therefore, does not provide much range in the retinal locations that can be analyzed in a testing session. In contrast, multifocal ERG (mfERG) provides local responses from multiple regions of the retina simultaneously.

The mfERG technique was developed by Erich Sutter in 1990's (Sutter 1991; Sutter and Tran 1992; Bearse and Sutter 1996). The original mfERG stimulus similar to that used in this dissertation consists of an array of black and white hexagons presented on a standard CRT monitor (Figure 1-2). The number of hexagons can be varied; typically, 61 or 103 hexagons are used in the clinic. The rate of change of contrast of the hexagons is based on the frame rate of the monitor and is controlled by a pseudo random sequence called the m-sequence. Each frame in the m-sequence is 13.3 ms for a 75 Hz CRT monitor. In order to obtain a waveform similar to the full field ERG, the m-sequence can be slowed by interleaving blank frames (Hood et al. 1997). Previous studies have shown that the slow sequence mfERG technique can be used for detecting inner retinal function. Various components of the slow sequunce mfERG such as the multifocal oscillatory potentials (mfOPs) (Fortune et al. 2003; Rangaswamy et al. 2003; Rangaswamy et al. 2006; Zhou et al. 2007), multifocal photopic negative

response (mfPhNR) (Luo et al. 2014; Kaneko et al. 2015) using different stimulus paradigms change significantly in glaucoma. Moreover, recent studies have suggested that, mfERG can be used as an effective tool to detect very early loss of function in experimental glaucoma (Fortune et al. 2012; Fortune et al. 2015).

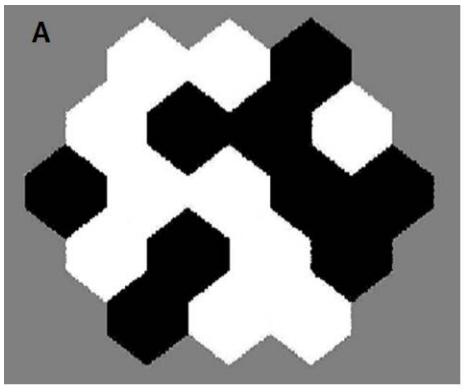

B

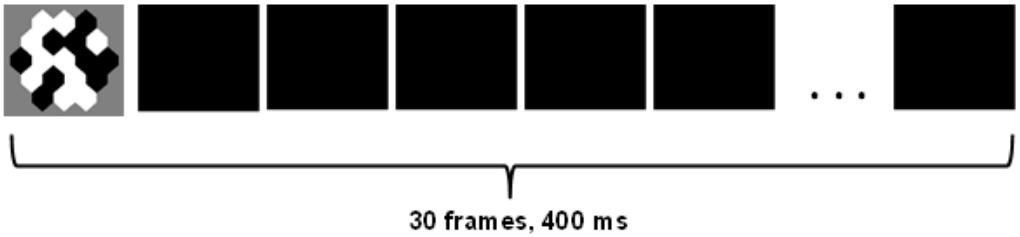

Figure 1-2: A: mfERG stimulus array. A mfERG stimulus array consisting of 19 hexagons is shown here. This stimulus was used in the studies reported in this dissertation. **B: Slow sequence protocol.** The figure shows a sequence with 30 frames with an initial frame with focal flashes followed by 29 black frames. Each frame changes every 13.3 ms and the total sequence takes 400 ms.

1.5 Structural and functional changes in glaucoma

Glaucomatous damage involves various changes in the structure and function of RGCs, their axons (RNFL) and the ONH that can be quantified in noninvasive testing. Some of the changes, including those most commonly reported, and some more recently observed that are relevant to this disseration, are briefly descibed in the next section.

1.5.1 Structural changes

1.5.1.1 Peripapillary retinal nerve fiber layer (RNFL) changes

Evidence in early glaucoma of a nerve fiber bundle defect was reported in 1972 by Hoyt and Newman. They observed a wedge shaped nerve fiber bundle defect using red free fundoscopy in ocular hypertensive patients with no visual field defects (Hoyt and Newman 1972). Later, Schuman and coworkers demonstrated a difference in RNFL thickness between glaucomatous and non glaucomatous eyes using OCT (Schuman et al. 1995a; Schuman et al. 1995b). Further more, Sommer and collegues reported that in a longitudinal study, 60% of OHT eyes had NFL defects prior to visual field defects (Sommer et al. 1991). With the advent of Fourier domain or spectral domain OCT (SD OCT), measurement of the peripapillary RNFLT has become the convention in clinical diagnosis of glaucoma (Zangwill and Bowd 2006; Townsend et al. 2009; Vizzeri et al. 2009) and considered to be more sensitive than visual sensitivity measured using SAP (Wollstein et al. 2005; Harwerth et al. 2007). However, a recent study found that approximately 10% to 15% of axonal loss determined in post mortem axon counts (Cull et al. 2012) occurred prior to thinning of RNFL. Following this study, several investigators have reported that the RNFLT may not be the earliest structural measure to change in glaucoma (Strouthidis et al. 2011; Fortune et al. 2013a; He et al. 2014; Patel et al. 2014; Fortune et al. 2015; Ivers et al. 2015).

1.5.1.2 Macular ganglion cell inner plexiform layer (GCIPL) changes

RGCs are the main neurons damaged in glaucoma. With the advancement in OCT technology, Ishikawa et al were able to segment the different layers of the retina from time domain OCT scans of the macula. The layers included the retinal ganglion cell + inner plexiform layer (RGC+IPL), the macular nerve fiber layer (mRNFL), outer nuclear layer and the outer plexiform + photoreceptor layer. In that study, they demonstrated the diagnostic accuracy of the macular ganglion cell complex, GCC (mRNFL, RGC + IPL layers) equal to the peripapillary RNFL thickness in distinguishing glaucomatous eyes from normal eyes (Ishikawa et al. 2005). Following this, other investigators using SD OCT have found the GCC to have comparable accuracy to the peripapillary RNFLT in diagnosing glaucomatous changes (Tan et al. 2009; Garas et al. 2011; Schulze et al. 2011; Akashi et al. 2013). Other studies that delineated the ganglion cell + inner plexiform layer (GCIPL, excludes mRNFL layer), also found good capability on par with peripapillary RNFL and ONH rim measurements (Mwanza et al. 2012; Francoz et al. 2014; Jung et al. 2014) in distinguishing normal and glaucoma patients.

1.5.1.3 Optic nerve head (ONH) changes

The ONH is an important anatomic structure through which axons of RGCs pass to the brain. RGC axons pass through a 3-dimensional sieve like structure in the ONH called the lamina cribrosa (LC). The LC is made up of connective tissue beams covered by astrocytes and contains capillaries. Early studies have suggested that the primary site for glaucomatous injury is at the level of the ONH (Quigley and Addicks 1980a; Quigley et al. 1981; Quigley 1982). This is supported by the finding that, changes in the optic disc topography (mean position of disc, MPD) occur immediately after acute increase of IOP in experimental glaucoma (Burgoyne et al. 1994). Also,

recent studies found a profound deformation of the neural canal, alterations in the prelaminar tissue thickness and posterior displacement of LC in enucleated eyes from monkeys with early experimental glaucoma (Downs et al. 2007; Yang et al. 2007a). Now, with the help of ultra-high resolution OCT, it is easier to image and quantify these deep structures of the ONH (Strouthidis et al. 2010). Strouthidis et al (2011) were able to identify deep ONH structures such as the Bruch's membrane/retinal pigment epithelium (BM/RPE), neural canal opening (NCO) and the anterior lamina cribrosa surface (ALCS) and found changes in ALCS depth and thinning of the neuroretinal rim at a very early stage of experimental glaucoma prior to RNFL thinning (Strouthidis et al. 2011). In addition to this, other investigators found early changes in these ONH measures including in minimum rim width (MRW), ALCS depth (ALCSD), prelaminar tissure thickness measured with OCT (He et al. 2014; Patel et al. 2014) and changes in lamina pore geometry measured with an adaptive optics scanning laser ophthamoscope (Ivers et al. 2015) prior to RNFL thinning in an experimental glaucoma model. More evidence of these early changes was reported in human glaucoma patients and suspects as well (Chauhan et al. 2013; Furlanetto et al. 2013; Patel et al. 2014).

1.5.2 Functional changes

1.5.2.1 Early inner retinal functional changes

As noted previously, in 1986, Marx et al., reported reduced PERG amplitude in a monkey model of unilateral experimental glaucoma. This loss of RGC function preceded optic neve head cupping (Marx et al. 1986) and occurred as early as two weeks after initiation of sustained IOP elevation (Marx et al. 1988). Since then, other investigators have found compelling evidence to suggest loss of RGC function at a very early stage in glaucoma. In rats (Fortune et al. 2004) with moderate IOP elevation,

it was found that the loss of RGC function measured using the STR preceded morphologic optic nerve damage. RGC dysfunction, as reflected by reduced PERG amplitude preceded RNFL thinning in DBA/2J mice (Saleh et al. 2007). Recent work using the mfERG technique demonstrated loss of high frequency components prior to thinning of RNFL (Fortune et al. 2012) or loss of axons (Fortune et al. 2015) in an NHP experimental glaucoma model. In addition to this, early loss of function has been reported in human subjects with optic neuropathies (Gotoh et al. 2004). The change in inner retinal function reflected by the reduction of PhNR amplitude preceded thinning of RNFL. Altogether, these studies suggest that reduced inner retinal function occurs at a very early stage in glaucoma and this can be quantified using the ERG.

1.5.2.2 Visual sensitivity changes

Damage to RGCs in glaucoma is reflected as a reduction in visual field sensitivity. Standard automated perimetry (SAP), therefore, has been used as a primary test for measuring visual function in glaucoma. SAP uses small flashed stimuli randomly presented on a white background. The standard stimulus size used in the Humphrey visual field analyzer (HVF) is 0.43^{o} corresponding to Goldman size III. Different test strategies are used for visual field testing. The HVF 24-2 protocol tests 54 locations while the 30-2 tests 76 locations. In both protocols, test locations are separated by six degrees and central 30 degrees of the visual field is tested (24-2: measures 24 degrees temporally and 30 degrees nasally). Many studies have reported that early glaucomatous visual field defects involve nasal, arcuate scotomas which mostly occur in the superior field (inferior retina) and superior field defects may involve the central macular region (Nicholas and Werner 1980; Heijl and Lundqvist 1984). Additionaly, early macular damage in glaucoma has now been reported by several studies, e.g. (Anctil and Anderson 1984; Pickett et al. 1985). However, it is difficult to

test visual sensitivity in the central 10° with 24-2 test strategy since it has only 4 points in that region. Recent studies have found the 10-2 visual field testing protocol to be more sensitive than the 24-2 protocol in detecting macular sensitivity loss in glaucoma (Hood et al. 2011; Hood et al. 2013; Traynis et al. 2014; Grillo et al. 2016). 10-2 test protocol in the HVF analyzer tests 64 points in the central 10 degrees and the points are 2 degrees apart, with the standard stimulus size.

1.6 Structure-function relationship in glaucoma

It is important to study structure-function relationships in glaucoma to understand the natural course of the disease and also to design strategies for early diagnosis and therepeutic care. Although various investigators have contributed to reaching this goal, it is yet to be fully understood.

Harwerth et al demonstrated that in NHP experimental glaucoma, proportional loss of visual sensitivity and corresponding ganglion cell loss are non-linearly related and a substantial amount of RGC loss (assessed by counting cells in post mortem tissue) was required before significant reduction in sensitivity can be observed (Harwerth et al. 1999a). Subsequently, they showed that the RGC counts derived from the SAP sensitivity (dB) and the axonal count in decibels (dB) (logarithmic scale) derived from OCT were linearly related (Harwerth et al. 2007) which supports the finding that the structural and functional changes were in agreement with each other when expressed in terms of RGCs. Similarly, the model showed good linear relationship between the two measures in early glaucoma patients when both the measures were expressed on a logarithmic scale (Wheat et al. 2012). Other studies also showed that RNFL thickness and visual sensitivity expressed on a linear scale were linearly related in glaucoma (Hood 2007; Hood et al. 2007).

Furthermore, another study reported that the visual sensitivity losses (1/lambert) in glaucoma was linearly related to PERG amplitude reduction and reduction in neuroretinal rim area (Garway-Heath et al. 2002). These studies and others, e.g. (Viswanathan et al. 2001; Rangaswamy et al. 2006; Kaneko et al. 2015) suggest that all these structural and functional measures are related and accurate interpretation of the specific relationships is essential.

1.7 Potential mechanisms involved in RGC dysfunction and degeneration in glaucoma

It is important to identify the pathophysiological mechanisms that lead to RGC dysfunction, and cell death, since recent studies have shown that reducing IOP-related stress signals theraepeutically can improve RGC function and prevent neuronal loss (Hare et al. 2004; Ventura and Porciatti 2005; Niyadurupola et al. 2013). Several mechanisms are thought to be involved in glaucomatous damage and it is difficult to isolate one cause. Some of the mechanisms involved in RGC functional loss and cell death are discussed below. However, these mechanisms are not mutually exclusive and one or many events may be responsible for glaucomatous damage.

1.7.1 Early biomechanical alterations

In glaucoma, elevated IOP is a major risk factor and decreasing the IOP can reduce the risk of visual damage (Gordon et al. 2002; Kass et al. 2002). A major effect of increased IOP (stress) is directed to the ONH specifically in the LC region, causing deformation (strain). This deformation is two fold: one force acts perpendicularly on the anterior laminar surface and pushes it posteriorly and the other force acts parallel to laminar surface and causes expansion of the neural (scleral) canal (Burgoyne et al. 2005; Downs et al. 2008). The susceptibilty and the extent of this deformation depends

on the tissue properties of the lamina and the sclera. Once this stress crosses beyond normal limits, it causes perrmanant deformation in the ONH (Bellezza et al. 2003; Downs et al. 2007), damage to the connective tissue and extracellular matrix (Morrison et al. 1990; Burgoyne et al. 1995). Furthermore, biomechanical stress due to increased IOP at the ONH causes deformation (Burgoyne et al. 2005; Downs et al. 2007; Yang et al. 2007a; Downs et al. 2008) of the laminar tissue and triggers molecular responses in astrocytes and connective tissue remodeling (Yang et al. 2011).

1.7.2 Reduced axonal transport

The axons of RGCs connect the eye to the brain. They enter the ONH at a 90° angle and pass through the complex structure of the lamina cribrosa to reach the brain via the optic nerve before the optic chiasm and optic tract beyond the chiasm. During this long journey, the axons are susceptible to damage due to mechanical or ischemic factors. These axons carry certain important neuronal components from the eye to the brain and also transport neutrotrophic factors from the brain to the RGCs. The former process is known as anterograde and the latter as retrograde axonal transport. This axonal transport is a highly energy dependent mechanism (Griffin and Watson 1988). Anterograde transport moves components used in neurotransmitter metabolism and proteins (neurofilament proteins, microfilaments etc) synthesized in retinal ganglion cell bodies to the axons and terminals. Retrograde transport is fast and involves delivering neurotrophic factors to the cell body (Morgan 2004). Hence, axonal transport is necessary for cell survival and for maintaining proper function. In the ONH, both anterograde and retrograde axoplasmic flow can be distrupted due to elevation in IOP (Anderson and Hendrickson 1974; Minckler et al. 1977; Quigley and Anderson 1977; Fahy et al. 2016). Similarly, deformation of the lamina cribrosa due to mechanical

stress can distrupt axonal transport (Strouthidis and Girard 2013). Furthermore, studies in rodent models of glaucoma have shown that axoplasmic flow is disrupted before cell death (Kim et al. 2004; Buckingham et al. 2008).

1.7.3 Vascular changes

For a long time, vascular alterations have been implicated in glaucomatous damage. The vascular theory (Fechtner and Weinreb 1994) states that glaucomatous damage is a result of reduced ocular blood flow which is a consequence of elevated IOP. Blood supply to the ONH is divided into four regions. The anterior-most nerve fiber layer receives blood supply from the small retinal arteries; the next region, the prelaminar region is supplied by branches of the peripapillary choroidal arterioles; posterior to this, the laminar region receives its blood supply from the short posterior ciliary arteries; and the most posterior region, the retrolaminar region receives its supply from the centripetal pial plexus and the axial centrifugal branches from the central retinal artery (Hayreh 2001b). Blood flow is calculated as the ratio of the perfusion pressure to the resistance to outflow (Hayreh 2001a). Perfusion pressure is the difference between the arterial pressure in the vessels of the ONH and the IOP. The resistance to outflow can be altered by the condition and quality of the vessels (Anderson 1996). Vessel quality can be altered by disruption of autoregulation of blood flow in the ONH (Grunwald et al. 1984; Pillunat et al. 1986; Pillunat et al. 1987), imbalance in the distribution of vascular endothelial vasoactive agents (nitric oxide, endothelins, oxygen free radicals etc) (Neufeld et al. 1997) and increased blood viscosity (O'Brien et al. 1997). Similarly, perfusion pressure may be affected by alterations in arterial pressure and IOP. Perfusion pressure and IOP are inversely related. Therefore, as the IOP increases, perfusion pressure decreases and the blood supply to the ONH decreases.

Changes in the blood flow have also been reported in glaucomatous eyes. Recently, several investigators were able to quantify ocular blood flow using doppler imaging (Yamazaki and Drance 1997; Galassi et al. 2003) and OCT angiography (Jia et al. 2014) and they found abnormalities in peripapillary vessel density and peripapillary blood flow in glaucoma (Liu et al. 2015). In addition, longitudinal changes in ocular blood flow were observed in monkeys with unilateral experimental glaucoma and these changes were strongly correlated with RNFLT (Cull et al. 2013).

1.7.4 Glial cell activation

The central nervous system (CNS), including the retina and the brain, has two types of glial cells: macroglia and microglia. The macroglial cells include astrocytes, ependymal cells and radial cells.

Müller glia, which are radial macroglia are the predominant type of glial cells in the retina. Müller glia have a wide range of functions which include, but are not limited to, water and potassium ion (K^+) homeostasis, glutamate metabolism and they also have a role in clearing cell debris and neurotoxins (Bringmann and Reichenbach 2001; Newman 2004). Müller cells react to an injury or stress and undergo a process described as “gliosis”. Glial fibrillary acidic protein (GFAP) is a marker for reactive Müller cells (Bringmann et al. 2006). Müller cell activation has been reported at a very early stage in glaucoma. In rats with increased IOP, Müller cell activation and increased expression of GFAP was detected very early after IOP elevation (Wang et al. 2000; Kanamori et al. 2005). In glaucoma, reactive Müller glia may participate in various mechanisms that might be detrimental to RGCs. For instance, glutamate toxicity is one among many factors contributing to RGC death (David et al. 1988). Müller cells play an important role in clearing the glutamate released by the neurons (Riepe and Norenburg 1977). A significant disruption in retinal glutamate uptake and

disruption of the glutamine/glutamate cycle was demonstrated in rats with elevated IOP (Moreno et al. 2005). Apart from glutamate toxicity, glial activation can upregulate NF-kB activity (Lebrun-Julien et al. 2009) that leads to the increased expression of (TNF)-α which contributes to loss of RGCs. Apart from this, more recently, alterations in the PhNR of the full field flash ERG were noted in human patients with a KCNJ10 mutation that affects potassium ions buffering in Müller cells(Thompson et al. 2011).

Another type of macroglia, astrocytes, are found in the RNFL, ONH and lamina cribrosa region. Their main function is to provide support to axons along with maintaining extracellular pH and ion balance (Magistretti 2006; Obara et al. 2008). They also help in water (Tait et al. 2008) and Na^+ homeostasis (Bowman et al. 1984). Like the Müller glia, ONH astrocytes also become reactive to injury or stress (Varela and Hernandez 1997). In glaucoma, astrocytes are activated due to stress induced by elevated IOP and they remodel the extracellular matrix (ECM) (Hernandez 2000; Tezel et al. 2001). Astrocytes in the ONH and laminar region have been shown to become reactive and upregulate expression of matrix metalloproteinases (MMPs) and degrade the ECM (Hernandez 1992; Hernandez et al. 1994; Johnson et al. 1996; Varela and Hernandez 1997; Hernandez 2000; Agapova et al. 2003). Reactive astrocytes were found to express increased amounts of neurotoxic substances such as nitric oxide, TNFα and endothelins that promote RGC death (Neufeld et al. 1997; Yan et al. 2000; Chauhan 2008).

The ONH also contains other glial cells that are negative to GFAP. These are the lamina cribrosa cells. Lamina cribrosa cells are present with in the cribriform plates and along with the astrocytes, they help in maintenance of ECM (Hernandez et al. 1988).

Lastly, microglial cells are responsible for innate immunity and are present in the retina and brain. Similar to macroglial activation, microglial activation has also been

reported at a very early stage in DBA/2J genetic mouse model of glaucoma (Bosco et al. 2011). Although the exact mechanism of microglial activation leading to RGC death is not well understood, reducing microglial activity has been shown to delay RGC death in optic nerve injury models (Baptiste et al. 2005).

1.7.5 Dendritic shrinkage and synaptic degeneration

There is substantial evidence for RGC dendritic alterations in glaucoma. RGC dendrite arbor abnormalities appeared at a very early stage (Weber et al. 1998) in a NHP model of glaucoma and correlated with functional deficits (Weber and Harman 2005). Other studies have shown that RGCs undergo morphological alterations such as dendritic arbor retraction (Morgan et al. 2006), and cell shrinkage before cell death (Morgan et al. 2000). The underlying mechanisms for the changes in the RGC dendrites and accompanying synapse degeneration are still not fully explored, However, recent studies suggest a key role for a complement cascade mechanism in synapse elimination in glaucoma (Ren and Danias 2010; Rosen and Stevens 2010). Complement activation causes upregulation of C1q in DBA/2J mice at a very early stage of glaucomatous damage prior to cell death (Stevens et al. 2007).

In summary, the mechanisms for glaucomatous damage described in this section are suggestive of the hypothesis that various neuronal and non-neuronal mechanisms for degeneration in glaucoma and some of the early morphological changes were accompanied or preceded by early functional deficits. Electrophysiological assessment is sensitive to these functional deficits and can be used as an adjunct biomarker for detecting glaucomatous changes.

1.8 Major Goal of the research in this dissertation

The various studies cited in the previous sections suggest that the earliest glaucomatous damage involves both inner retinal functional changes and structural changes in the ONH. The SD OCT is a valuable tool to measure structural changes in inner retina and ONH objectively. Similarly, it is crucial to develop a functional biomarker, which is objective and can detect early changes in glaucoma. The goal of the research in this dissertation therefore, was to explore the utility of the ERG in detecting early functional changes in glaucoma, and to compare changes in the ERG, longitudinally, with the structural changes measured using SD OCT in the inner retina and ONH in a NHP model of experimental glaucoma. Working towards this goal, we designed the following specific aims, which utilized two ERG techniques: mfERG and full field ERG.

1.9 Specific aims

1. To compare the global and local functional changes detected by the mfERG with structural changes measured by SD OCT in the inner retina (retinal nerve fiber layer, RNFL and macular ganglion cell inner plexiform layer, GCIPL) and ONH (anterior lamina cribrosa depth, ALCSD and minimum rim width, MRW). To determine the temporal order in which these parameters indicate damage in eyes with experimental glaucoma, two different slow sequence mfERG protocols were used:

    a. *A modified slow sequence protocol adjusted to maximize the mfPhNR amplitude without completely sacrificing spatial localization.*

    Previous studies in our lab, using 103 hexagons and 14 frames (Luo et al. 2014) were hampered by recording of small mfERG signals, and this was particularly true for the mfPhNR outside the macular region. In this study, firstly, we aimed to address this issue by altering the mfERG protocol to acquire a larger mfERG signal without losing all local resolution. The second objective was to compare the local

changes in RGC function as reflected by the mfPhNR and mfOPs to the structural changes in the inner retina and ONH to determine which of these parameters is most sensitive to early changes in glaucoma. The results of this experiment are presented in Chapter 2.

b. *The slow sequence mfERG protocol that was used in previous studies in the lab, with a one frame multifocal flash, followed by 14 dark frames (F14) and a mfERG display of 103 hexagons.*

The current study now presents longitudinal results in individual subjects for the F14 stimulus and compares functional mfERG changes to changes in ONH structural parameters that were not measured in our previous studies (Rangaswamy et al. 2006; Luo et al. 2014). The study also compares the temporal order of functional changes detected with the slow sequence F14 stimulus with changes in the mfERG obtained using the mfERG protocol in Specific Aim 1-a. The results for this sub aim are presented in Chapter 3.

2. To assess the utility of a simple and relatively short test of RGC function, the photopic negative response (PhNR) of the full field (FF) light-adapted flash ERG, for early detection and longitudinal assessment of experimental glaucoma. Changes in FF-PhNR amplitudes were compared with structural changes in inner retina and ONH, and with changes in mfPhNR found in specific aim 1-a. The results of this specific aim are presented in Chapter 4.

Addressing these specific aims will provide evidence to support the application of electro diagnostic techniques in early detection of glaucoma, which ultimately could lead to early therapeutic intervention and preservation of vision.

CHAPTER 2

Longitudinal evaluation of local and global changes in structure and function in experimental glaucoma

Contributing authors:

Nimesh B Patel[1], Kevin M Ivers[1], Nripun Sredar[2], Suresh Viswanathan[3], Jason Porter[1], Ronald S Harwerth[1], Laura J Frishman[1]

[1]College of Optometry, University of Houston, Texas, USA, [2]Medical College of Wisconsin, Milwaukee, Wisconsin, USA, [3]State University of New York, College of Optometry, New York, New York, USA

Abstract

PURPOSE: To apply the multifocal electroretinogram (mfERG) technique to detecting loss of retinal ganglion cell (RGC) function in a nonhuman primate model of experimental glaucoma and to determine the relationship between the mfERG measures and structural parameters obtained using spectral domain optical coherence tomography (SD OCT) over time.

METHODS: OCT scans and mfERG recordings were acquired in ten macaque monkeys: three normal and seven with unilateral experimental glaucoma induced by elevation of intraocular pressure (IOP). Macular ganglion cell inner plexiform layer (m-GCIPL), peripapillary retinal nerve fiber layer (RNFL) thickness, and optic nerve head (ONH) parameters, minimum rim width (MRW) and anterior lamina cribrosa depth (ALCSD) were quantified in control (Con) and experimental (Exp) eyes. The mfERG protocol was modified to maximize photopic negative response (mfPhNR) amplitude. Global (g), sectoral (s), macular (m) mfPhNR and oscillatory potentials (mfOPs) amplitudes were measured. Time points for the earliest changes in structure and function were analyzed (paired t-test, repeated measures MIXED and Kaplan-Meir (K-M) survival analysis).

RESULTS: In Exp eyes, mfPhNR and mfOPs amplitudes showed early reductions with increased cumulative IOP. g-mfPhNR amplitude was linearly related to MRW (R^2=0.66, *P*<0.01) and ALCSD (R^2=0.54, *P*<0.01) but showed an exponential relationship to g-RNFLT (R^2=0.58, *P*<0.01). ONH structural changes either preceded or coincided with functional losses and g-RNFLT was the last parameter to change (K-M survival, P<0.05). s-RNFLT showed changes prior to g-RNFLT (P<0.05, paired t-test).

CONCLUSIONS: The results show that inner retinal function and ONH structural parameters change prior to RNFL thinning, suggesting that mfERG can be used to detect early functional changes in glaucoma.

2.1 Introduction

Glaucoma is a family of diseases that causes permanent damage to retinal ganglion cells (RGCs) and their axons that form the retinal nerve fiber layer (RNFL) and optic nerve (Quigley et al. 1988). It is the leading cause of irreversible vision loss worldwide (Quigley and Broman 2006), and it has been estimated that by 2040, nearly 112 million people will be affected by glaucoma (Tham et al. 2014). Therefore, it is important to develop strategies for early diagnosis, monitoring of progression and successful prevention of damage due to this disease. Although standard automated perimetry (SAP) is used in the clinic to detect changes in visual sensitivity, considerable loss of retinal ganglion cells can occur in glaucoma before visual field defects are reliably predictive of those losses (Quigley et al. 1989; Harwerth et al. 1999a).

Various imaging techniques have proven utility in detecting structural changes in glaucoma. Optical coherence tomography (OCT), and particularly spectral domain (SD) OCT, is an excellent technique for documenting changes in structure that take place in the retina and optic nerve head (ONH). Commonly in glaucoma, changes are detected in RNFL thickness (RNFLT) (Zangwill and Bowd 2006; Townsend et al. 2009) and macular retinal ganglion cell and inner plexiform layer thickness (GCIPLT) (Na et al. 2012; Arintawati et al. 2013). However, a histomorphometric study in a nonhuman primate (NHP) model of experimental glaucoma found that approximately 10-15% of the optic nerve axons were lost before any loss of RNFLT was apparent (Cull et al. 2012), and recent evidence indicates that the RNFLT might not be the first structural parameter to change in glaucoma. Longitudinal studies of NHP experimental glaucoma (Strouthidis et al. 2011; He et al. 2014) and cross-sectional studies in humans (Chauhan et al. 2013; Furlanetto et al. 2013; Patel et al. 2014) have observed that optic nerve head neuroretinal tissue parameters such as the minimum rim width (MRW) and anterior lamina cribrosa depth (ALCSD) change prior to thinning of RNFL. This is consistent with

the view that the primary site of glaucomatous injury is within the ONH (Quigley et al. 1981; Yang et al. 2007a).

In addition to structural changes, inner retinal function also is affected in glaucoma, as reflected by two related measures of RGC function in the electroretinogram, the response to pattern reversal in the pattern ERG (PERG) (Marx et al. 1988; Johnson et al. 1989; Ventura et al. 2005; Bach and Hoffmann 2008) and the photopic negative response (PhNR) in the full field flash ERG (Viswanathan et al. 1999; Viswanathan et al. 2000; Viswanathan et al. 2001). Other ERG techniques such as the focal ERG (Kondo et al. 2008; Tamada et al. 2010; Nakamura et al. 2011) and multifocal ERG (mfERG) (Sutter and Tran 1992) have been used to assess inner retinal function, e.g. (Hood et al. 1999; Frishman et al. 2000). The advantage of mfERG over focal ERG is that mfERG allows acquisition of responses from several different retinal regions simultaneously, whereas focal ERG samples only one region at a time. Various stimulus paradigms have been used to study effects of glaucoma on specific waves of the flash ERG and mfERG. For example, high frequency multifocal oscillatory potentials (mfOPs) and multifocal PhNR (or the N2 wave), are two mfERG components that show reduced amplitude in experimental glaucoma in NHP (Rangaswamy et al. 2006; Luo et al. 2011; Fortune et al. 2012; Luo et al. 2014). Changes in mfPhNR have also been observed in glaucoma patients (Kaneko et al. 2015). In studies using the mfERG, significant relationships have been observed between local mfERG responses and local structural measures, and increasing evidence suggests that losses in RGC function occur prior to thinning of the RNFL (Fortune et al. 2012; He et al. 2014) or loss of optic nerve axons (Fortune et al. 2015).

Although several studies, including those cited above, have shown the mfERG to be a useful tool for assessing inner retinal function, the time course of the changes in different mfERG measures, and their relation to structural measures over time in

glaucoma have not been fully explored. The purpose of this study was to apply the mfERG technique to detecting loss of RGC function in a NHP model of experimental glaucoma and to determine the relationship between the mfERG measures and structural parameters (in retina, RNFL, GCIPL, and optic nerve head, MRW and ALCSD) over time.

2.2 Methods

2.2.1 Animals and animal preparation

mfERGs were recorded from ten adult monkeys *(Macaca mulatta),* 3.3 to 6.3 years of age, 3 females, 7 males. Seven monkeys had unilateral experimental glaucoma induced by laser photocoagulation of the trabecular meshwork (Gaasterland and Kupfer 1974; Quigley and Hohman 1983; Pederson and Gaasterland 1984), one eye each of two normal monkeys was injected intravitreally with tetrodotoxin (TTX), and a normal eye of an additional monkey was used for adjusting stimulus parameters. Some of these animals were subjects in other studies as well e.g. (Patel et al. 2014; Ivers et al. 2015). All animal care and experimental procedures adhered to the ARVO statement for the use of animals in ophthalmic and research and were approved by the Institutional Animal Care and Use Committee of the University of Houston.

Preparation was similar to that in previously studies, e.g. (Luo et al. 2014). Animals were anesthetized intramuscularly with ketamine (20-25 mg/kg.hr) and xylazine (0.8-0.9 mg/kg.hr). Atropine sulphate (0.04 mg/kg) was administered subcutaneously, and intraocular pressure (IOP) was measured using Tono-pen XL (Reichert, Inc., Depew, NY, USA). IOP reducing medications (Iopidine, Alcon laboratories Inc., Fort Worth, TX, USA or Combigan, Allergan, Inc., Irvine, CA, USA) were used before imaging sessions or recording sessions to prevent acute effects of elevated IOP on the structural or functional measurements. Heart rate and blood oxygen were monitored using a pulse

oximeter (model 9847V; Nonin Medical, Inc USA) and body temperature was maintained between 36.5 and 38°C with a thermostatically controlled blanket (TC1000-Temperature Controller; CWE, Ardmore, PA). Pupils were dilated using topical tropicamide (1%) and phenylephrine hydrochloride (2.5%). SD OCT measurements (see below) were made using Spectralis HRA+OCT (Heidelberg Engineering, Germany) at approximately 2-3 week intervals for each monkey. mfERG recordings were made on the same days as imaging sessions, although not always as frequently. For OCT experiments, a head mount with a bite bar was used to stabilize the monkey's head. A plano-power contact lens was used to maintain optical quality. For the mfERGs, eyes were refracted and appropriate contact lenses were fitted. The monkey's head was positioned with a small bead-filled pillow under the chin to eliminate tilt and to direct the eyes toward the middle of the mfERG stimulus display. A modified direct ophthalmoscope (American Optical Co. Buffalo, NY) was used to locate the fovea of the eye being tested and accurately align it with the center of the stimulus. All seven experimental glaucoma monkeys had at least one baseline imaging session prior to the first laser treatment and four (OHT- 70, OHT-71, OHT-72, OHT-75) of the seven monkeys had at least one baseline mfERG session. The time course of changes in the other three monkeys who were studied earlier (OHT-64, OHT- 66 and OHT- 67) was markedly longer due differences in the lasering protocol, and therefore these monkeys were not included in most of the longitudinal time point analyses.

2.2.2 Multifocal electroretinogram

The mfERG stimulus consisted of an array of 19 unstretched black and white hexagons (Visual Evoked Response Imaging System; VERIS 4.1, Electro-Diagnostic Imaging, Inc., Redwood City, CA) presented on a standard CRT monitor. The stimulus display subtended angles of 35° X 34° on the retina at a viewing distance of 46 cm

(Figure 2-1 A). Each hexagon was flashed based on a pseudo random m-sequence (Sutter 1991). The maximum luminance of the white hexagons was 215 cd/m^2 (2.67 cd.s/m^2 per flash) and the black hexagons were 10 cd/m^2. The surround had a mean luminance of 132 cd/m^2. The slow sequence protocol consisted of 30 frames (F30) with a focal flash in the initial 1 to 6 frames, followed by 29 to 24 dark frames. The monitor frame rate was 75 Hz, making each 30 frame sequence 400 ms in duration. The protocol was modified by including additional initial frames with focal flashes to extend the stimulus duration up to the point where further additional flashes no longer increased mfPhNR amplitude. This was done because it has been reported for focal ERGs, that PhNR amplitude increases with stimulus duration up to about 50 ms (Kondo et al. 2008). The outcomes of the experiments to establish optimal stimulus duration for the present study are presented in the first section of the results. The mfERG signals were sampled at 1200 Hz and filtered between 1 and 300 Hz. The total duration of an epoch was approximately seven minutes. Three recording epochs were obtained and combined using VERIS. The raw data were exported for offline analysis. Figure 2-1 B shows the mfERG protocol with five initial focal flashes followed by 25 blank frames (F30-5).

2.2.3 mfERG offline processing and analysis

mfERGs were analyzed offline using MATLAB (MATLAB; The MathWorks, Natick, MA). Two components, namely 1) mfPhNR (Figure 2-1 C, *left inset*) and 2) high frequency mfOPs (Figure 2-1C, *right inset*) were measured. For the mfPhNR, mfERG signals were filtered with a low pass filter (55 Hz) and amplitude was measured from baseline to the minimum point in the trough occurring after the first positive peak. mfPhNR amplitude in experimental glaucoma (Exp) eyes was measured at the latency of mfPhNR in the control (Con) eye. For the high frequency mfOPs, signals were filtered using a bandpass filter (100 - 200 Hz) and the mfOPs were quantified using the root

mean square (RMS) amplitude within a signal window of 60 ms (Rangaswamy et al. 2003; Rangaswamy et al. 2006).

2.2.4 Intravitreal injections

Intravitreal injections of 40 to 50 µL of tetrodotoxin citrate (TTX) diluted with sterile balanced saline solution to 10^{-4}M were administered nasally and temporally into the vitreous cavity of one eye of 2 monkeys using a sterile 30-gauge needle inserted through the pars plana behind the limbus. The final concentration of TTX, based on a 2.1 ml vitreous volume would be 1.2 – 2.1 µM (Rangaswamy et al. 2003). mfERGs were recorded before and after TTX administration.

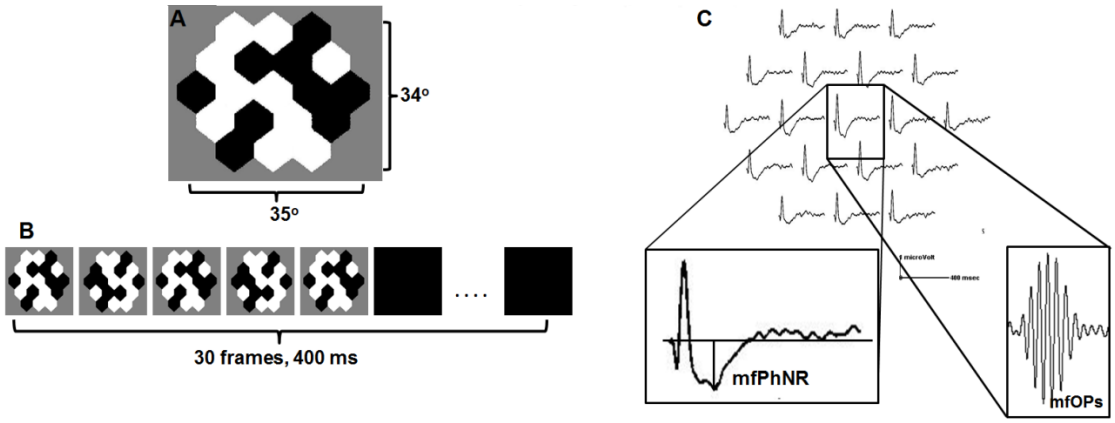

Figure 2-1: **(A)** mfERG stimulus display. **(B)** Slow sequence mfERG protocol showing five initial focal flashes followed by 25 dark frames. The duration of each sequence was 400 ms and the total duration of each recording was 7 min. **(C)** mfERG F30 responses from the 19 hexagons in the stimulus array. ***Left inset:*** Low pass (55 Hz) filtered mfERG signal. The mfPhNR was measured from baseline to trough. ***Right inset:*** Bandpass filtered mfOPs (100-200 Hz).

2.2.5 Optical coherence tomography and data analysis

All images were obtained with Spectralis HRA+OCT. Three scanning protocols were used: 1) a standard 12° peripapillary circular scan (1536 point B scan) centered on the ONH to measure RNFL thickness, 2) a 49 line 20° x 20° raster scan centered on the fovea to measure macular GCIPLT and 3) 48 radial B-scans acquired over a 20° area (1024 A-scans per B-scan) to measure MRW and ALCSD.

The RNFL was segmented using the OCT's software and these data were exported. Segmentation errors were corrected using a custom MATLAB program (Patel et al. 2014). ONH features including the termination points of the RPE/BM interface, the anterior lamina cribrosa (ALCS) points and the internal limiting membrane were marked in as many radial scans as possible in MATLAB (Sredar et al. 2013; Ivers et al. 2015). Minimum rim width (MRW), defined as the minimum distance from each of the RPE/BM termination points to ILM, was calculated on each side of the neural canal opening in the B-scan. Mean anterior lamina cribrosa surface depth (ALCSD) was calculated as the average distance between a plane best-fit to the Bruch's membrane opening (BMO) points and a thin-plate spline surface that was fit to the marked ALCS points (Sredar et al. 2013). Figure 2-2 shows a SD OCT image with RNFL (Figure 2-2 A) and ONH structures marked (Figure 2-2 B and Figure 2-2 C). A custom MATLAB program was used to segment the ILM, RNFL and ganglion cell inner plexiform layers (GCIPL). The GCIPL thickness is shown in Figure 2-2 D.

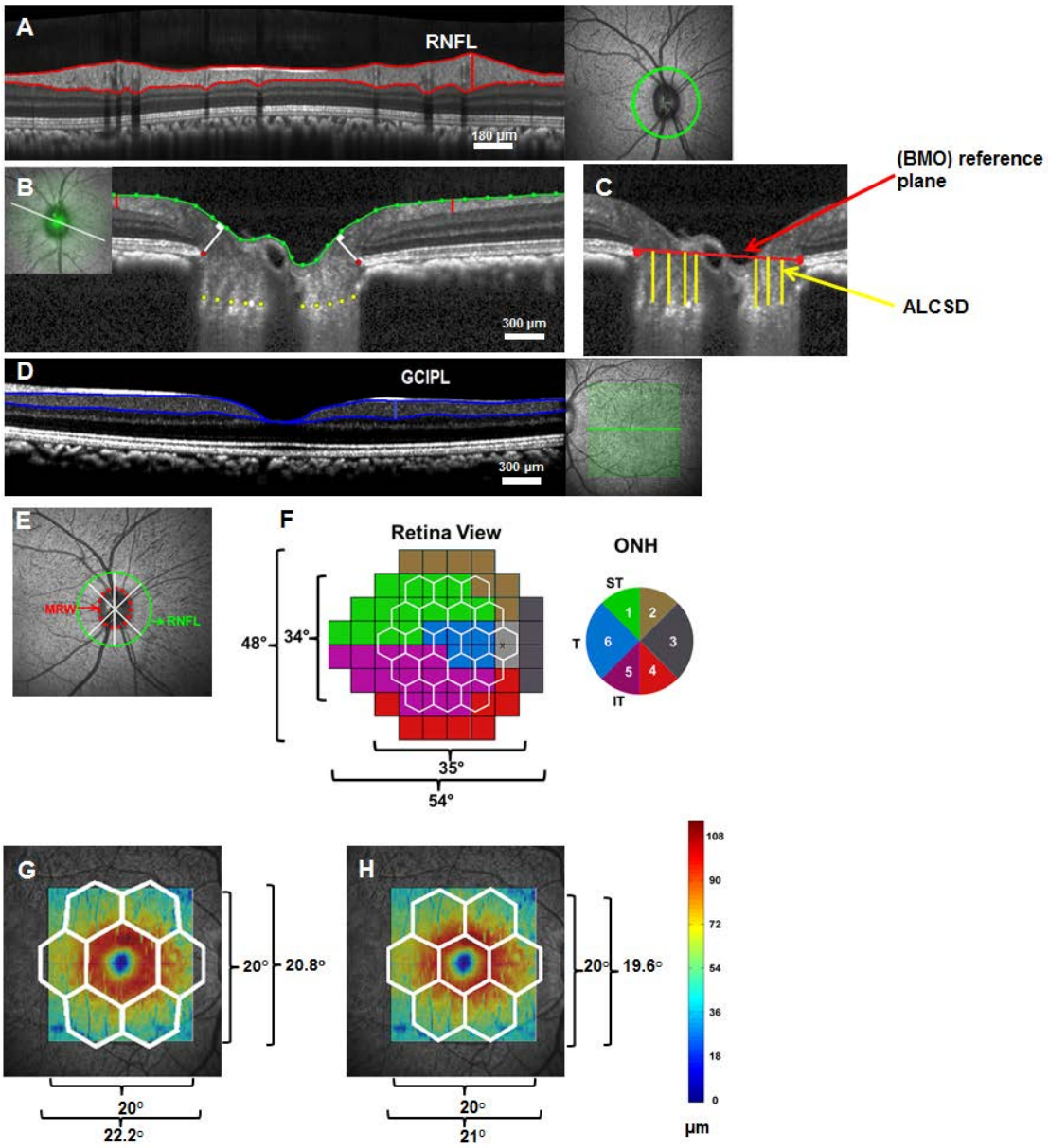

Figure 2-2: OCT segmentation and structure-function comparisons (A): A OCT circular B-scan showing the RNFL between the two red lines. The scan location is indicated by the green circle around the ONH in the inset. **(B):** A single OCT radial B-scan of the ONH. The inset shows the corresponding en face SLO image of the ONH and the location of all the radial B-scans. The scan shows ONH structures including termination points of the RPE/BM interface (red dots) and the ALCS (yellow dots), the semi-automatically segmented ILM (green dots) and the MRW (white line). An

approximate location of the RNFL peripapillary scan is shown as two vertical red lines (12°) on either side of the ONH. **(C):** B–scan showing the BMO reference plane (red line), the plane best fit to the BMO points on either side of the neural canal opening and the ALCSD (yellow lines). The mean ALCSD is the average of the distance between the BMO reference place and the thin-plate spline surface that was fit to the marked ALCS points. **(D)** A single OCT raster B-scan centered on the fovea. The scan shows the GCIPL thickness between the two blue lines. The inset shows the corresponding SLO image and the location of all B-scans. **(E)** Structure-function mapping for mfERG measures and structural parameters (RNFL and MRW) for the ONH. SLO image of the ONH showing the location of the peripapillary scan (green circle) and the location of BMO points (red dotted ellipse). The ONH was divided into 6 sectors based on a Garway Heath map (Garway-Heath et al. 2002). **(F)** *(Left)*: Position of the mfERG stimulus overlaid on the visual field map, which was flipped to retina view. *(Right)*: ONH map showing the projections of the axons from the corresponding regions of the visual field map. Each color-coded region in the visual field map corresponds to an ONH sector. **(G)** Projection of the mfERG stimulus array on the GCIPL map, corrected for RGC displacement, and **(H)** not corrected for RGC displacement. Calibration bars (μm on the retina) in panels A-C were scaled to take account of the shorter axial length of normal adult monkeys, compared to the axial length in normal adult humans, as described in Patel et al (Patel et al. 2011)

2.2.6 Comparison of mfPhNR and mfOPs with RNFLT and MRW

mfPhNRs were quantified both globally (g) and locally (sectorally, s). For the global mfPhNR (g-mfPhNR), mfERG responses from all 19 hexagons were added together and the mfPhNR amplitude was measured from the summed response. For the "global" temporal high frequency mfOPs (temp mfOPs), the mfOPs in the eight temporal hexagons were added together and RMS amplitude of the temporal mfOPs was computed. Only temporal mfOPs were analyzed because previous studies in the lab showed that temp mfOPs were larger, and more sensitive to glaucoma than nasal mfOPs (Rangaswamy et al. 2006), and this was confirmed in the present study (see Discussion Chapter 5, Figure 5-1, which also shows that mfPhNR did not display the naso-temporal differences in amplitude seen for the OPs). OCT RNFL and MRW parameters also were computed globally (g-RNFLT, g-MRW). Sectoral values for these parameters were then computed (s-RNFLT and s-MRW) for both Con and Exp eyes of animals with experimental glaucoma (Figure 2-2).

In order to evaluate the relationship between mfERG responses and sectoral structural measures, it was necessary to define the topographic relationships between the measures. Relations between visual field locations and corresponding regions of the ONH were previously mapped for humans by Garway-Heath et al in two slightly different formats (Garway-Heath et al. 2000; Garway-Heath et al. 2002). Figure 2-2 E shows the location of the measured RNFLT and the MRW around the ONH divided into 6 sectors indicated by the white lines. Figure 2-2 F shows the mfERG stimulus array, superimposed on the 2002 Garway Heath et al map (Garway-Heath et al. 2002). For a given ONH sector, the contributions of the mfERG responses were summed over all of the hexagons present in the corresponding visual field location. If only part of a hexagon was present in the corresponding visual field location, the response from that hexagon was scaled appropriately. Of the six sectors defined for the ONH, only the three

temporal sectors (1, 5 and 6) were used for comparing sectoral mfERG (s-mfPhNR and s-mfOPs) and structure (s-RNFLT, s-MRW) because the mfERG stimulus did not cover the far nasal regions corresponding to sectors 2, 3, and 4. For mfOPs, only responses from the region corresponding to the superior temporal (sector 1) and inferior temporal (sector 5) were used for sectoral analysis. Sector 6 was not used because it was dominated by axons of the papillomacular bundle, corresponding to nasal macular locations where OPs were small and not analyzed.

2.2.7 Comparison of mfPhNR amplitude with macular GCIPL thickness

In order to obtain an accurate comparison between the mfPhNR and the macular GCIPL thickness, it is necessary to account for RGC displacement in the foveal region (Drasdo et al. 2007). Recent studies have used the RGC displacement model of Drasdo et al to study macular structure-function relationships (Hood and Raza 2011; Hood et al. 2011; Luo et al. 2014), and it was adopted for the present study. In brief, the mfERG stimulus array was scaled based on RGC lateral displacement and the central seven hexagons were then projected on the GCIPL thickness map. Figures 2-2 G and 2-2 H show the mfERG stimulus array overlaid on the GCIPLT map with (G) and without (H) scaling. Thickness values for pixels covered by the central seven hexagons (macular, m-GCIPL) were averaged and compared with the corresponding macular mfPhNR (m-mfPhNR) amplitude.

2.2.8 Biometric measurements and scaling

Axial length, corneal curvature and anterior chamber depth were measured using a non-contact ocular biometer (IOLMaster; Carl Zeiss Meditec, AG, Jena, Germany). These measurements were included in the three surface (anterior corneal curvature,

posterior corneal curvature and anterior lens curvature) formula of the model eye and for calculating lateral magnification of the OCT scans (Ivers et al. 2011; Patel et al. 2011).

2.2.9 Statistical Analysis

Repeated measures ANOVA was done to compare the mfPhNR amplitudes for different numbers of multifocal flashes in normal monkey eyes. Post hoc tests with Tukey corrections were used for multiple comparisons (SPSS Statistics Version 20, IBM Corporation, Somers, NY). Linear and nonlinear regression analyses were used to compare structure–function and structure–structure relationships (SigmaPlot 10.0, Systat software Inc, San Jose, CA) for individual monkeys from all recording sessions. Both global (average) and local structure function relationships were analyzed. Appropriateness of nonlinear fits was supported by Akaike information criteria (AICc) analysis (Burnham and Anderson 2004) (GraphPad Prism version 6.0, GraphPad Software, La Jolla, CA). For the longitudinal analysis, for individual animals the 95% confidence limits for each parameter (mfPhNR, mfOPs, RNFLT, GCIPLT, MRW and ALCSD) were calculated for the Con eye across all experimental sessions and the percent change of each parameter in the Exp eye from the mean of the Con eye values was plotted against time. The time of first significant change was defined as the first time point for which the parameter fell outside the lower (or upper for ALCSD) limit of the 95% confidence interval (CI), with subsequent time points also outside the 95% CI. The determined first time points for the various structural and functional measures were compared using Kaplan-Meir (K-M) survival analysis for a subset of four monkeys with experimental glaucoma. Log rank test (χ^2) was performed on the K-M curves to test for significant difference. (SPSS Statistics Version 20, IBM Corporation, Somers, NY). An additional repeated measure ANOVA using PROC MIXED and paired t-test in SAS (SAS; SAS Institute, Inc., Cary, NC) were used for the whole set of experimental animals

(n=7) to compare the time points of change across global and local structural and functional parameters.

2.3 Results

2.3.1 Adjustment of the mfERG stimulus duration to maximize mfPhNR amplitude

The number of initial frames with multifocal flashes in the mfERG stimulus was increased from one to five or six frames followed by 29 to 24 dark frames in a 30 frame sequence (F30). The effect of increasing the number of flashes on the mfERG was evaluated in five normal eyes of five different monkeys. As shown by the plots in Figure 2-3, mfPhNR amplitudes increased for each eye with increasing initial flashes up to five flashes, but did not increase for the sixth flash, when it was presented. Assuming integration of the response over time, the estimated effective duration of the five focal flashes was at least 53.3 ms. The mfPhNR amplitude was greatest for five flashes (P<0.05, repeated measures ANOVA, Tukey), and the F30-5 protocol was adopted for mfERG recording in the longitudinal study described in this chapter.

2.3.2 Reduction of mfPhNR amplitude after TTX injection and in experimental glaucoma

To determine the contribution of spiking neurons to the mfPhNR, mfERGs were recorded in two monkeys before and after intravitreal injection of TTX, an agent that blocks the Na^+ dependent spiking of inner retinal neurons (Bloomfield 1996; Stafford and Dacey 1997). Previous studies in the laboratory showed that full field PhNR and OPs in the mfERG are reduced by intravitreal injection of TTX (Viswanathan et al. 1999) (Rangaswamy et al. 2003). Figure 2-4 A shows the global mfERG, summed over the entire stimulus array recorded with the F30-5 (five focal flashes) protocol before TTX

(black line) and after TTX *(red line)*. The plot shows that mfPhNR amplitude was reduced although not fully eliminated by TTX. Similar effects of TTX were observed for one focal flash in this animal and in the other animal.

For comparison, global mfERG results from a representative monkey eye with advanced experimental glaucoma are shown in Figure 2-4 B. g-mfPhNR amplitude and g-RNFLT were greatly reduced in the Exp eye compared to the Con eye.

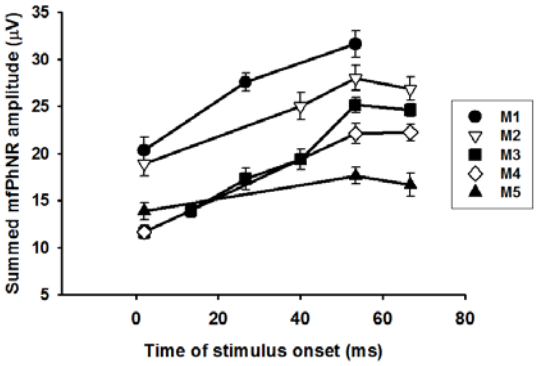

Figure 2-3: Plot of the mfPhNR amplitude (mean ± SEM) elicited by presentation of one to six successive focal flashes for five normal monkey eyes (n= 5). mfPhNR amplitudes were plotted against time of stimulus presentation for each successive flash with the first focal flash occurring at time zero. The estimated stimulus duration for five successive focal flashes in the 30 frame sequence was at least 53.3 ms.

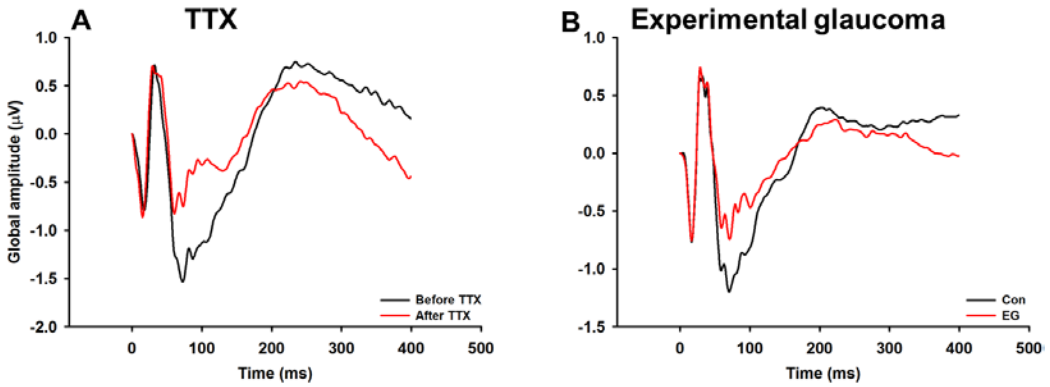

Figure 2-4: Effect of pharmacological blockade of inner retinal spiking activity by TTX and of experimental glaucoma on mfERG. (A) mfERG of one monkey before *(black line)* and after *(red line)* TTX injection. **(B)** mfERG of one monkey (OHT-66) with advanced experimental glaucoma (RNFLT = 46 µm). *Black line* represents Con eye and *red line* represents Exp eye. For this plot, the summed global amplitude was divided by the number of hexagons (19).

2.3.3 Relationship between intraocular pressure (IOP) and global structural and functional measures

IOP data and the time course of experimental glaucoma for the seven monkeys are presented in Table 2-1. IOP was measured longitudinally in the monkeys with unilateral experimental glaucoma and the relation of different global structural and functional measures to cumulative IOP was assessed. Cumulative IOP difference was calculated by integrating the IOP difference between the Con and Exp eye over time, expressed in mm Hg.days (Yang et al. 2011). Day zero was defined as the day of the first laser treatment. The relation between cumulative IOP and g-mfPhNR, temp mfOPs, m-GCIPLT, g-RNFLT and g-MRW were adequately described using an exponential decay function ($f=y0+a*e^{(-t*x)}$, Figure 2-5 A-E) and the relation between cumulative IOP and ALCSD (Figure 2-5 F) was described using an exponential rise to maximum function ($f=y0+a*(1-e^{(-t*x)})$). The exponential fits (Figure 2-5 A-C, E, and F) were compared with linear fits using AICc analysis, which favored the exponential fits. The values of exponent "t" for g-mfPhNR, temp mfOPs, macular GCIPLT, MRW and ALCSD were similar but were consistently larger than for the RNFLT, indicating that the RNFL changed more slowly than the other functional and structural measures. The exponential relationships shown in Figure 2-5 did not change when we plotted the average or median of the individual monkeys' data.

Table 2-1: IOP data for the control and experimental glaucoma eyes from the time of first laser session

Animal ID	Age (years)	Follow up time from 1st laser session (days)	Number of laser sessions	Mean IOP ± SD (mmHg)		Peak IOP (mmHg)		Cumulative IOP difference (mmHg.days)*	g-RNFLT in the last imaging session (µm)	
				Con	Exp	Con	Exp		Con	Exp
OHT- 64	4.3	554	10	14.0 ± 2.4	28.5 ± 13.6	18	48	7327	102	74
OHT- 66	3.2	518	7	13.7 ± 1.0	33.5 ± 12.4	15	47	9731	101	46
OHT- 67	3.3	651	12	14.0 ± 2.3	26.1 ± 10.3	18	41	8840	115	106
OHT- 70	5.5	406	5	11.5 ± 2.7	30.4 ± 11.0	15	44	7440	119	52
OHT- 71	3.5	595	3	14.3 ± 3.6	40.0 ± 13.0	20	54	15431	118	67
OHT- 72	3.6	588	3	15.2 ± 2.1	35.3 ± 10.0	19	48	12222	111	81
OHT- 75	6.3	69	2	11.3 ± 2.2	16.8 ± 7.6	19	26	362	102	89

*Cumulative IOP difference = AUC (IOP. time $_{Exp}$) - AUC (IOP. time $_{Con}$)

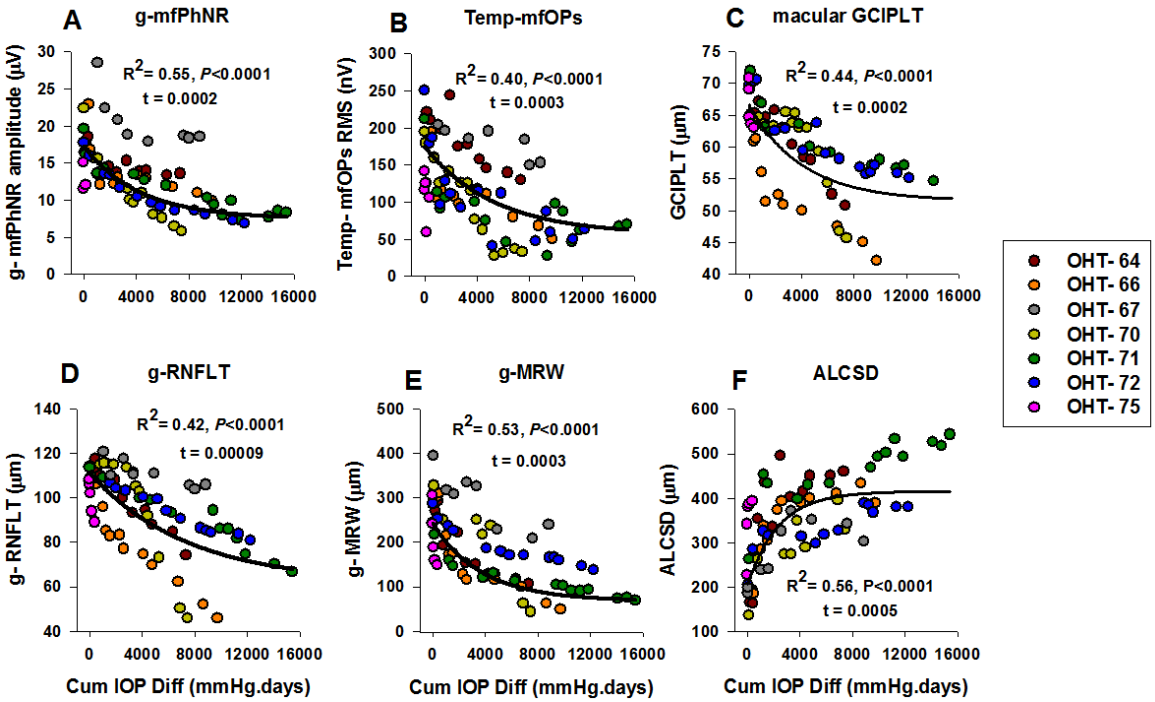

Figure 2-5: Relationship between structural and functional measures and IOP. (A) g-mfPhNR amplitude, **(B)** temp mfOPs, **(C)** m-GCIPLT**, (D)** g-RNFL thickness, **(E)** g-MRW, **(F)** ALCSD as a function of cumulative IOP difference. Each colored symbol represents data from the Exp eye of one monkey. An exponential decay function was used to describe the effect of elevated IOP on the g-mfPhNR, temp mfOPs, g-MRW and g-RNFLT and an exponential rise to maximum function was used for ALCSD. AICc supported the exponential fits over linear fits: *(Difference in AICc; g-mfPhNR= 2.0, temp-mfOPs= 7.0, m-GCIPLT= 4.2, g-MRW= 3.4, ALCSD= 7.38).*

2.3.4 Global structure-function and structure–structure relationships

The main purpose of this study was to analyze the relation between inner retinal functional measures and concurrent alterations in structural measures in experimental glaucoma as they changed over time. In previous studies, full field and focal PhNR amplitudes were strongly correlated with RNFLT and with corresponding rim areas and cup-disc ratios. (Machida et al. 2008; Tamada et al. 2010). Strong relationships therefore might be expected between mfPhNR amplitude and retinal (RNFLT and m-GPIPLT) and ONH measures (MRW and ALCSD). Figure 2-6 shows comparisons of global structural and functional measures for Con and Exp eyes combined (Figure 2-6 A-F). g-mfPhNR amplitude was linearly related to g-MRW (R^2=0.66, *P*<0.0001, Figure 2-6 A) and ALCSD (R^2=0.54, *P*<0.0001, Figure 2-6 B). Similarly, m-mfPhNR was linearly related to m-GCIPLT (R^2=0.47, P<0.0001, Figure 2-6 D). However, unlike the linear relationship with ONH measures and m-GCIPLT, g-mfPhNR amplitude was nonlinearly related to g-RNFLT (Figure 2-6 E); the relationship was more suitably described by an exponential growth equation $f=y0+a*e^{(t*x)}$ (R^2=0.58, P<0.0001; AICc analysis). Figure 2-6 E shows that g-mfPhNR amplitude was reduced markedly when g-RNFLT had hardly changed, and that much of the change in g-RNFLT occurred after changes in g-mfPhNR amplitude were complete. Averaging parameters of the fits for individual animals yielded similar results to fits across animals, which are shown in these, and subsequent figures. The time points for initial changes in structural and functional measures are specifically addressed later in the results.

g-MRW and ALCSD, were linearly related (Figure 2-6 F) and strongly correlated (R^2=0.68, P<0.0001). In contrast, the relationship between g-MRW and g-RNFLT (Figure 2-6 G) was better described by an exponential rise to maximum equation, $f=y0+a*(1-e^{(-t*x)})$, (R^2=0.78, P<0.0001; AICc analysis). This non-linear relationship was consistent with previous findings in NHP experimental glaucoma and glaucoma patients (Patel et al.

2014) suggesting that ONH parameters begin to change at earlier stages of glaucoma than RNFLT. The relationship between structural and functional measures was not altered by including or excluding the Con eye data when curve fitting.

2.3.5 Local structure-function relationship

An advantage of the mfERG over the full field ERG is that it allows us to measure local changes in function. Figures 2-7 A and B show the relationship between thickness of a sectoral region of the peripapillary RNFL (s-RNFLT, see Figure 2-7 A) and the local PhNR amplitude (s-mfPhNR) in the corresponding retinal region populated by the RGCs whose axons form the RNFL in that sector (Garway-Heath et al. 2002). These relationships are illustrated for Con and Exp eyes separately in the figure. Unlike the nonlinear relationship found between the global mfPhNR and RNFLT, the s-mfPhNR was linearly related to the s-RNFLT in both Con and Exp eyes. The s-mfPhNR and s-MRW, like the global measures of the same parameters, also were linearly related (Figures 2-7 C and D) in both Con and Exp eyes. For the temp mfOPs, there was not a significant relationship in Con eyes with either s-RNFLT or s-MRW (Figure 2-7 E and Figure 2-7 G). However, in Exp eyes, similar to s-mfPhNR results, temp mfOPs were linearly related to both s-RNFLT (Figure 2-7 F) and s-MRW (Figure 2-7 H).

2.3.6 Relationship between g-mfPhNR and temporal RNFLT

As noted above, only the temporal sectors of the ONH 1, 5 and 6 received input from RGCs stimulated by the multifocal array. The nasal side of the ONH did not receive axons from stimulated RGCs. Therefore, we examined the relationship between the g-mfPhNR and the averaged temporal RNFLT from sectors 1, 5 and 6 only (Figure 2-8), and found that temporal RNFLT, unlike global RNFLT which contained the nasal sectors,

was linearly related to g-mfPhNR amplitude (R^2=0.40, P<0.0001). The relationship did not change when we included or excluded Con eye data.

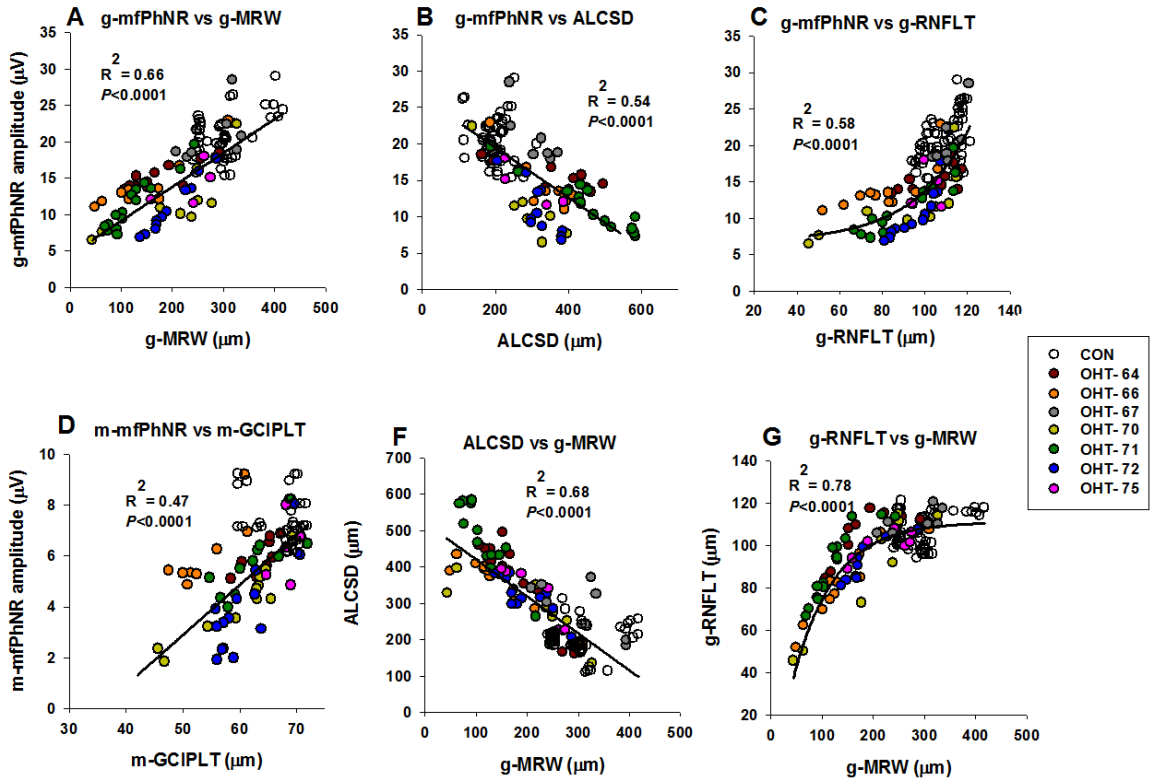

Figure 2-6: Global structure-function and structure-structure relationships in experimental glaucoma. *Top panel:* **(A)** Global mfPhNR amplitude versus global MRW. **(B)** Global mfPhNR amplitude versus ALCSD. **(C)** Global mfPhNR amplitude versus global RNFLT, difference in AICc = 8.2. *Bottom Panel:* **(D)** macular mfPhNR versus macular GCIPLT. **(E)** mean ALCSD versus global MRW. **(F)** Global RNFLT versus global MRW, difference in AICc = 37.1. Each colored symbol represents one time point for one monkey. *Open circles* correspond to Con eyes and *filled circles,* to Exp eyes.

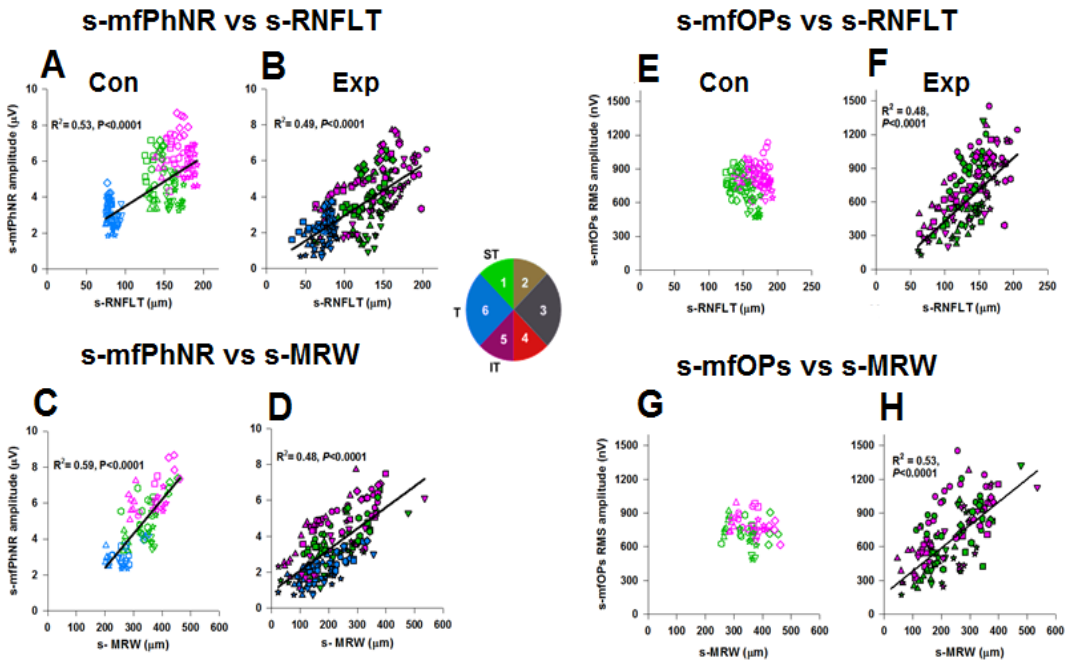

Figure 2-7: Relation of mfPhNR to local structure in control and experimental glaucoma eyes. *Left panel:* Local mfPhNR versus Local structure. **(A)** s-mfPhNR amplitude as a function of s-RNFLT in Con eyes. **(B)** s-mfPhNR amplitude as a function of s-RNFLT in Exp eyes, **(C)** s-mfPhNR amplitude as a function of s-MRW in Con eyes. **(D)** s-mfPhNR amplitude as a function of s-MRW in Exp eyes. *Right Panel:* Local mfOPs versus Local structure. **(E)** s-mfOPs amplitude as a function of s-RNFLT in control eyes. **(F)** s-mfOPs amplitude as a function of s-RNFLT in Exp eyes, **(G)** s-mfOPs amplitude as a function of s-MRW in control eyes. **(H)** s-mfOPs amplitude as a function of s-MRW in Exp eyes. Only data from superior-temporal sector *(Green, 1)* and inferior-temporal sectors *(Purple, 5)* were used in the s-mfOPs analysis. Each symbol corresponds to data from one animal for one time point: *open symbols* for Con eyes and *closed symbols,* for Exp eyes. The colors, purple, green and blue correspond to sectors 5, 1 and 6 respectively in the ONH, as shown in the inset.

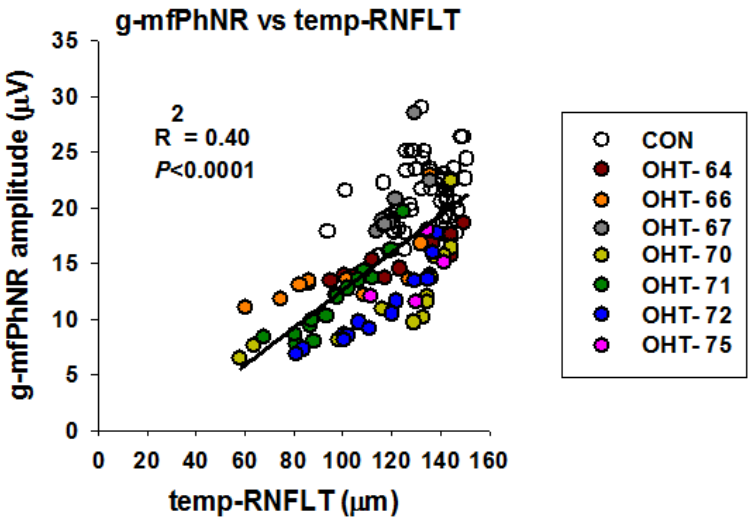

Figure 2-8: Relation of global mfPhNR amplitude to the temporal RNFLT. Each colored symbol represents one time point for one monkey. *Open circles* correspond to Con eyes and *filled circles*, to Exp eyes.

2.3.7 Longitudinal analysis of structural and functional changes

Next, we examined, more directly, the time necessary for significant changes to occur in structural and functional measures for Exp eyes, to determine which measure(s) changed earliest. We first determined the mean and variability (95% CI) for Con eye of the structural and functional measures made over the 4 to 8 OCT and mfERG sessions for each animal. Then we calculated the percent change of each parameter in the Exp eye from the mean for that parameter in the Con eye and plotted the data against time from the initial laser treatment (e.g. Figure 2-9). The time of the first significant change for a parameter for the Exp eye was defined as the first time point for which the parameter crossed the lower (or upper) limit of the Con eye's 95% confidence interval, when the values at subsequent time points were also outside that measure of variability.

2.3.7.1 Global longitudinal analysis

Figure 2-9 illustrates the time course of changes in global parameters in one animal (OHT-70). For this animal, the ONH measures in panels C and D (g-MRW and ALCSD), and macular parameters m-mfPhNR (E) and m-GCIPLT (F) changed at 98 days, closely followed by g-mfPhNR (A) at 112 days. However, g-RNFLT (B) changed only after 273 days. Over all in the seven monkeys, we observed from these longitudinal plots that the ONH measures (MRW and ALCSD) changed first accompanied by mfPhNR changes in one monkey and the g-RNFLT was consistently the last parameter to change. Statistical analyses are presented in a later section.

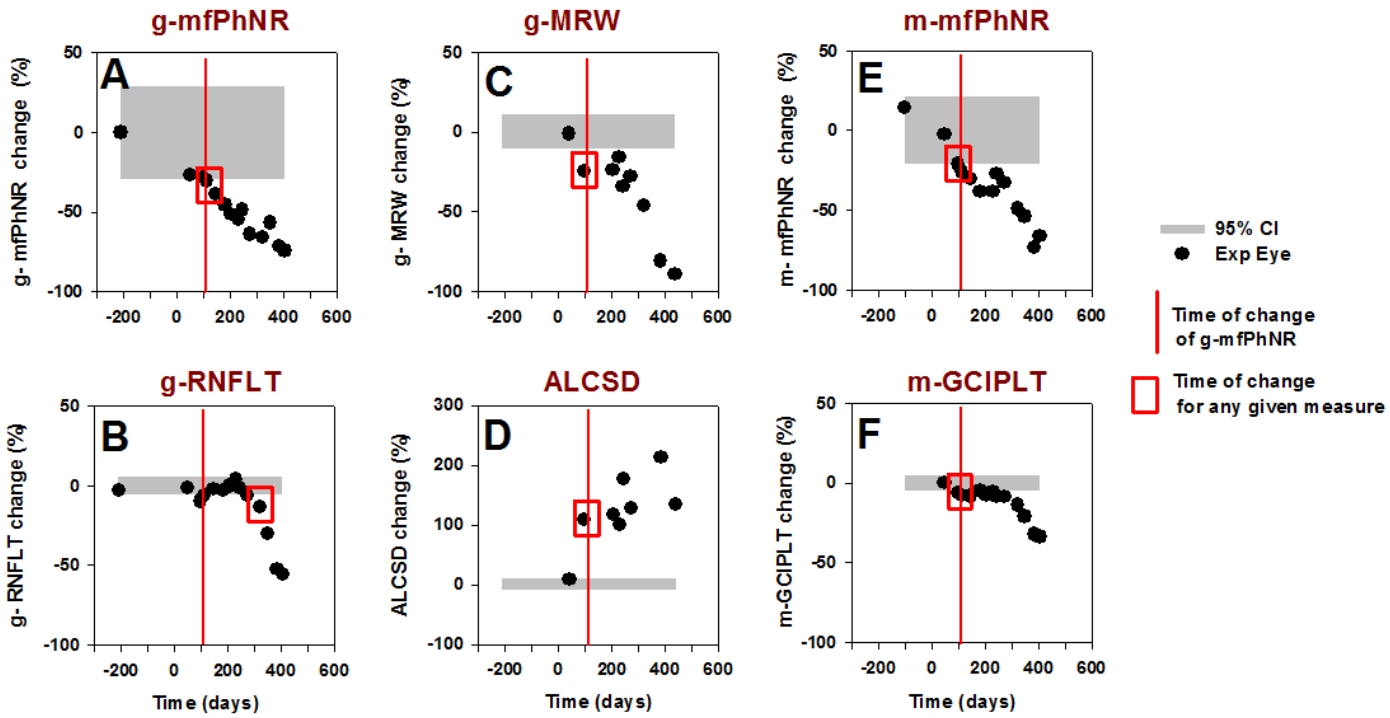

Figure 2-9: Longitudinal analysis of global structure-function measures in experimental glaucoma (OHT-70). (A) Global mfPhNR amplitude percent change, **(B)** Global RNFLT percent change, **(C)** Global MRW percent change, **(D)** ALCSD percent change, **(E)** macular mfPhNR percent change, **(F)** macular GCIPLT percent change *Grey* band represents the 95% CI from the control eye. *Black* symbols represent the percent change in the Exp eye from the mean for the Con eye. Zero (0) represents the time of the first laser session. *Red* vertical line corresponds to the time of first significant change of g-mfPhNR amplitude. *Red* squares indicate the time of first significant change for that measure.

2.3.7.2 Sectoral longitudinal analysis

Figure 2-10 (A-I) illustrates the time course of changes in locally measured parameters, for one animal (OHT 71). The inset shows the ONH with the sectors color-coded. In this monkey, s-MRW (Middle row 2-10 D-F) and s-mfPhNR (Top A-B) were the first parameters to change at 42 days in sectors 1 and 6 followed by s-RNFLT at 84 days (Bottom 2-10 H). Overall, in the seven monkeys, either the s-MRW or s-mfPhNR was the first parameter to change and s-RNFLT was the last. The results for the four animals that were in the second group (see Methods) are summarized by the Kaplan-Meier (K-M) analysis in the next section.

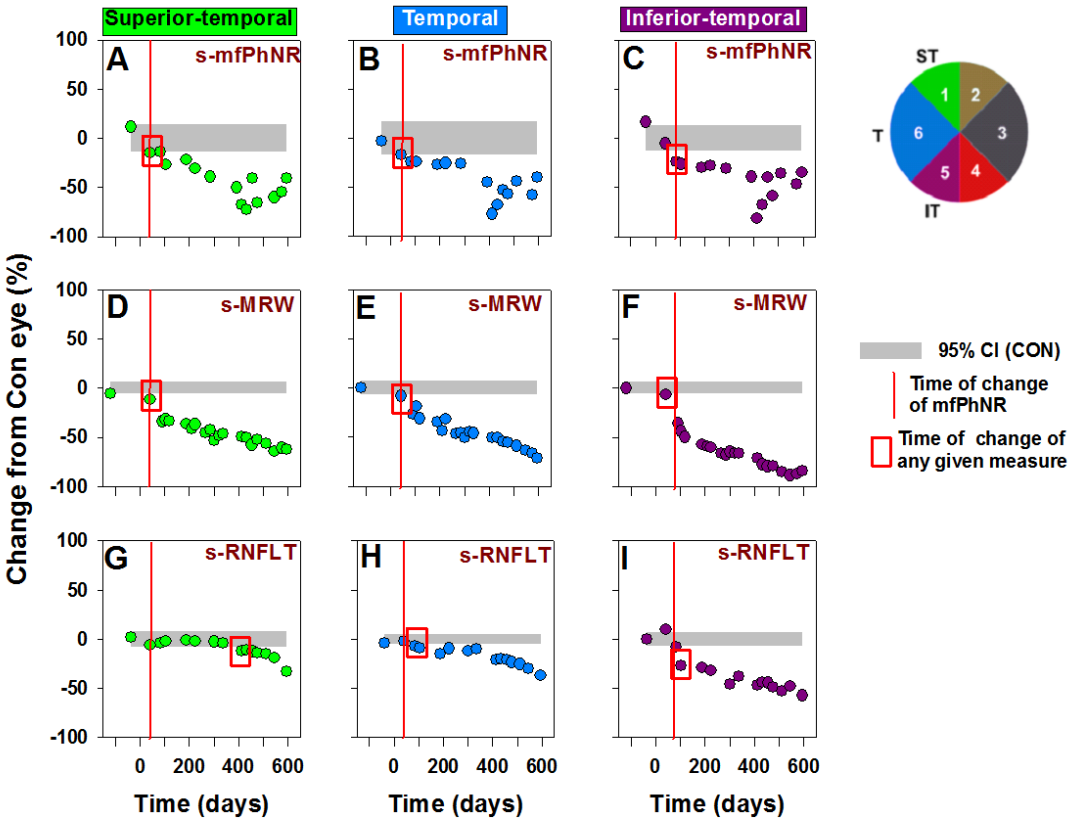

Figure 2-10: Longitudinal analysis of sectoral structure-function measures in experimental glaucoma (OHT- 71). Sectoral mfPhNR amplitude percent change *(A-C)*. sectoral MRW percent change *(D-F)*. sectoral RNFLT percent change *(G-I)*. *Inset:* ONH map with color coded sectors. *Grey* band represents the 95% CI from the Con eye in different sectors. *Green* filled symbols represent percent change in the Exp eye in sector 1, *Purple* filled symbols, percent change in the Exp eye in sector 5. *Blue* filled symbols, percent change in the Exp eye in sector 6. Time 0 represents the time of first laser treatment. *Red* vertical line corresponds to the time of first significant change of s-mfPhNR amplitude. *Red* squares indicate the time of first significant change in the plotted measure.

2.3.8 Comparison of time points for the first significant change

From the longitudinal analysis, it was evident that the RNFLT (global and sectoral) was consistently the last measure to change in Exp eyes. ONH parameters tended to change earliest, closely followed or concurrently with changes in mfPhNR amplitude. In order to distinguish time points for first significant change for the various structural and functional parameters more directly, a survival analysis was done for the four animals in the second group (see Methods). Kaplan-Meier (K-M) curves (Figure 2-11) were plotted for each measure and the cumulative probability of the first time point showing significant change was determined for that measure. Figure 2-11 A shows the K-M survival plots for the global structural parameters (g-RNFLT, g-MRW, and ALCSD). From the figure, it is evident that the global ONH (g-MRW and ALCSD) parameters were the first to change and the g-RNFLT was the last to change; the K-M survival curve for RNFLT was significantly different from curves for ONH parameters (g-MRW, χ^2=4.9; ALCSD, χ^2=4.8, *P*<0.05, Log Rank). Figure 2-11 B shows the K-M curve for g-mfPhNR. We did not find a significant difference between ONH (Figure 2.11 A) and g-mfPhNR (Figure 2.11 B) curves but the g-mfPhNR curve looked earlier than g-RNFLT curve. Although the difference in K-M curves did not achieve statistical significance (χ^2=2.3, *P*=0.13) in the subset of four monkeys, time points for change in g-mfPhNR were significantly earlier than time points for g-RNFLT when we compared data for all seven monkeys with experimental glaucoma (*P<0.05*, n=7, repeated measures, PROC MIXED).

A comparison of K-M survival plots for global (Figure 2-11 A) and sectoral structural measures (Figure 2-11 C), indicates that s-RNFLT changed earlier than g-RNFLT, but no difference was seen in s-MRW vs g-MRW curves. Again, although we did not find a significant difference in the subset of four animals based on the K-M analysis (χ^2= 0.97, *P*= 0.3), a significant difference was found between the sectoral and global

RNFLT when we compared time points of first significant changes for all seven animals (P<0.05, n=7, paired t-test).

Figure 2-11 D shows the time points for local functional changes (s-mfPhNR). No significant difference was found between local structural and local functional measures although in the plot, s-mfPhNR changed slightly before s-RNFLT. Finally, we also did not find a significant difference between macular structural (Figure 2-11 E) and functional (2-11 F) parameters.

To sum up, the overall trend in monkeys with experimental glaucoma was that changes in function and ONH structure preceded global RNFLT changes, and local changes in inner retinal structure, s-RNFLT and m-GCIPLT, preceded global changes in g-RNFLT.

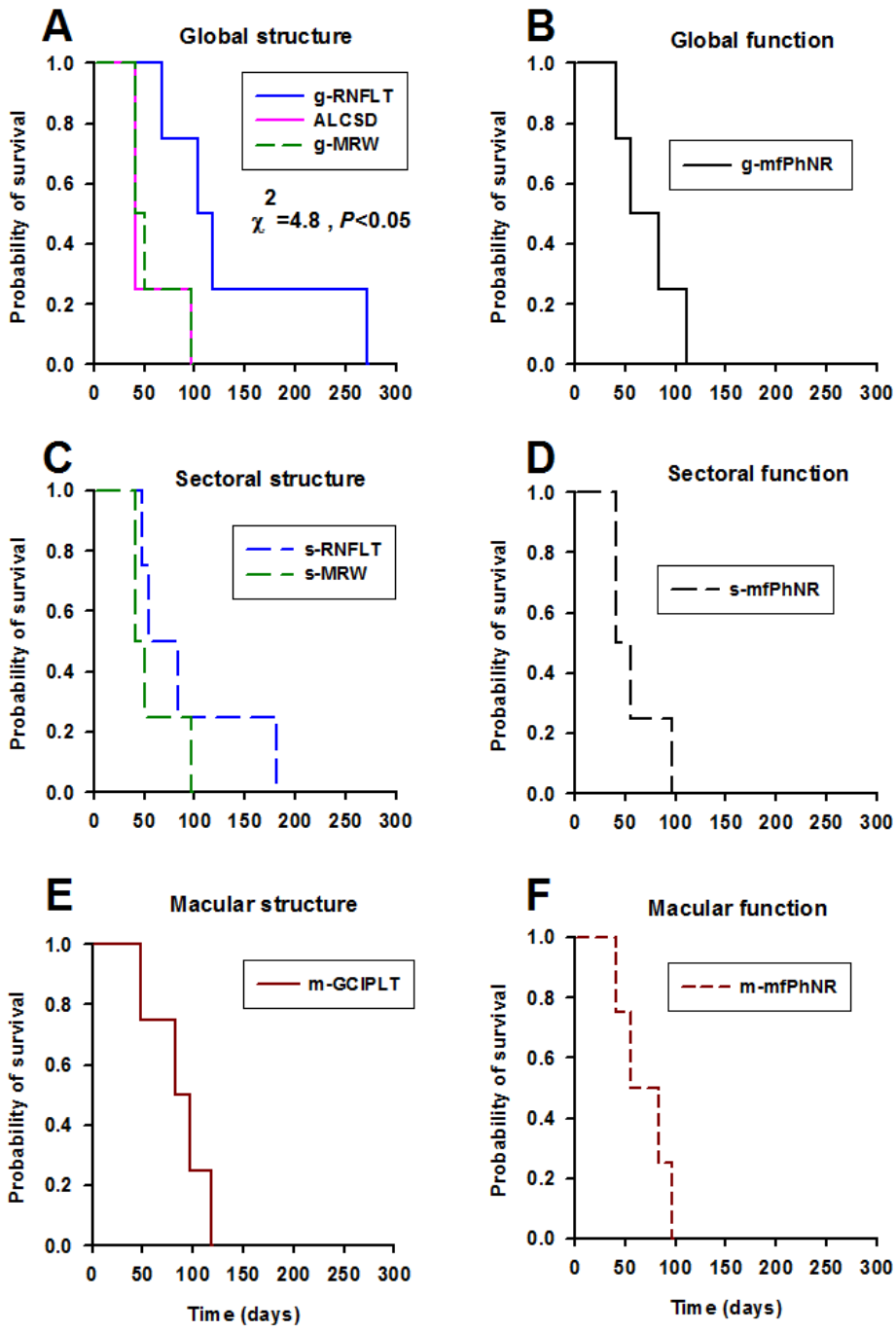

Figure 2-11: Kaplan-Meier survival analysis comparing time points for the first significant change in structural and functional parameters in experimental glaucoma eyes. (A) Global structure (g-RNFLT, g-MRW and ALCSD). **(B)** Local structure (s-RNFLT, s-MRW). **(C)** Global function (g-mfPhNR). **(D)** Local function (s-mfPhNR. **(E)** Macular structure (m-GCIPLT). **(F)** Macular function (m-mfPhNR).

2.4 Discussion

In this study, we examined longitudinal changes in inner retinal function and compared them with changes in the structure of inner retina and the optic nerve head in macaque eyes with experimental glaucoma. Previous studies have shown that changes in functional measures occur prior to RNFL thinning (Fortune et al. 2012; He et al. 2014) and structural changes in the ONH occur prior to RNFL thinning in experimental glaucoma (Strouthidis et al. 2011; He et al. 2014; Patel et al. 2014; Ivers et al. 2015), and our study confirmed and extended these findings. The unique outcome of our study was that the earliest changes in mfPhNR amplitude occurred almost concurrently with changes in ONH structure (MRW and ALCSD). Additionally we found that local measures of mfPhNR and RNFL were well correlated. We also found changes in local RNFLT preceded global changes, whereas no such difference was observed for MRW.

2.4.1 Early changes in ONH structure and inner retinal function in Exp eyes

It is evident from previous studies that glaucomatous damage occurs early at the level of the ONH when IOP is elevated (Quigley and Green 1979; Quigley et al. 1981; Burgoyne et al. 2005; Quigley 2005). The stress due to elevated IOP causes deformation of the ONH and connective tissue remodeling (Bellezza et al. 2000; Bellezza et al. 2003; Burgoyne et al. 2004; Burgoyne et al. 2005; Downs et al. 2007; Yang et al. 2007a; Yang et al. 2007b). Quantification of these changes in experimental glaucoma has shown, as we also observed (Figure 2-11 A), reduced neuroretinal rim width and increased ALCS depth that occurred prior to RNFL thinning (Strouthidis et al. 2011), suggesting that changes in ONH structure occur prior to axonal loss. Axonal loss may be masked in the RNFL however, as ~10-15% axonal loss in the optic nerve has been reported in macaques with experimental glaucoma prior to RNFL thinning (Cull et al. 2012). Glial changes in the RNFL (Wang et al. 2002) and varicosities in the axons

(Wang et al. 2003) or edema may cause an artificial thickening of the RNFL which could mask the thinning caused by reduced axon count. Our observation of sectoral thinning when global RNFL had not changed (Figure 2-11 A and C) would be consistent with such masking. Regardless of the underlying reason for the difference, there is a growing consensus that MRW is more sensitive than RNFL in distinguishing glaucoma patients (Chauhan et al. 2013) and suspects (Patel et al. 2014)) from healthy control subjects.

Similar to the structural changes in ONH, we found that inner retinal function was reduced relatively early compared to thinning of the RNFL (Figure 2-11 A and B) as cumulative IOP increased in Exp eyes (Figure 2-5 A). The finding that reductions in mfPhNR amplitude occurred concurrently with changes in ONH parameters raises the possibility that these changes are related. Although the PhNR is dependent upon the activity of RGCs, a contribution of glial cells to the generation of the slow wave is likely (Raz-Prag et al. 2010; Thompson et al. 2011). A role for activated glial cells in glaucomatous damage has been reported (Hernandez and Pena 1997; Carter-Dawson et al. 1998; Wang et al. 2000; Kanamori et al. 2005). It may be the case that, early reduction in mfPhNR amplitude is due to non-neuronal/glial changes and at later stages of sustained elevated IOP, the mfPhNR amplitude declines as RGC activity declines.

Another interpretation of the early changes in PhNR amplitude is that the inner retina itself is sensitive to changes in IOP, and effects on inner retina (e.g. RGC dendrites) precede axonal loss or cell death (Morgan et al. 2000; Shou et al. 2003; Morgan et al. 2006). For instance, Weber et al reported a significant reduction in RGC dendritic arbor size in a NHP (bead) model of experimental glaucoma, and that this change occurred prior to reduction in axon diameter and cell shrinkage (Weber et al. 1998). Subsequent studies by Weber and collaborators also found changes in visual function of RGCs (Weber and Harman 2005). They hypothesized that reduced axonal transport of trophic factors from target cells caused dendritic arbor retraction in RGCs,

which lead to reduced visual function. This idea was further supported by results of treatment of RGCs in Exp eyes with BDNF, which improved cell survival and preserved dendritic morphology. Additionally BDNF treated eyes showed enhanced PERG responses compared to untreated eyes (Weber and Harman 2008; Weber et al. 2008).

Taken together, the concurrent very early changes in ONH parameters and inner retinal function measured by the PhNR or OPs raises the possibility of a dual effect of IOP related stress, resulting in both conformational changes in the ONH, and the functional changes in the inner retina.

2.4.2 Early changes in the sectoral RNFLT prior to the global RNFLT

Another difference of this study from previous studies e.g. (Patel et al. 2011; Fortune et al. 2013a; He et al. 2014) is that we compared local changes in structure with local functional changes. We found that local s-RNFLT showed changes significantly before the g-RNFLT in Exp eyes (Figure 2-9, Figure 2-10, Figure 2-11 A and C). One possibility for this finding could be that small RNFLT changes occurring in one sector could have been missed in the global average (or. as noted above, masked. by swelling in other regions). As the disease progresses, the dimensions of the defect will increase, involving multiple sectors of the ONH region, leading to global RNFLT changes. This idea is supported by the difference in the relationship between g-mfPhNR versus g-RNFLT (Figure 2-7 C) which is nonlinear, and between g-mfPhNR versus temporal (sectors 1, 5, 6) RNFLT only (Figure 2-8), which is linear. Further, studies in human glaucoma patients have shown that the superior and inferior poles of the ONH are most susceptible to glaucomatous damage (Jonas et al. 1993; Hood et al. 2013; Kim et al. 2014) and that local visual field changes correlate well with local changes in the RNFLT (Gardiner et al. 2016). In our study, we found a good correlation between local inner retinal functional measures (s-mfPhNR and s-mfOPs) and local s-RNFLT (Figure 2-7 B,

Figure 2-7 F), suggesting that the mfPhNR can be used to track progression of RGC loss in glaucoma, as well as being useful for early detection.

In contrast to the RNFLT, where local changes were seen earlier than global changes, this difference did not occur between local versus global ONH parameters (Figure 2-11 A, Figure 2-11 C). One possible explanation could be that the biomechanical effects of increased IOP are different for RNFL and MRW due to location. Very early changes in g-MRW and s-MRW were more likely to be due to conformational changes than neuronal loss (Strouthidis et al. 2011). The direct effects of pressure may not have affected RNFL, and the changes in thickness that were measured occurred after axons died. In support of this idea, numbers of surviving axons were found to be correlated better with the RNFLT than with the MRW in experimental glaucoma (Fortune et al. 2016), and reduction in visual function (mean deviation, MD) was better correlated better with RNFLT than with MRW in glaucoma patients (Gardiner et al. 2014). No significant difference was observed between MRW and RNFLT in detection of established glaucoma, although MRW performed better in discriminating glaucoma suspects from healthy controls (Patel et al. 2014).

2.4.3 Relationship between function (mfPhNR) and inner retinal structures (m-GCIPLT and g-RNFLT)

In our study, we found that macular GCIPL tended to show thinning earlier than peripapillary RNFLT, although the measures were not significantly different. (Figure 2-10 A and 2-10 E). GCIPLT may be a more direct measure for comparison with the local functional changes than the RNFL. Although we used a map to trace the trajectories of RGC axons from retina to ONH, each sector of the ONH has overlapping axons coming from several retinal locations. m-GCIPLT directly reflects RGC layer thickness in the macula where the RGC density is high (Curcio and Allen 1990). In addition, the

coefficient of variation of the peripapillary RNFLT (9.1%) is slightly greater than the m-GCIPLT (7.1%) (Calculated from data of Mwanza et al) (Mwanza et al. 2012) and peripapillary RNFLT can be confounded by blood vessels, glial tissue or edema. Furthermore, various studies have reported early macular damage in glaucoma (Hood et al. 2011; Raza et al. 2011; Hood et al. 2013). Therefore, a combination of these factors could be the reason for the trend toward better sensitivity of m-GCIPLT than the g-RNFLT.

Studies using the focal macular ERG have reported regional differences in the PhNR amplitude (larger in superior and nasal macula than elsewhere) (Kurimoto et al. 2009) and also showed that the focal PhNR was better than the full field in detecting functional changes in glaucoma (Machida et al. 2011). However, in the present study, we did not see naso/temporal differences in mfPhNR amplitudes in control eyes (shown in chapter 5, Figure 5-1, to be a supplemental figure in a publication). The reason for this discrepancy could be that Kurimoto et al used a red stimulus flash on a blue rod saturating background, which is reported to be the best stimulus to elicit PhNR response (Rangaswamy et al., 2007), whereas we used a white hexagon in the mfERG. Secondly, the stimuli used in the focal macular ERG studies were hemi circular (15° in diameter) and could separate the superior/ inferior and nasal/ temporal halves distinctively. On the other hand, it was not possible to have distinct hemifield separation in the foveal region with the mfERG stimulus provided by VERIS.

2.4.4 Comparison of the mfERG-F30 with the slow sequence F14 protocol

The motivation for designing the F30 protocol with 19 hexagons, and 5 multifocal flashes was to increase the mfPhNR amplitude to improve dynamic range while preserving some spatial resolution. Previous studies from our lab using the slow sequence F14 protocol and a display of 103 hexagons showed that changes in mfPhNR

amplitude correlated well with the structural changes in inner retina (Luo et al. 2014). However, the mfPhNR-F14 signal was small, and difficult to measure in the peripheral portions of the mfERG array. Additionally the amplitude of the mfPhNR F30-5 in the present studies was larger than that for the F-14 protocol (Figure 2-3 and Chapter 3), and less variable mfPhNR-F30 (CV=9.1%) than the mfPhNR-F14 (CV=14.1%) (shown in Chapter 3 in more detail). In addition, mfPhNR amplitude using the F30-5 protocol was linearly related to the thickness of the local RNFL over the mfERG array (Figures 2-7 B and 2-8).

2.4.5 Time difference between mfPhNR and RNFL changes

Our results indicate a significant difference in the onset of changes between mfPhNR amplitude and thickness of the RNFL in experimental glaucoma. Similar observations were made for PERG amplitude in monkeys with experimental glaucoma where there was a reduction in the PERG prior to clinically significant cupping of the ONH (Marx et al. 1986) and in DBA/2J mice where there was a reduction in PERG amplitude before RNFL thinning (Saleh et al. 2007). Other studies using full field and mfERG in experimental models (rat and monkeys) also have reported a reduction in ganglion cell function prior to RNFL thinning (in vivo) and axon loss assessed post mortem in optic nerve sections (Fortune et al. 2004; Fortune et al. 2012). Altogether, these findings suggest that increased IOP alters RGC function at an early stage and RNFLT at a later stage of experimental glaucoma. The time difference for changes in the two measures (mfERG and RNFLT) opens the door for potential therapeutic intervention to preserve RGC structural integrity and restore function. A recovery of RGC function has been shown in recent studies in glaucomatous and OHT patients in which reducing IOP caused a recovery of amplitude in the full field PhNR (Niyadurupola et al. 2013) or PERG (Ventura and Porciatti 2005; Sehi et al. 2010). It will be interesting to look for a

reversal of losses due to lowering IOP both in structure, i.e. MRW and function (mfPhNR) early in glaucoma.

2.5 Conclusions

In this study, we found that the mfERG, and specifically the mfPhNR and temporal mfOPs could be used to detect early functional changes in glaucoma. These functional changes occur concurrently with early changes in the optic nerve head structure, detected by OCT. Therefore, the mfERG along with measures of ONH can be used as early biomarkers to detect changes in glaucoma and to facilitate, and monitor the effects of therapeutic interventions to preserve vision.

CHAPTER 3

Longitudinal evaluation of local functional changes using two slow sequence multifocal electroretinogram protocols: relation of functional changes to structural changes in inner retina and optic nerve head in experimental glaucoma

Contributing authors:

Nimesh B Patel[1], Kevin M Ivers[1], Nripun Sredar[2], Jason Porter[1], Ronald S Harwerth[1], Laura J Frishman[1]

[1]College of Optometry, University of Houston, Texas, USA, [2]Medical College of Wisconsin, Milwaukee, Wisconsin, USA

Abstract

PURPOSE: To evaluate and compare the utility of the slow sequence multifocal electroretinogram (mfERG) protocol using 14 frames (F14) with a protocol using a slower sequence (30 frames) and larger hexagons, in assessing inner retinal functional changes in experimental glaucoma and to compare the functional changes with structural changes in inner retina and optic nerve head (ONH) measured using spectral domain optical coherence tomography (SD OCT).

METHODS: Seven monkeys with unilateral experimental glaucoma were followed longitudinally with functional and structural assessments. Two mfERG protocols were used to assess the photopic negative responses (mfPhNR): (1) F14: mfERG stimulus display of an array of 103 hexagons, m- sequence with 1 focal flash followed by 14 dark frames (F14). (2) F30-5: mfERG display of 19 hexagons, m-sequence with 5 focal flashes followed by 25 dark frames (used in Chapter 2). Structural parameters included the macular ganglion cell inner plexiform thickness (m-GCIPLT), peripapillary retinal nerve fiber layer thickness (RNFLT), minimum rim width (MRW), anterior lamina cribrosa depth (ALCSD). Structural and functional parameters were measured both globally (g) and locally (sector, s; macular, m). Variability and reproducibility of mfPhNR for the two mfERG protocols were calculated for control eyes using coefficient of variation (CV) and intra class correlations (ICC). Structure-function relationships and time points of early change were analyzed (Kaplan-Meir (K-M) survival analysis) in Exp eyes.

RESULTS: In Exp eyes, the mfPhNR-F14 amplitude showed early reductions that were coincident with structural changes in ONH measures but prior to thinning of the RNFL. In control eyes, the CV for the g-mfPhNR-F30 (9.1) was significantly smaller than for the g-mfPhNR-F14 (14.1) (P<0.05, paired t-test). The ICC for both mfPhNRs were greater

than 0.80. Although CVs were different, the time points of the first significant changes in mfPhNR amplitude for the two different mfERG protocols were similar.

CONCLUSIONS: The two mfERG protocols detected functional changes concurrently and at the same early time that structural changes in the ONH were seen, indicating that both slow sequence mfERG protocols can be used as objective functional biomarkers to detect early damage in glaucoma.

3.1 Introduction

The electroretinogram (ERG) is a noninvasive technique for measuring retinal function. The photopic negative response (PhNR) of the full field light-adapted flash ERG reflects retinal ganglion cell (RGC) activity and is found to be sensitive to changes in glaucoma (Viswanathan et al. 1999; Viswanathan et al. 2001; Machida et al. 2008). With the advent of the multifocal electroretinogram (mfERG), it has been possible to record responses to a change in contrast from multiple regions of the retina simultaneously (Sutter 1991; Sutter and Tran 1992; Bearse and Sutter 1996). Typical mfERG arrays consist of 61 or 103 hexagons covering approximately the central 35 degrees of the retina. The contrast of the hexagons is reversed based on a pseudorandom sequence called the m-sequence. Each frame in the m-sequence occurs every 13.3 ms for a 75 Hz CRT monitor. Various studies have used the mfERG to assess functional loss in glaucoma. Hood et al found that the mfERG waveform can be more accurately related to the well-established full field flash ERG components by inserting dark frames after the initial focal flash to slow the m-sequence (Hood et al. 1997). In the initial study, Hood et al, added seven dark frames after the first focal flash and found that the resulting waveform containing an a-wave, b-wave and oscillatory potentials that were similar in appearance to those components in the full field flash ERG. Subsequent studies have identified specific measures in the slow sequence mfERG that change significantly in glaucoma. For instance, a reduction in the multifocal fast oscillatory potentials (mfOPs) and a loss of naso-temporal asymmetry in mfOPs amplitude has been reported in both human glaucoma patients and in a nonhuman primate (macaque) model of experimental glaucoma (Fortune et al. 2003; Rangaswamy et al. 2006; Zhou et al. 2007). More recent studies demonstrated a reduction in the amplitude of the multifocal photopic negative response (mfPhNR) when using the slow sequence protocol in glaucomatous eyes and these functional

abnormalities correlated well with reduction of macular ganglion cell inner plexiform layer thickness (GCIPLT)(Luo et al. 2014).

In addition to functional losses in glaucoma, structural abnormalities also occur and some of these, specifically in the optic nerve head (ONH), occur at a very early stage of glaucoma (Quigley and Addicks 1980a; Quigley et al. 1981; Quigley 1982; Quigley et al. 1982). For example, in the macaque, changes in optic disc topography (mean position of disc, MPD) have been observed immediately after acute increase of intraocular pressure (IOP) (Burgoyne et al. 1994) and recent studies have reported profound deformation of the neural canal, alterations in prelaminar tissue thickness and posterior displacement of LC in eyes enucleated from monkeys with early experimental glaucoma (Downs et al. 2007; Yang et al. 2007a). Furthermore, changes in anterior lamina cribrosa surface depth (ALSCD) and thinning of the neuroretinal rim width (minimum rim width, MRW) was observed at a very early stage of experimental glaucoma in macaques prior to thinning of the retinal nerve fiber layer (RNFL) (Strouthidis et al. 2011). The MRW was found to be sensitive enough to distinguish glaucoma suspects (Patel et al. 2014) and glaucoma patients from normal control subjects (Chauhan et al. 2013). Additionally, changes in lamina pore geometry (assessed with adaptive optics scanning laser ophthalmoscope) (Patel et al. 2014; Ivers et al. 2015) were also observed to occur prior to RNFL thinning in experimental glaucoma in macaque.

Several studies have found that functional changes, documented using the mfERG, also occur prior to the RNFL thinning in glaucoma (Fortune et al. 2012; Fortune et al. 2015). Similar results can be found in studies that used other ERG techniques such as the pattern ERG (PERG) in mice (Saleh et al. 2007). Although these studies indicate that mfERG changes occur early, whether these changes occur as early as the ONH changes in glaucoma has not been fully explored. One recent

longitudinal study of macaque experimental glaucoma reported that mfERG changes occur prior to RNFL changes but later than ONH changes (He et al. 2014). However, this study considered only average (global) changes over the whole mfERG array and average structural changes, and did not consider local changes in individual animals in these measures.

In the previous chapter, a modified slow sequence stimulus was used with 30 frames and 5 initial focal flashes with a display with an array of 19 hexagons. Using that stimulus, the earliest significant change in mfPhNR amplitude was coincident with earliest changes in ONH structure and changes in both measures preceded thinning of RNFL in experimental glaucoma. In the same recording sessions, we also recorded slow sequence mfERGs using the F14 protocol.

The main purpose of this study was to investigate longitudinal changes in inner retinal function using the slow sequence mfERG stimulus (14 interleaved frames after one focal flash, F14) that was used in several previous studies in the lab and to compare functional changes with structural changes in the inner retina (RNFL and GCIPL) and the ONH both locally and globally in experimental glaucoma. In addition, this study aimed to compare outcomes using the F14 protocol with those using the mfERG protocol with 30 frames and five focal flashes (F30-5) that was used in Chapter 2 and to determine whether one of these mfERG protocols is better than the other in detecting glaucomatous damage.

3.2 Methods

3.2.1 Animals and preparation.

mfERGs were recorded from seven adult monkeys *(Macaca mulatta),* 3.3 to 6.3 years of age, *2 females, 5 males* with unilateral experimental glaucoma induced by laser photocoagulation of the trabecular meshwork (Gaasterland and Kupfer 1974;

Quigley and Hohman 1983; Pederson and Gaasterland 1984), These animals were subjects for the experiments described in other chapters of this dissertation and in other studies as well (Patel et al. 2014; Ivers et al. 2015). All animal care and experimental procedures adhered to the ARVO statement for the use of animals in ophthalmic and research and were approved by the Institutional Animal Care and Use Committee of the University of Houston. The animal preparation was similar to that in previously studies, e.g. (Luo et al. 2014), as described in the Methods section of Chapter 2.

3.2.2 Multifocal electroretinogram

Two mfERG protocols were used in almost all recording sessions; (1) A slow sequence protocol with an initial focal flash and followed by 14 dark frames in each m-step (F14), and (2) the slower sequence described in Chapter 2 and below. The first mfERG stimulus consisted of an array of 103 unstretched hexagons (Visual Evoked response imaging system; VERIS 4.1, Electro-Diagnostic imaging, Inc., Redwood City, CA) presented on a standard CRT monitor, and subtended angles of 35º X 34º on the retina at a viewing distance of 46 cm. Each hexagon was flashed based on a pseudorandom m-sequence (Sutter 1991). The luminance of the white hexagons was 200 cd/m^2 (one flash was 2.67 cd.s/m^2) and the black hexagons and surround, 15 cd/m^2 (Figure 3-1 A). The slow sequence protocol consisted of a focal flash followed by 14 dark frames. Each frame was 13.3 ms. With the monitor frame rate of 75 Hz, each m-step was 200 ms in duration (Figure 3-1 B). Two recording epochs were combined using VERIS. The second mfERG stimulus was a slow sequence mfERG protocol that was altered to increase the amplitude of the local responses. It had 30 frames, of which the first 5 frames had focal flashes (F30-5). The stimulus array subtending the same angles

on the retina as the F14 stimulus array consisted of only 19 unstretched hexagons. More details of the stimulus can be found in Chapter 2.

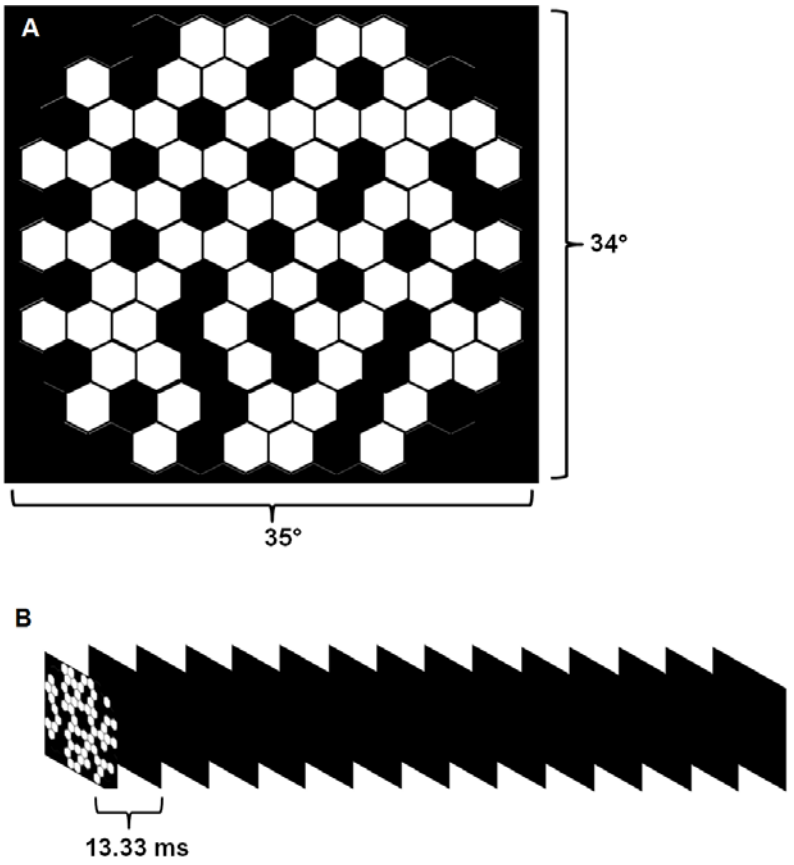

Figure 3-1: (A) mfERG stimulus display with 103 hexagons (B) Slow sequence mfERG F14 protocol – Slow sequence mfERG protocol showing one initial multifocal flash followed by 14 dark frames. A frame occurred every 13.3 ms and the duration of the sequence was 200 ms.

3.2.3 mfERG offline processing and analysis

mfERG signals from both protocols were sampled at 1200 Hz, filtered between 1 and 300 Hz, and analyzed offline using MATLAB (MATLAB; The MathWorks, Natick MA). Multifocal photopic negative responses from both protocols; mfPhNR-F14 (Figure 3-2) and mfPhNR-F30 were obtained after applying a low pass filter (55 Hz) and measured from baseline to the minimum trough occurring after the positive peak. mfPhNRs were measured globally (g-mfPhNR), sectorally with respect to regions of the optic nerve head (s-mfPhNR) and centrally in the macula (m-mfPhNR).

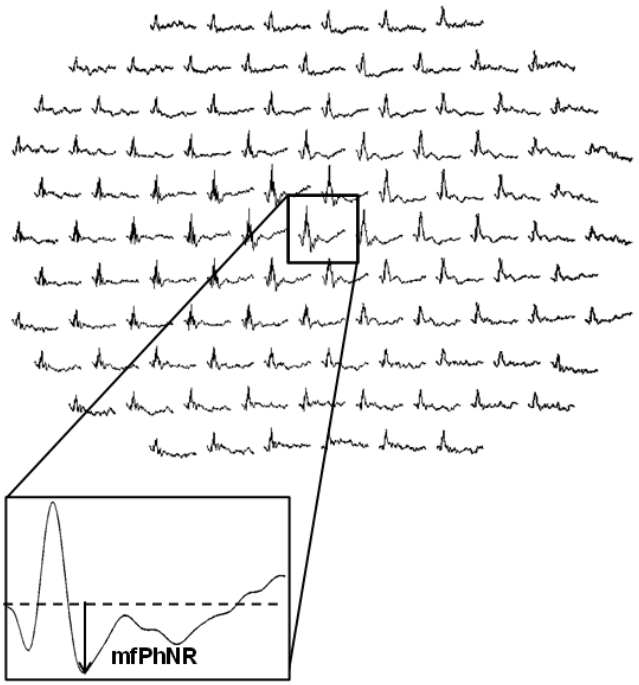

Figure 3-2: mfERG F14 responses from 103 hexagons. Inset: Low pass (55 Hz) filtered mfERG signal showing the mfPhNR. The mfPhNR was measured from the baseline to the trough.

3.2.4 Optical coherence tomography and data analysis

All imaging data were obtained using Spectralis HRA+OCT (Heidelberg Engineering, Germany) as described in Chapter 2. Three scanning protocols were used. 1) A standard 12° peripapillary circular scan (1536 point B scan) centered on the ONH to measure RNFL thickness, 2) a 49 line 20° x 20° raster scan centered on the fovea to measure macular GCIPL thickness (GCIPLT) and 3) 48 radial B-scans were acquired over a 20° area (1024 A-scans per B-scan) to measure MRW and ALCSD. Global (g-RNFLT, g-MRW, ALCSD) and local structural (s-RNFLT, s-MRW, and m-GCIPLT) measures were obtained.

3.2.5 Comparison of mfPhNR-F14 amplitude with RNFLT and MRW

mfPhNRs were quantified both globally and sectorally. For the global mfPhNR (g-mfPhNR), mfERG responses from all 103 hexagons (or 19 hexagons from mfPhNR-F30) were added together and the mfPhNR amplitude was measured from the summed response. Similarly the SD OCT ONH and RNFL parameters were computed globally (g-RNFLT, g-MRW) and sectorally (s-RNFLT and s-MRW) for both eyes of each animal with unilateral experimental glaucoma. For comparing the corresponding regions from the mfERG and the OCT measurements, we used a map designed by Garway-Heath et al (Garway-Heath et al. 2002). Figure 3-3 shows the mfERG stimulus array with 103 hexagons superimposed on the map. Details of comparing the two regions were presented in the previous chapter. Briefly, the sectoral (s-mfPhNR) responses were compared with the corresponding structural measures (s-RNFLT, s-MRW) for each of the ONH sectors studied. Of the six sectors defined for the ONH, only the temporal three sectors (1, 5 and 6) were used for the mfPhNR and structural comparisons because the mfERG stimulus did not cover retinal regions corresponding to the other sectors.

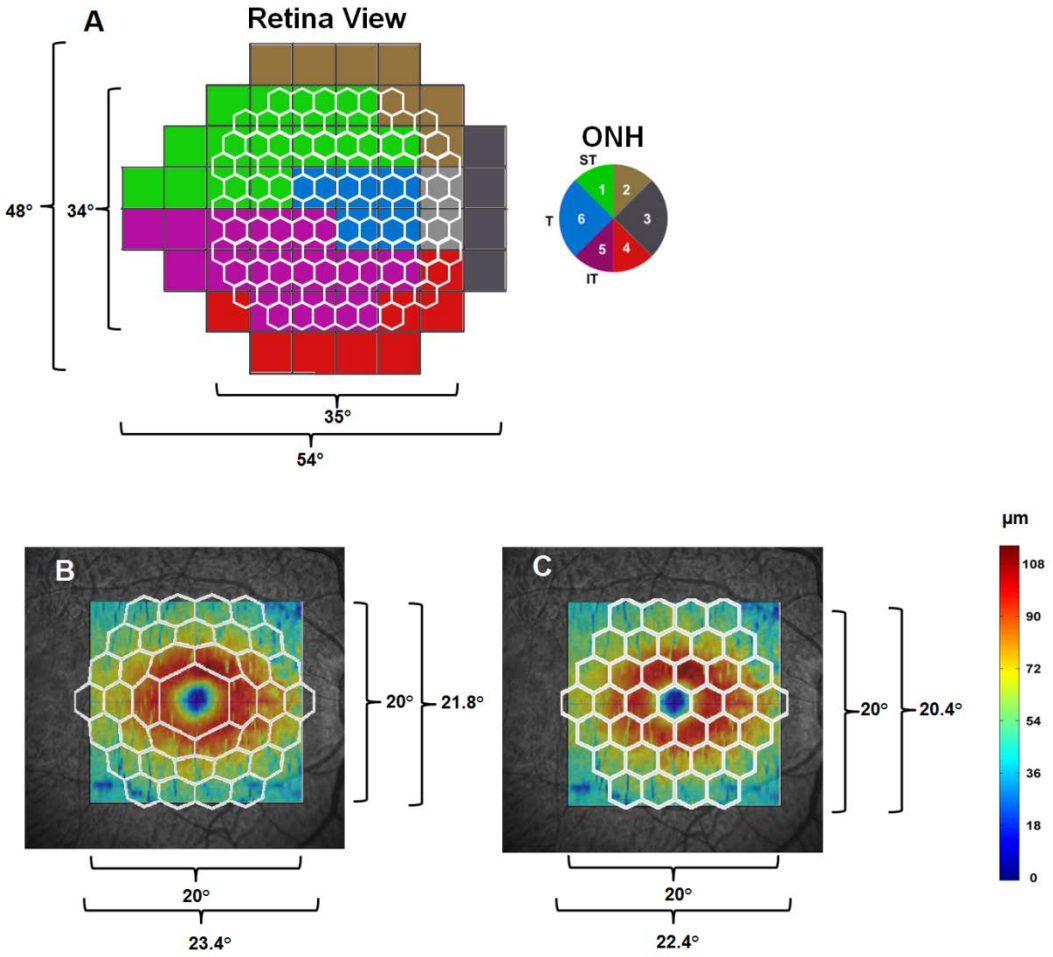

Figure 3-3: Structure-function mapping for mfERG measures and structural parameters (RNFL, MRW and m-GCIPLT) and for the ONH. (A) (Left): Position of mfERG stimulus overlaid on the visual field map (Garway-Heath et al., 2002). The visual field map was flipped to retina view. (Right): ONH map showing projections of axons from corresponding regions of the visual field map. Each color coded region in the visual field map corresponds to an ONH sector. **(B)** Projection of mfERG stimulus array on the GCIPL map. Corrected for RGC displacement, **(C)** Not corrected for RGC displacement.

3.2.6 Comparison of mfPhNR amplitude with macular GCIPLT

For accurate comparison between the mfPhNR and macular GCIPL thickness, we used the RGC displacement model of Drasdo et al for retina in and near the foveal region (Drasdo et al. 2007). The method of comparing these two measures was explained in detail in a previous study (Luo et al. 2014). In brief, the mfERG stimulus was scaled based on the RGC lateral displacement and the hexagon array (central 37 of the 103 hexagons) was then projected on the GCIPL thickness profile map. Figures 3-3 B and C show the mfERG stimulus array superimposed on the GCIPL thickness map with (B) and without (C) RGC displacement. Based on the amount of RGC displacement, RGC projections of the hexagon array were adjusted. Thickness values of the pixels within a hexagon or portion of a hexagon were averaged and compared with the corresponding mfPhNR values.

3.2.7 Biometric measurements and scaling

Axial length, corneal curvature and anterior chamber depth were measured using a non-contact ocular biometer (IOLMaster; Carl Zeiss Meditec, AG, Jena, Germany). These measurements were included in the three surface (anterior corneal curvature, posterior corneal curvature and anterior lens curvature) formula of the model eye and for calculating the lateral magnification of the OCT scans (Ivers et al. 2011; Patel et al. 2011).

3.2.8 Statistical Analysis

The coefficient of variation (CV) for each of the various structural and functional parameters in control eyes was calculated using Excel (Microsoft Excel 2010; Microsoft Corporation, USA). The analysis was limited to four sessions for all animals because

one animal was only tested in four sessions. Reproducibility for the two functional measures (mfPhNR-F14 and mfPhnR-F30) was calculated using the intraclass correlation coefficient (ICC) (SPSS Statistics Version 20, IBM Corporation, Somers, NY). Linear and nonlinear regression analyses were used to compare structure–function relationships (SigmaPlot 10.0, Systat software Inc, San Jose, CA). Nonlinear fits were supported by Akaike information criteria (AICc) analysis (Burnham and Anderson 2004) (GraphPad Prism version 6.0, GraphPad Software, La Jolla, CA). For the longitudinal analysis, 95% confidence limits of each parameter (mfPhNR, mfOPs, RNFL, MRW and ALCSD) were calculated for the Con eye across all experimental sessions and the percent decrease in each parameter in the Exp eye from the mean of the control eye values was plotted against time. The time of the first significant change in a given parameter was defined as the first time point for which the value of the parameter fell outside the lower (or upper) limit of the 95% confidence interval with subsequent time points also outside the limit. The time points of the first significant change in the various structural and functional measures were assessed for a group of four monkeys (see Chapter 2) using Kaplan-Meir (K-M) survival analysis. Log rank test (χ^2) was performed on the K-M curves to test for significant difference (SPSS Statistics Version 20, IBM Corporation, Somers, NY). An additional repeated measure ANOVA using PROC MIXED and paired t-test in SAS (SAS; SAS Institute, Inc., Cary, NC) were used for the whole set of experimental animals (n=7) to compare the time points of change between global and local structural and functional parameters.

3.3 Results

mfERGs were recorded and OCT measurements were made longitudinally in seven monkeys with unilateral experimental glaucoma.

3.3.1 mfPhNR coefficient of variability (CV) and intraclass coefficient (ICC)

Global and local coefficient of variation (100 X [standard deviation/mean]) for the mfPhNR-F14 and mfPhNR-F30-5 amplitudes in the control eyes from four sessions for the seven monkeys are given in Table 3-1 A and 3-1 B. Table 3-1 A shows that for global measures, CV for g-mfPhNR-F30-5 amplitude (9.1 %) was significantly lower than for g-mfPhNR-F13 amplitude (14.1 %) (P<0.05, paired t-test). Similarly, for local functional parameters in Table 3-1 B, CV for the F30-5 protocol was lower than for the F14 protocol and it was significantly lower in sector 1 (P<0.05, paired t-test).

We also calculated the intraclass coefficient (ICC) for global and local mfPhNR amplitudes (Table 3-2) for the two protocols in the control eyes. Both protocols had an ICC >0.80 and the mfPhNR-F30-5 had a consistently higher ICC than the F14 protocol indicating very good reproducibility.

3.3.2 Reduction of mfPhNR (F14) and mfPhNR (F30-5) amplitude in experimental glaucoma

Reductions in mfPhNR amplitudes (F14 and F30-5) were present in both early and advanced stages of experimental glaucoma. Figure 3-4 shows the mfERG traces from the last experimental session for the two protocols (A, mfERG F14, B, mfERG F30-5) for one animal (OHT-66) and illustrates the reduction in mfPhNR amplitudes in the Exp eye (red) compared to Con eye (blue). Similar results were observed for other animals.

Table 3-1: Comparison of coefficient of variation of global and sectoral mfERGs for the F14 versus the F30-5 protocol.

A. Global Animal ID	Coefficient of variation (CV) (%) (CON)	
	g-mfPhNR-F14	g-mfPhNR-F30-5
OHT- 64	12.2	9.4
OHT- 66	16.3	7.0
OHT- 67	18.3	12.0
OHT- 70	18.6	11.3
OHT- 71	16.1	8.4
OHT- 72	5.1	7.2
OHT- 75	12.1	8.4
Mean (SD)	14.1 (4.7) *	9.1 (2.0)

B. Sectoral Animal ID	Coefficient of variation (CV) (%) (CON)					
	s-mfPhNR-F14			s-mfPhNR-F30-5		
	Sec 1	Sec 5	Sec 6	Sec 1	Sec 5	Sec 6
OHT- 64	7.8	8.5	11.9	8.0	6.8	7.7
OHT- 66	20.4	19.5	7.3	14.4	7.4	13.7
OHT- 67	15.0	16.9	20.5	6.3	6.9	7.2
OHT- 70	9.9	9.0	15.6	9.3	11.4	10.0
OHT- 71	12.0	8.0	9.9	11.0	16.7	15.2
OHT- 72	12.1	11.2	6.3	6.3	4.8	11.1
OHT- 75	16.6	23.4	20.0	7.6	7.6	8.1
Mean (SD)	13.4 (4.3) *	13.8 (6.1)	13.1 (5.8)	9.0 (2.9)	8.8 (4.0)	10.4 (3.1)

* $P<0.05$, paired t-test

Table 3-2: Intraclass coefficient (ICC) for the global and sectoral mfPhNR amplitudes from F14 and F30-5 protocols

Animal ID	ICC (CON)	
	mfPhNR-F14	mfPhNR-F30-5
Global	0.83	0.88
Sector 1	0.85	0.93
Sector 5	0.89	0.93
Sector 6	0.89	0.94

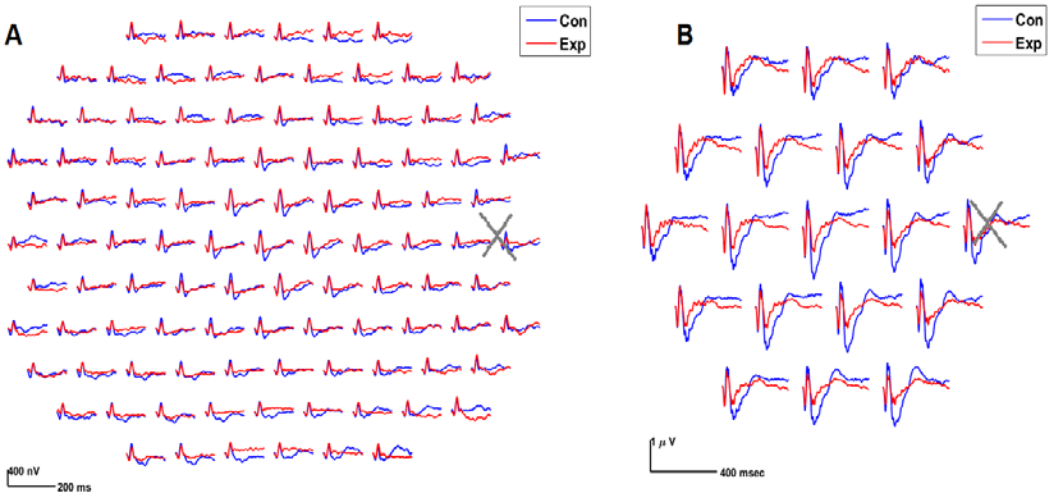

Figure 3-4: Effect of experimental glaucoma on the mfERG for one monkey (OHT-66) with advanced experimental glaucoma (RNFLT= 46 µm). **(A)** mfERG–F14 **(B**) mfERG–F30-5. *Blue line* represents Con eye and *red line* represents Exp eye. Grey cross corresponds to the approximate location of the ONH.

3.3.3 Effect of cumulative IOP on the mfPhNR amplitude

Longitudinal IOP data and the time course of experimental glaucoma for the seven monkeys that we studied were reported in Chapter 2, Table 2.1. The relationships between mfPhNR amplitudes for the two mfERG protocols and cumulative IOP are illustrated in Figure 3-5. For the F14 stimulus, mfPhNR amplitude (Figure 3-5 A) showed an exponential relationship with cumulative IOP. For comparison, in Figure 3-5 B there also was an exponential relationship between mfPhNR-F30-5 and cumulative IOP (from Chapter 2). Both mfPhNR measures showed an early reduction in amplitude relative to the growth of cumulative IOP, and similar reductions were noted in the ONH measures (Chapter 2). The exponential fits were supported by AICc analysis.

3.3.4 Global structure–functional relationship

The relationship between mfERG-F14 components and inner retinal structural measures (GCIPLT and RNFLT) were evaluated in previous studies (Luo et al. 2014). However, the relation between mfPhNR-F14 amplitude and ONH measures was not explored. Figure 3-6 shows the relationship between g-mfPhNR-F14 amplitude and the global structural measures (RNFLT, MRW and ALCSD) over all experimental sessions. G-mfPhNR-F14 amplitude was linearly related to ONH measures, g-MRW and ALCSD (Figure 3-6 A and Figure 3-6 B) whereas the relationship with g-RNFLT was exponential (Figure 3-6 C), as seen for mfPhNR 30-5 in Chapter 2 when all sectors of RNFL were included.

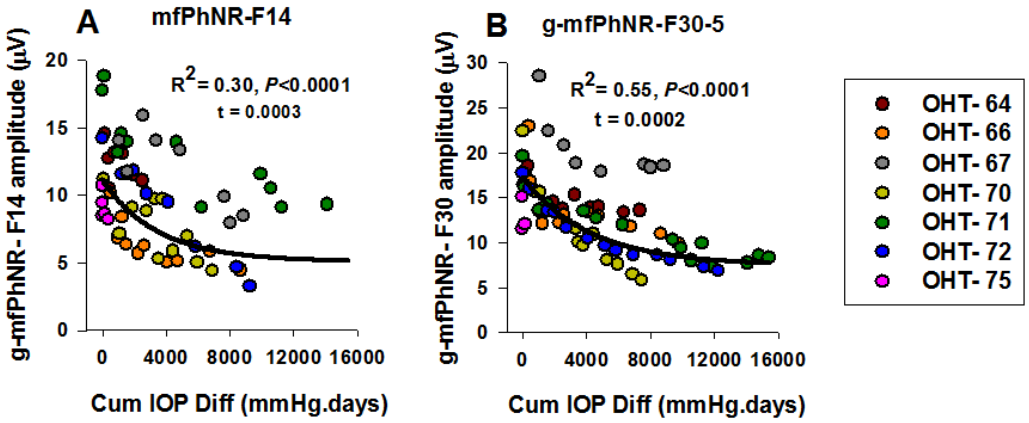

Figure 3-5: Relationship between structural and functional measures and IOP. **(A)** global mfPhNR–F14 amplitude**, (B)** global mfPhNR-F30-5 amplitude*. Each colored symbol represents data from the Exp eye of one monkey for one time point. An exponential decay function was used to describe the effect of IOP insult on g-mfPhNR-F14, g-mfPhNR-F30-5. The exponential fits were supported by AICc analysis. (Difference in AICc for g-mfPhNR-F14: 4.3, and for g=mfPhNR F30-5: 2.0)

* Plots from Chapter 2.

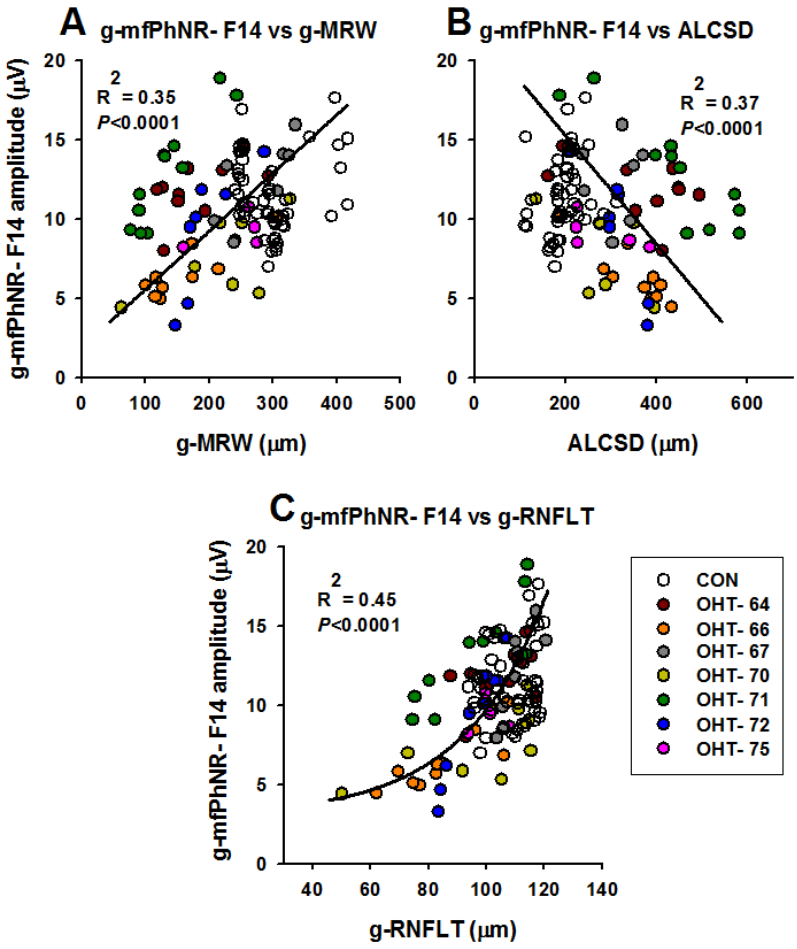

Figure 3-6: Global structure-function relationship in experimental glaucoma. **(A)** Global mfPhNR-F14 amplitude versus global MRW. **(B)** Global mfPhNR-F14 amplitude versus ALCSD. **(C)** Global mfPhNR-F14 amplitude versus global RNFLT. (Difference in AICc for g-mfPhNR-F14 versus g-RNFLT: 2.0). Each colored symbol represents one time point for one monkey. *Open circles* correspond to Con eyes and *filled circles*,to Exp eyes.

3.3.5 Local structure-function relationship

In addition to global structure-function relationships, we also studied local relationships in Con and Exp eyes. As described in the Methods section, we used a map to determine cumulative mfPhNR amplitudes for ONH sectors and compared amplitudes with corresponding structural measures for those sectors. Figure 3-7 shows the relationship between s-mfPhNR, s-RNFLT (A-B) and s-MRW (C-D) in the Con (left) and Exp (right) eyes. In both Con and Exp eyes, local structure (s-MRW and s-RNFLT) and function (s-mfPhNR-F14) were linearly related, as they were for s-mfPhNR-F30 (Chapter 2). We also studied local structure-function relationship between macular GCIPLT and macular mfPhNR-F14 amplitude in Exp eyes (Figure 3-7 E). In order to study this structure-function relationship, we grouped the central 37 hexagons as rings (Center, R1, R2 and R3) as shown in the figure inset. We found that the m-mfPhNR-F14 amplitude was linearly related to m-GCIPLT. Across the different rings, the central hexagon showed more changes in some animals, and had a larger range of mfPhNR amplitudes compared to the rings.

3.3.6 Relationship between g-mfPhNR-F14 and temporal RNFLT

We also examined the relation between g-mfPhNR-F14 and the averaged temporal RNFLT (sector 1, sector 5 and sector 6) of the ONH (Fig 3-6 D). Since the temporal region of ONH received inputs from the RGCs stimulated by the mfERG, it was logical to compare global mfPhNR to that region only. In contrast to the global structure-function relationship, we found that the mfPhNR-F14 amplitudes were linearly related to the temporal RNFLT (R^2=0.28, P<0.0001, Figure 3-8). A similar result was found in Chapter 2 for the mfPhNR-30.

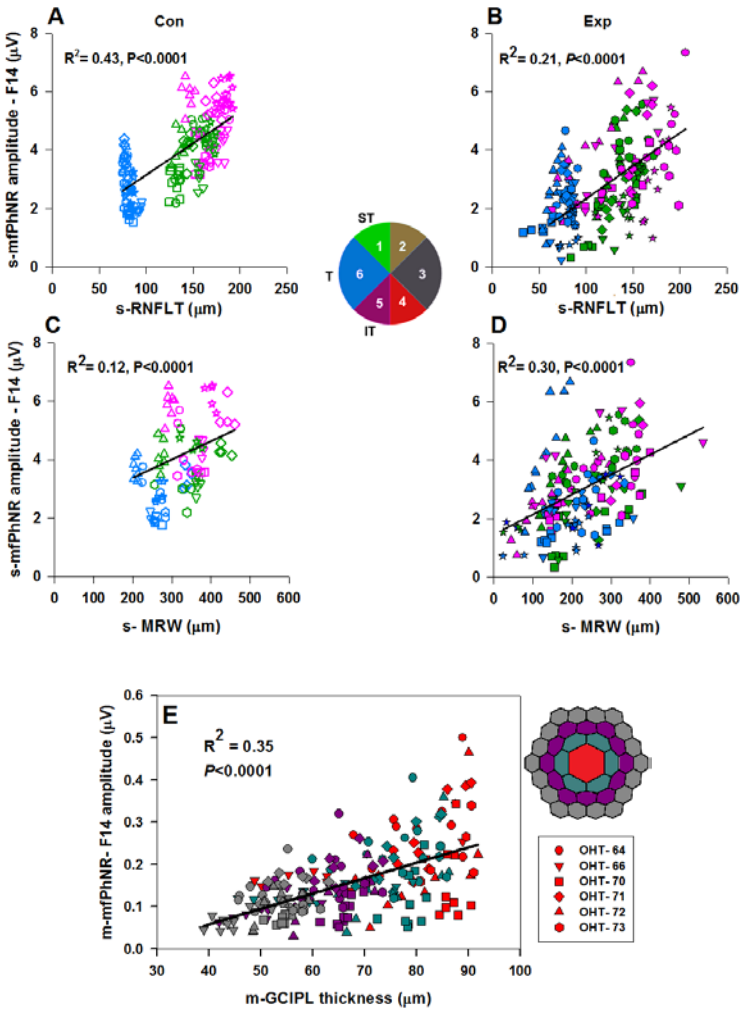

Figure 3-7: Local structure versus mfPhNR-F14 in control and experimental eyes. (A) s-mfPhNR-F14 amplitude as a function of s-RNFLT in control eyes. **(B)** s-mfPhNR-F14 amplitude as a function of s-RNFLT in Exp eyes, (**C)** s-mfPhNR-F14 amplitude as a function of s-MRW in control eyes. **(D)** s-mfPhNR amplitude as a function of s-MRW in Exp eyes. Each symbol corresponds to data from one animal from one session. *Open symbols* correspond to Con eyesand *filled symbols,* to Exp eyes. Colors purple, green and blue correspond to sectors 5, 1 and 6 respectively of the ONH shown in the inset. **(E)** m-mfPhNR-F14 amplitude as a function of m-GCIPLT in Exp eyes. Each symbol corresponds to the data from one animal for one session and each color corresponds to one of the rings shown in the inset.

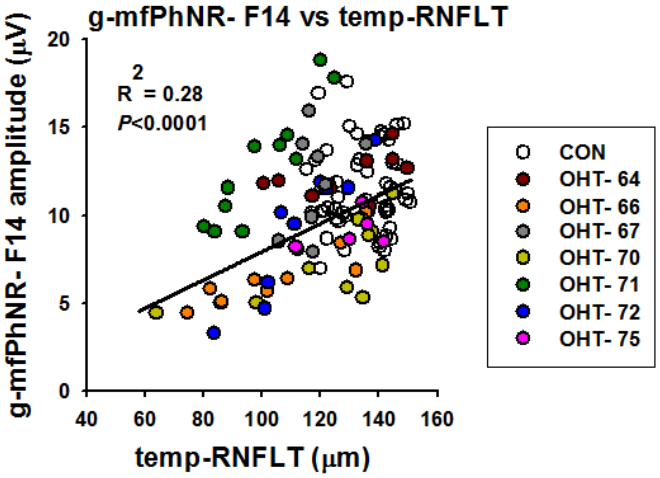

Figure 3-8: Comparison of global mfPhNR-F14 amplitude with the temporal RNFLT. Each colored symbol represents one time point for one monkey. *Open circles* correspond to Con eyes and *filled circles*, to Exp eyes.

3.3.7 Longitudinal analysis of structural and functional changes

To determine the time point of the first significant change in structural and functional measures, we did a longitudinal assessment of changes in Exp eyes. Only four monkeys (OHT-70, OHT-71, OHT-72 and OHT-73) were included in the analysis because these monkeys showed a similar duration to reach end points. The 95% confidence interval (CI) for each parameter was calculated for each Con eye across all experimental sessions. The time point of first significant change was defined as the time point at which the value of a given parameter crossed the lower (or upper for ALCSD) limit of the 95% CI.

3.3.7.1 Global longitudinal analysis

Figure 3-9 shows a longitudinal analysis of global structural (g-RNFLT, g-MRW and ALCSD and functional (mfPhNR-F14) measures in the Exp eye of one monkey. For this monkey (OHT-70), ONH parameters (panels C and D), m-GCIPLT (E) and m-mfPhNR (F) were the first to show a change at 98 days, closely followed by g-mfPhNR-F14 amplitude (A) at 112 days. The g-RNFLT was the last parameter to change at 273 days. The data for all four monkeys are shown in Table 3-3 A. For comparison, the table also shows the time of change in the Exp eye for the mfPhNR amplitude using the F30-5 protocol. The time points of first significant change in amplitude for both mfPhNR amplitudes (F14 and F30) were the same in three monkeys and in one monkey, change in mfPhNR-F30 occurred earlier.

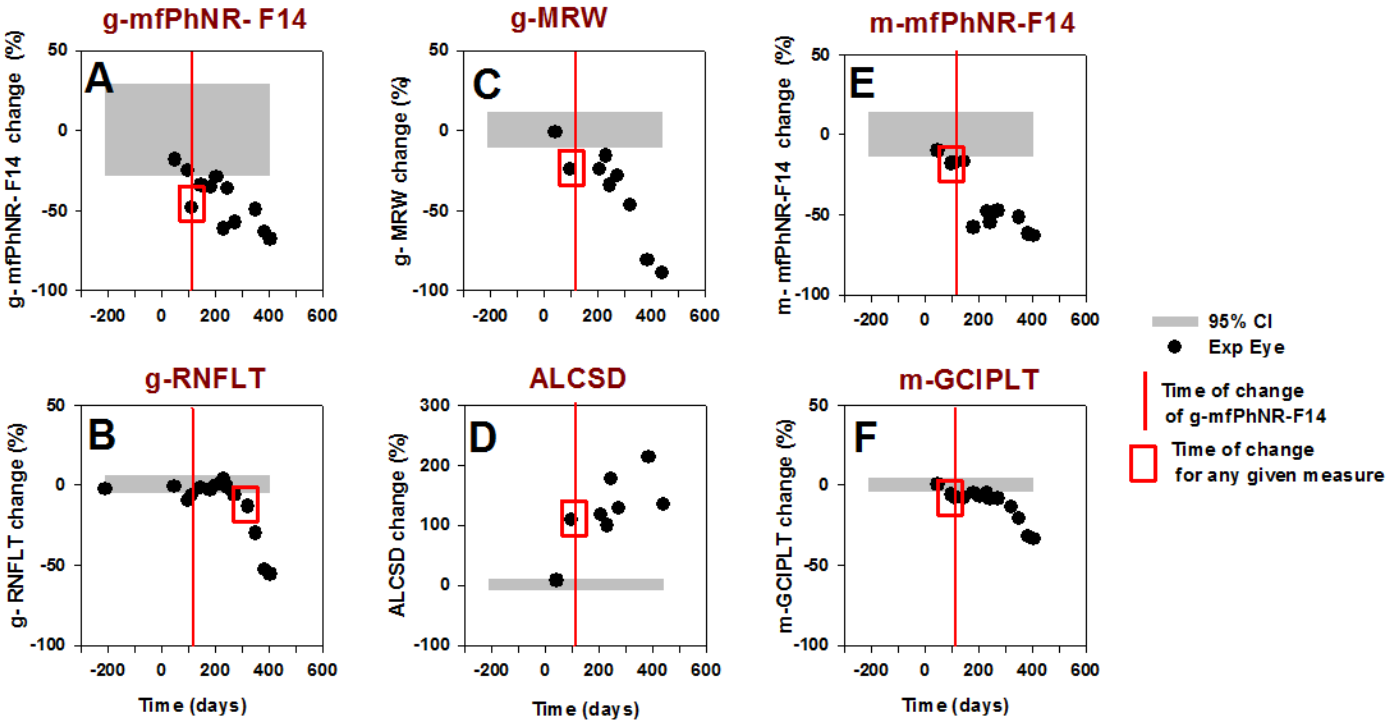

Figure 3-9: Longitudinal analysis of global structure-function measures in experimental glaucoma (OHT-70). (A) Global mfPhNR-F14 amplitude percent change, **(B)** Global RNFLT percent change*, **(C)** Global MRW percent change*, **(D)** ALCSD change*. **(E):** mfPhNR-F14 versus time. **(F)** m-GCIPLT*. *Grey* band represents the normal variability from the Con eye, 95% CI (Con). *Black* symbols represent the percent change in the Exp eye from the mean of the Con eye. Zero time (0) represents the time of the first laser treatment. *Red* vertical line corresponds to the time of first change of g-mfPhNR-F14 amplitude. *Red* squares indicate the time point of first significant change for that measure. * From Chapter 2

Table 3-3: Time point of the first significant change in global and local parameters

A. Global Animal ID	Time point of the first significant change (days)							
	g-mfPhNR-F14	g-mfPhNR-F30-5	m-mfPhNR-F14	m-mfPhNR-F30-5	g-RNFLT	m-GCIPLT	g-MRW	ALCSD
OHT- 70	112	112	98	98	273	98	98	98
OHT- 71	84	84	84	84	105	84	42	42
OHT- 72	119	56	56	56	154	119	42	42
OHT- 75	42	42	42	42	69	49	49	42

B. Local Animal ID	Time point of the first significant change (days)			
	s-mfPhNR-F14	s-mfPhNR-F30-5	s-RNFLT	s-MRW
OHT- 70	98	98	182	98
OHT- 71	42	42	84	42
OHT- 72	56	56	56	42
OHT- 75	42	42	49	49

3.3.7.2 Sectoral longitudinal analysis

Local changes in function (s-mfPhNR-F14) and corresponding structure (s-RNFLT and s-MRW) also were studied over time in Exp eyes, using the percent change from Con eye, as calculated for global measures. Figure 3-10 A-I shows longitudinal changes in local structure and function for the Exp eye of one monkey (OHT-71). In this figure, the top, middle and the bottom panel correspond to longitudinal changes in s-mfPhNR (A-C), s-MRW (D-F) and s-RNFLT (G-I) in the Exp eye. Each color corresponds to a sector of the ONH. In this monkey, s-MRW changed first at 42 days followed by the -mfPhNR and s-RNFLT at 84 days. The time points for changes in all monkeys are shown in Table 3-3 B. Changes in s-mfPhNR coincided with the changes in the MRW in two out of four monkeys and was earlier in one monkey. Change in s-RNFLT coincided with the change in s-mfPhNR in one monkey, but was the last parameter to change in the other three monkeys. In order to study these time points further for statistical significance, a survival analysis was done.

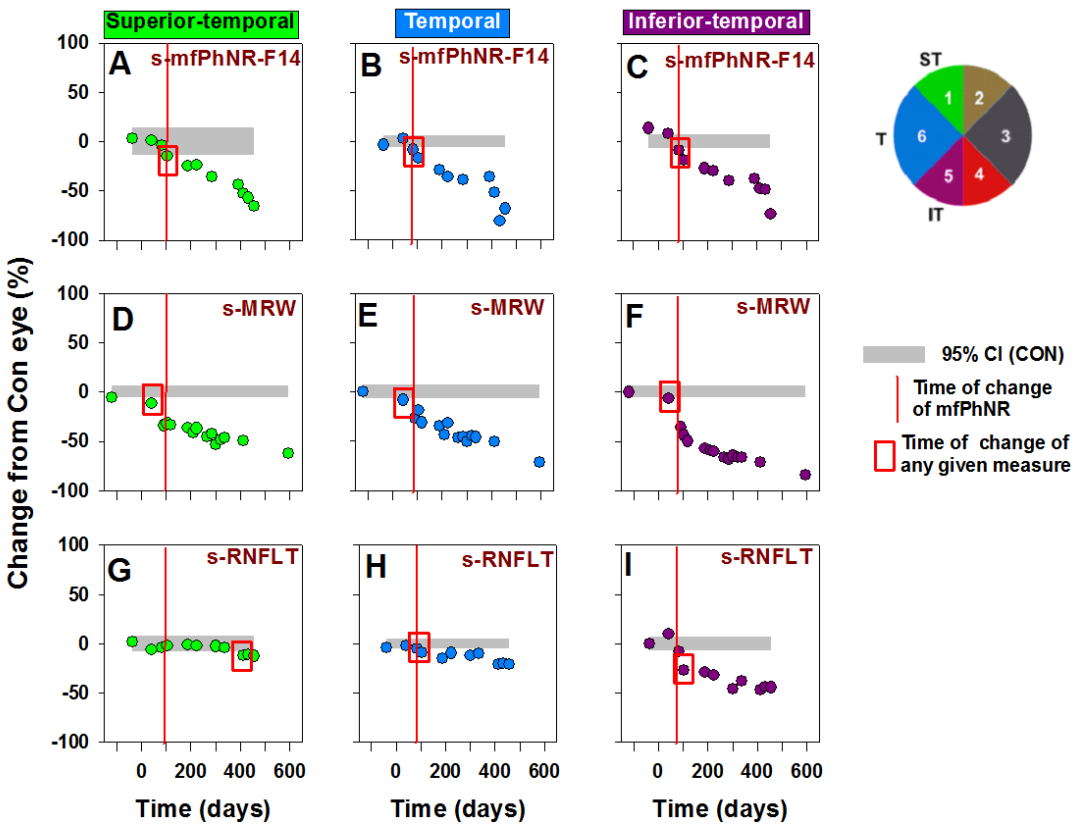

Figure 3-10: Longitudinal analysis of sectoral structure-function measures in experimental glaucoma (OHT- 71). *Top panel (A-C):* Sectoral mfPhNR amplitude percent change, *Middle panel (D-F):* sectoral MRW percent change *, *Bottom panel (G-I):* sectoral RNFLT percent change *, *Inset:* ONH map with color coded sectors. *Grey* band represents the control eye variability (95% CI (Con)) in different sectors. *Green* filled symbols represent percent change in the Exp eye in sector 1, *Purple* filled symbols, in sector 5. *Blue* filled symbols, in sector 6. Time zero, 0 represents time of the first laser treatment. *Red* vertical line corresponds to time of first significant change of s-mfPhNR amplitude. *Red* squares indicate time of first significant change of a particular measure. * From Chapter 2.

3.3.8 Comparisons of time points for the first significant change

To compare the time points for first significant change in structure and function, a survival analysis was done. Figure 3-11 shows Kaplan–Meier (K-M) survival curves for the various structural and functional measures. Log rank test was used to test for statistical significance ($P<0.05$). Consistent with the results in Chapter 2 for the F30-5 protocol, in this study, we did not find a significant difference between K-M survival curves for g-mfPhNR-F14 amplitude and the two ONH parameters. Although g-mfPhNR-F14 showed changes prior to the g-RNFLT (Figure 3-11 A and Figure 3-11 B), the K-M curves based on the group of four monkeys did not show a significant difference ($\chi^2=0.7$, P=0.3). However, if we included the other group of three monkeys, time points of change for the g-mfPhNR-F14 were significantly earlier than for g-RNFLT ($P<0.05$, n=7, repeated measures, PROC MIXED).

When we compared the mfPhNRs from the two protocols, two K-M curves were not significantly different (Figure 3-11 B) although the F30-5 curve looked slightly earlier. In addition, sectoral and macular functional (F14 and F30-5) measures changed at the same time (Figure 3-11 D and 3-11F). To summarize, the overall trend was that functional changes measured by the two mfPhNR protocols occurred concurrently with structural changes in the ONH and preceded g-RNFLT changes in experimental glaucoma.

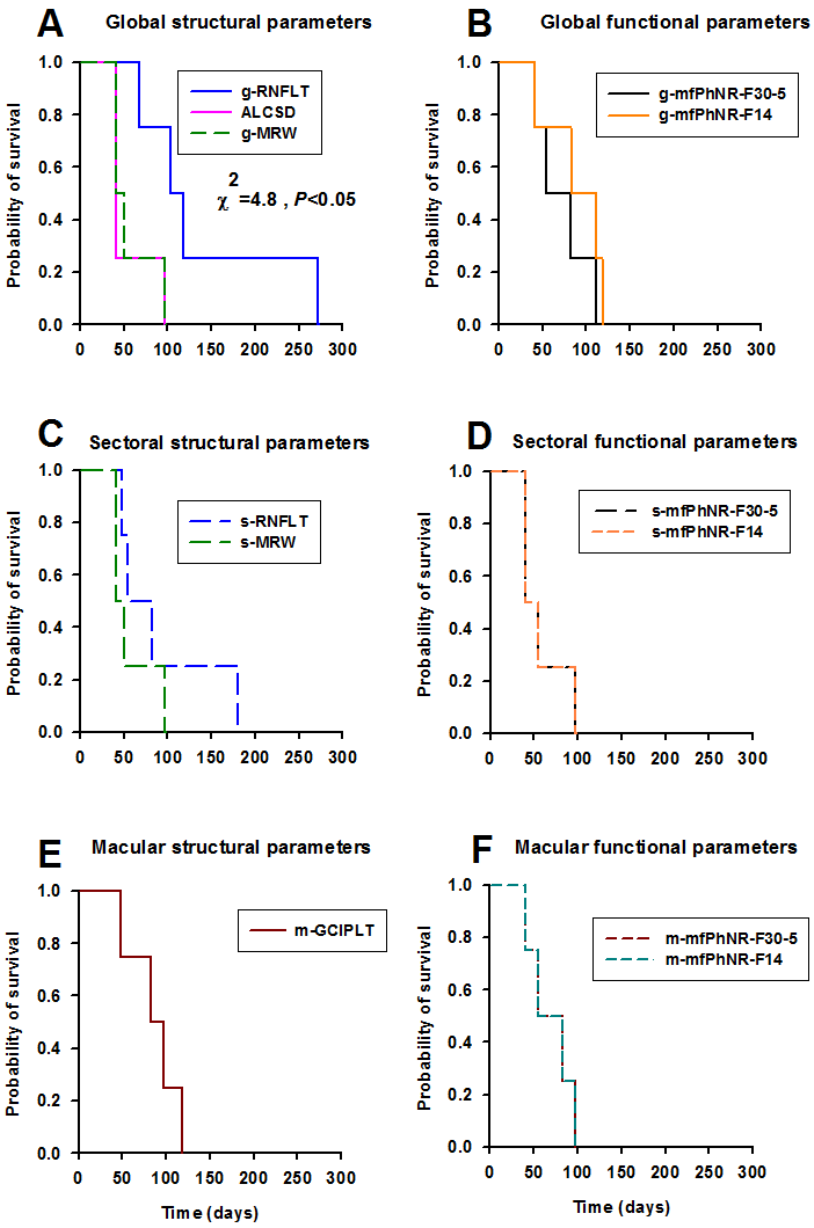

Figure 3-11: Kaplan-Meier survival analysis comparing time points for the first significant change in experimental glaucoma eyes. (A) For global structural parameters (g-RNFLT, g-MRW and ALCSD)*. **(B)** For global functional parameters (g-mfPhNR F30-5 and F14). **(C)** For local structural parameters (s-RNFLT, s-MRW)*. **(D)** For local functional parameters (s-mfPhNR F30-5 and F14). **(E)** For macular structure (m-GCIPLT). **(F)** For macular function (m-mfPhNR F30-5 and F14).* From Chapter 2.

3.4 Discussion

In the present chapter, we analyzed the relationship between the slow sequence mfPhNR-F14 amplitude and structural measures, RNFLT, m-GCIPLT, MRW and ALCSD both globally and locally over time in experimental glaucoma. One of the main findings of this chapter was that, the changes in mfPhNR-F14 amplitude preceded changes in the RNFL and mostly occurred at the same time as changes in the ONH structure in Exp eyes. Another important finding was that, mfPhNR amplitudes from the F14 and F30-5 protocols changed concurrently. In addition to these findings, we also found linear relationships between local functional and structural measures for both mfERG protocols (Figures 3-7 and 3-8).

3.4.1 Early changes in mfPhNR-F14 and ONH in experimental glaucoma

Slow sequence mfERG has been useful for assessing functional changes in glaucoma. Various investigators have used different slow sequence protocols to evaluate components in the mfERG that reflect activity of RGCs (e.g. high frequency component, PhNR) (Rangaswamy et al. 2006; Fortune et al. 2012; He et al. 2014; Luo et al. 2014; Kaneko et al. 2015). Among these, two studies showed that the high frequency component in the slow sequence mfERG showed early glaucomatous changes and these changes occurred prior to RNFL thinning (Fortune et al. 2012; He et al. 2014). Two other studies showed the utility of mfPhNR in studying changes in macular function in experimental glaucoma and in glaucoma patients (Luo et al. 2014; Kaneko et al. 2015). However, none of the previous studies compared the timing of changes in the mfERG with the timing of changes in ONH parameters (MRW and ALCSD) in glaucoma. The finding (similar to the finding for F30-5 used in Chapter 2) that mfPhNR-F14 amplitude shows early reduction prior to RNFL thinning and these changes occur at the

same time as the ONH changes suggests that the slow sequence mfPhNR can used as an early biomarker along with the SD OCT ONH measures in glaucoma.

This study is in agreement with previous studies in showing that changes in deep ONH structures occur prior to RNFL thinning in experimental glaucoma (Strouthidis et al. 2011; Fortune et al. 2013b; He et al. 2014). It is known that stress due to elevated IOP triggers conformational changes resulting in deformation of the ONH and leads to connective tissue remodeling (Bellezza et al. 2000; Bellezza et al. 2003; Burgoyne et al. 2004; Burgoyne et al. 2005; Downs et al. 2007; Yang et al. 2007a; Yang et al. 2007b). Glial cells in the ONH, i.e., astrocytes and lamina cribrosa cells, play an important role in laminar extracellular matrix (ECM) remodeling resulting in damage to axons. IOP induced stress leads to activation of glial cells resulting in degradation of the ECM and these changes could be reflected as deformations of the ONH (Morgan 2000; Hernandez et al. 2008; Crawford Downs et al. 2011; Wallace and O'Brien 2016). Recent studies of experimental glaucoma and of human glaucoma patients have suggested that early changes in the ONH (MRW and ALCSD) could be nonneuronal, whereas, RNFL thinning that happens later is related to axonal loss (Strouthidis et al. 2011; Chauhan et al. 2013).

Early functional changes in inner retina and optic nerve head could also be related to early effects on glia activity. A role for retinal glial cells in glaucomatous damage has been well documented (Carter-Dawson et al. 1998; Wang et al. 2000; Kanamori et al. 2005). The slow time course of the PhNR waveform is thought to reflect a role for potassium currents in glia cells in generating the response (Viswanathan et al. 1999; Raz-Prag et al. 2010; Thompson et al. 2011; Niyadurupola et al. 2013). Disruption of the glial currents could be reflected in a reduction in the amplitude.

3.4.2 F14 and F30-5 mfERG protocols

The CV for mfPhNR amplitude in control eyes was significantly larger for the F14 protocol than for the F30-5 protocol. Although this larger variability did not cause differences in the time of onset of changes in mfPhNR amplitude between the two protocols overall, in one monkey (OHT-72), global mfPhNR-F30-5 showed changes before the F14. This difference was noted in two other monkeys from the earlier experimental glaucoma group as well (OHT- 64 and OHT- 67) (see supplemental Table 3-4). The reason for this could be that, F14 protocol tested 103 hexagons and used a single flash, which produced small amplitude and variable local responses particularly in peripheral hexagons. This variability was reflected in the global response. On the other hand, the F30-5 stimulus tested only 19 regions, with five flashes to amplify responses, so responses in peripheral regions were robust, and the overall variability was less than for the F14 protocol. In the plots relating the macular mfPhNR and the m-GCIPLT the mfPhNR-F14 showed a greater range of amplitudes for the central hexagon (Figure 3-7 E) than the mfPhNR-F30-5 (Figure 3-12 included below). One reason for this could be that the central hexagon (as well as the other hexagons) in the F14 stimulus was smaller and the mfPhNR was therefore more susceptible to contamination by eye movements compared to the F30-5 stimulus that had a bigger central hexagon. In general, larger hexagons for the F30-5 protocol lead to larger responses over the stimulated regions, and fewer delays during recording sessions for realignment of the stimulus due to small eye movements.

3.5 Conclusions

In summary, in this chapter, we found that early structural changes in the ONH were accompanied by early functional changes in inner retina as reflected by mfPhNR-

F14 amplitude and these changes occurred prior to RNFL thinning. mfPhNR amplitudes for the two mfERG protocols (F14 and F30-5) had similar relationships with structural measures and showed a significant change in amplitude in Exp eyes at about the same time. This suggests that either of the mfERG slow sequence protocols could be used as an adjunct biomarker along with the ONH measures to detect early changes in glaucoma. The ease of recording and larger signal for the F30-5 protocol makes it preferable to the F14 protocol.

3.6 Supplemental tables and figures

Table 3-4: Time point of the first significant change in the global functional parameters (all monkeys)

Animal ID	Time point of the first significant change (days)	
	g-mfPhNR-F14	g-mfPhNR-F30-5
OHT-64	267	238
OHT-66	168	168
OHT-67	371	315
OHT-70	112	112
OHT-71	84	84
OHT-72	119	56
OHT-75	42	42

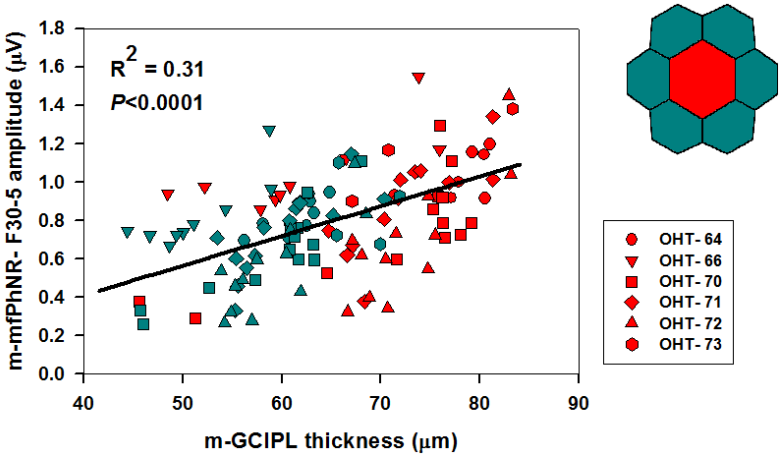

Figure 3-12: m-mfPhNR-F30-5 amplitude as a function of m-GCIPLT. Each symbol corresponds to the data from one animal for one session and each color correspond to the rings shown in the inset.

CHAPTER 4

Longitudinal effects of experimental glaucoma on photopic negative response (PhNR) of the full field flash versus the multifocal electroretinogram: relation to inner retinal and optic nerve head structure

Contributing authors:

Jacqueline J Yi[1], Nimesh B Patel[1], Kevin M Ivers[1], Nripun Sredar[2], Jason Porter[1], Ronald S Harwerth[1], Laura J Frishman[1]

[1]College of Optometry, University of Houston, Texas, United States of America

Abstract

PURPOSE: To compare longitudinal changes in inner retinal function in a macaque model of experimental glaucoma using the photopic negative response (PhNR) of the full field (FF) electroretinogram (ERG) versus the PhNR of the multifocal (mf) ERG, and to compare functional changes with concurrently imaged structural changes in inner retina and optic nerve head (ONH) measured using spectral domain optical coherence tomography (SD OCT).

METHODS: Unilateral experimental glaucoma was induced in seven monkeys by laser photocoagulation of the trabecular meshwork. The FF-PhNR was measured using red flashes on a blue rod saturating background in control (Con) and experimental (Exp) eyes. Multifocal (mf) PhNRs were measured using an array of 19 hexagons (30 frames with initial five frames of multifocal flashes) subtending angles of 35° X 34° on the retina. SD OCT was used to measure retinal nerve fiber layer (RNFL) thickness, macular ganglion cell inner plexiform thickness (m-GCIPLT) and ONH parameters (minimum rim width, MRW; anterior lamina cribrosa depth, ALCSD). Structure-function relations and time points of earliest significant changes were analyzed [Kaplan-Meir (K-M) survival analysis with log rank test] in Exp eyes.

RESULTS: In Exp eyes, both FF-PhNR, and global mfPhNR showed an exponential relationship with RNFLT and m-GCIPLT, and a linear relationship with ONH parameters. No significant difference was found in the time of the first significant change in amplitude of the FF-PhNR, mfPhNR or ONH parameters. However, changes in functional measures (mfPhNR and FF-PhNR) and ONH parameters were significantly earlier than thinning of the RNFL (P<0.05, K-M survival). Additionally, FF-PhNR showed changes significantly earlier than changes in m-GCIPLT (P<0.05, K-M survival).

CONCLUSIONS: Use of the full field ERG and ONH head scans can provide early indications of functional and structural alterations in experimental glaucoma.

4.1 Introduction

The electroretinogram (ERG) is a useful technique for assessing retinal function noninvasively. The application of the ERG to measuring function of retinal ganglion cells (RGCs) was first reported in 1981 in a study using a pattern reversal stimulus to assess the effects of unilateral optic nerve section in the cat (Mafei and Fiorentini 1981). Following this, Marx et al and then Johnson et al showed a reduction in pattern ERG (PERG) amplitudes in nonhuman primate model of experimental glaucoma (Marx et al. 1988; Johnson et al. 1989). Apart from the PERG technique, various other ERG techniques have been used to study inner retinal function. These include full field ERG (scotopic threshold response, STR (Frishman et al. 1996) and photopic negative response, PhNR (Viswanathan et al. 1999)), focal ERG (Miyake et al. 1981; Kondo et al. 2008; Machida et al. 2008) and multifocal ERG (mfERG) (Sutter and Tran 1992; Hood et al. 1999; Frishman et al. 2000; Fortune et al. 2002; Rangaswamy et al. 2006; Luo et al. 2011; Fortune et al. 2012) .

Of the various ERG responses, the PhNR, a negative wave following the b-wave, has advantages in recording RGC function compared to other responses such as the STR which requires complete dark adaptation or the PERG which requires fixation and accurate refractive correction (Viswanathan et al. 1999). The PhNR was found, initially, to be greatly reduced both in experimental glaucoma (Viswanathan et al. 1999) and in human glaucoma patients (Colotto et al. 2000; Viswanathan et al. 2001). In addition, PhNR amplitude was reduced by tetrodotoxin (TTX) which blocks sodium dependent action potentials generated by neurons in inner retina. Several studies have reported the efficacy of the PhNR in detecting inner retinal changes in glaucoma (Machida et al. 2008; North et al. 2010; Huang et al. 2012).

In glaucoma, both functional and structural damage of the RGCs and their axons occurs. The optic nerve head (ONH) is an important anatomic structure through

which the axons of the RGCs pass on the way to the brain. Various studies have suggested that the primary site for glaucomatous injury is at the level of the ONH (Quigley and Addicks 1980a; Quigley et al. 1981; Quigley 1982). Studies using spectral domain optical coherence tomography (SD OCT), have found new structural biomarkers that change early in glaucoma. Strouthidis et al found changes in anterior lamina cribrosa depth (ALCSD) and thinning of the neuroretinal rim at a very early stage of experimental glaucoma prior to RNFL thinning (Strouthidis et al. 2011). Chauhan and coworkers showed that the minimum rim width (MRW) measured from the BM opening (BMO) to the inner limiting membrane (ILM) in humans had greater diagnostic accuracy than RNFLT in detecting glaucomatous changes (Chauhan et al. 2013). Other investigators showed that ONH structure changed early both in experimental glaucoma (He et al. 2014; Patel et al. 2014) and in human glaucoma suspects (Patel et al. 2014).

Recent studies have reported reductions in inner retinal function measured using the mfERG (Fortune et al. 2012); Chapter 2 of this dissertation) and the PERG (Saleh et al. 2007) preceded thinning of RNFL. However, some of the constraints for recording the mfERG or PERG in addition to the need for proper refraction and fixation are that, the signal to noise ratio for inner retinal signals, mf PhNR or mf Oscillatory potentials (OPs) can be low, and mfERG recordings can be time consuming. On the other hand the full field flash ERG has less stringent requirements (Bach and Poloschek 2013) and the signal to noise ratio is relatively large for the full field PhNR with optimal stimulus setting (Rangaswamy et al. 2007).

The main purpose of this study was to compare the utility of the full field PhNR in assessing early inner retinal functional changes in experimental glaucoma with that of the mfPhNR, as well as with structural measures obtained using OCT.

4.2 Methods

4.2.1 Animals and animal preparation

Full field light-adapted electroretinograms (ERGs) and multifocal electroretinograms (mfERGs) were recorded in the same sessions from seven adult monkeys with unilateral experimental glaucoma induced by laser photocoagulation of the trabecular meshwork. All animal care and experimental procedures adhered to ARVO statement for the use of animals in ophthalmic and research and were approved by the Institutional Animal Care Committee of the University of Houston. Animal preparation and procedures were similar to the previous studies, as described in Chapter 2.

4.2.2 ERG experiments

Two ERG protocols were used: (A) Full field light-adapted ERGs were recorded using Ganzfeld stimulator (Espion system; Diagnosys LLC, Lowell, MA). In this study, we used brief red flashes (λ_{max}= 650 nm, 0.044 - 5.68 cd.s/m^2) on a blue (λ_{max}= 462 nm, 10 cd/m^2) rod saturating background. Responses were averaged over 20 trials. A red flash was previously found to be an optimal stimulus for acquiring the photopic negative response (PhNR) in macaques and humans (Rangaswamy et al. 2007). Responses were also recorded in response to brief white flashes (0.044 - 11.36 cd.s/m^2) on a white background (40 cd/m^2), and a comparison of results are presented in a Table 4-2-C in the Results section. (B) A slow sequence mfERG protocol with 30 frames, of which the first five frames had multifocal flashes (F30-5). Detailed description of the stimulus was given in Chapter 2. In brief, the stimulus array consisted of 19 unstretched hexagons (Visual Evoked response imaging system; VERIS 4.1, Electro-Diagnostic imaging, Inc., Redwood City, CA) subtending angles of 35º X 34º on the retina at a viewing distance of 46 cm. The luminance of the white hexagons were 215 cd/m^2 (2.67 cd.s/m^2 for a flash) and the black hexagons were 10 cd/m^2. The surround had a mean luminance of 132

cd/m^2. With a monitor frame rate of 75 Hz, each sequence was 400 ms in duration. Three recording epochs were combined using VERIS.

4.2.3 ERG signal processing and analysis

The full field ERG signals were amplified, filtered (DC to 300 Hz) and sampled at 1000 Hz. Offline analysis of the ERG was done in MATLAB (MATLAB; The MathWorks, Natick MA). The amplitude of the full field photopic negative response (FF- PhNR) was measured as a 5-point average within the maximum trough occurring after the positive b-wave. In order to have similar stimulus conditions for both mfERG and full field ERG settings, we chose a flash strength of 2.84 cd.s/m^2 for the full field ERGs for analysis since the strength was close to that of the mfERG stimulus for a single flash (although we lengthened the mfERG stimulus to increase the flash energy).

The FF-PhNR stimulus response relation in the control eyes was fit with the generalized Naka-Rushton function (Fulton and Rushton 1978; Wang et al. 2012).

$$V = (V_{max} * I^n) / (I^n + I_0^n)$$

where, V is the response amplitude (μV), V_{max} is the maximum amplitude (μV), I is the stimulus strength, I_0 is the level of I at which V is half the full V_{max} value and n is the slope of the function when $I=I_0$. Curve fitting was done using Sigma plot (SigmaPlot 10.0, Systat software Inc, San Jose, CA).

The mfERG signals protocols were sampled at 1200 Hz and filtered between 1 and 300 Hz. The mfERGs were analyzed offline using MATLAB . The multifocal photopic negative response (mfPhNR-F30) was low pass filtered (55 Hz) and measured from baseline to minimum trough occurring after the positive peak. mfPhNRs were measured globally (g-mfPhNR), sectorally (s-mfPhNR) and centrally in the macula (m-mfPhNR). g-mfPhNR was calculated as the sum of mfERG signals from the 19 hexagons, s-mfPhNR was calculated as the cumulative sum of mfERG signals from the retinal regions

corresponding to specific sectors of the ONH and the m-mfPhNR was the sum of the mfERG signals from the macula in the central seven hexagons. Further details can be found in Chapter 2.

4.2.4 Optical coherence tomography and data analysis

All imaging data were obtained using Spectralis HRA+OCT (Heidelberg Engineering, Germany). Three scanning protocols were used. 1) A standard 12° peripapillary circular scan (1536 point B scan) centered on the ONH to measure RNFL thickness, 2) a 49 line 20° x 20° raster scan centered on the fovea to measure macular GCIPLT and 3) 48 radial B- scans were acquired over a 20° area (1024 A-scans per B-scan) to measure MRW and ALCSD. Segmentation and image analysis were described in detail in Chapter 2.

4.2.5 Statistical analysis

The coefficient of variation (CV) for the various structural and functional parameters in control eyes from four experimental sessions for each animal was calculated using Excel (Microsoft Excel 2010; Microsoft Corporation, USA). Reproducibility for the two functional measures (mfPhNR-F30 and FF-PhNR) was calculated using an intraclass correlation coefficient (ICC) SPSS Statistics Version 20, IBM Corporation, Somers, NY). Linear and nonlinear regression analyses were used describe structure-function relationships (SigmaPlot 10.0, Systat software Inc, San Jose, CA). Nonlinear fits, when appropriate, were supported by Akaike information criteria (AICc) analysis (Burnham and Anderson 2004) (GraphPad Prism version 6.0, GraphPad Software, La Jolla, CA For longitudinal analyses, 95% confidence intervals (CI) for each parameter (PhNR, g-RNFLT, m-GCIPLT, g-MRW and ALCSD) were calculated for each of the Con eye across all experimental sessions and the percent decrease of each

parameter in the Exp eye from the mean of the Con eye values in that animals was plotted against time. The first time of significant change for a particular parameter was defined as the first time point for which the amplitude fell outside the limit of the 95% CI with subsequent time points also outside the limit. Times of first significant changes in the various structural and functional measures were assessed using Kaplan-Meir (K-M) survival analysis. Log rank test (χ^2) was performed to test for a statistically significant difference (P<0.05) between the time points for the different parameters (SPSS Statistics Version 20, IBM Corporation, Somers, NY).

4.3 Results

4.3.1 Reduction of FF-PhNR amplitude at an early stage of IOP elevation

Figure 4-1 shows a representative full field photopic ERG trace in response to a stimulus strength flash of 2.84 cd.s/m^2 in a control monkey eye *(Blue, Con)* and in the fellow eye with induced experimental glaucoma (*Red*, *Exp*). PhNR amplitude was measured as a 5-point average within the broad maximum trough of the negative wave, as shown in the figure. The blue trace in the figure illustrates a reduction of FF-PhNR amplitude in the Exp eye. The illustrated reduction occurred at an early time, before there was a change in g-RNFLT. This ERG was recorded 84 days after IOP elevation.

In Figure 4-2, FF-PhNR amplitudes from Con eyes (A) and Exp eyes (B) at the time of first significant change (n=7) (see Methods) were fitted with a generalized Naka-Rushton function. In the Exp eye, amplitudes were reduced for all flash strengths. Parameters of the fits are shown in Table 4-1. In both Con eye and Exp eye (for which the first three flash strengths were skipped because there was no response), the FF-PhNR amplitude increased linearly with increase in stimulus strength before saturating as shown by the slope n (Con: 0.9; Exp: 0.9). Exp eyes showed a reduction of about 60% in V_{max} (Con: 22.4, Exp: 9.0) from Con eyes at the time of first significant change.

There was also reduction in the sensitivity for Exp eyes compared to the Con eyes denoted by I_0 (Con: 0.25, Exp: 0.5) although there was more variability in Exp eyes.

We selected a flash strength of 2.84 cd.s/m^2 for analysis. It was in the middle of the stimulus range that produced maximum responses; no significant difference in the amplitudes was found across the stimuli of 1.42, 2.84 and 5.68 cd.s/m^2 in control eyes (*P* = 0.7, repeated measures ANOVA). Stimuli of about 1.42 and 2.84 cd.s/m^2 were observed to produce saturation of PhNR amplitude previously by Rangaswamy et al (Rangaswamy et al. 2007). The choice of a stimulus that elicited a large amplitude response, gave a large range for measuring changes, and it met the criteria for matching the stimulus conditions in mfERG and full field ERG. We compared the variability of the FF-PhNR and mfPhNR-F30-5 measures from control eyes of the seven animals used in the study for the flash strength of 2.84 cd.s/m^2. Four experimental sessions were chosen randomly for each monkey for calculation of the variability. The coefficient of variation (CV) for FF-PhNR (10.1 %) was comparable to the CV for mfPhNR- F30-5 (9.1 %). The intraclass correlation coefficients (ICC) for FF-PhNR (0.95) and mfPhNR-F30-5 (0.88) were both above 0.80, indicating good reproducibility.

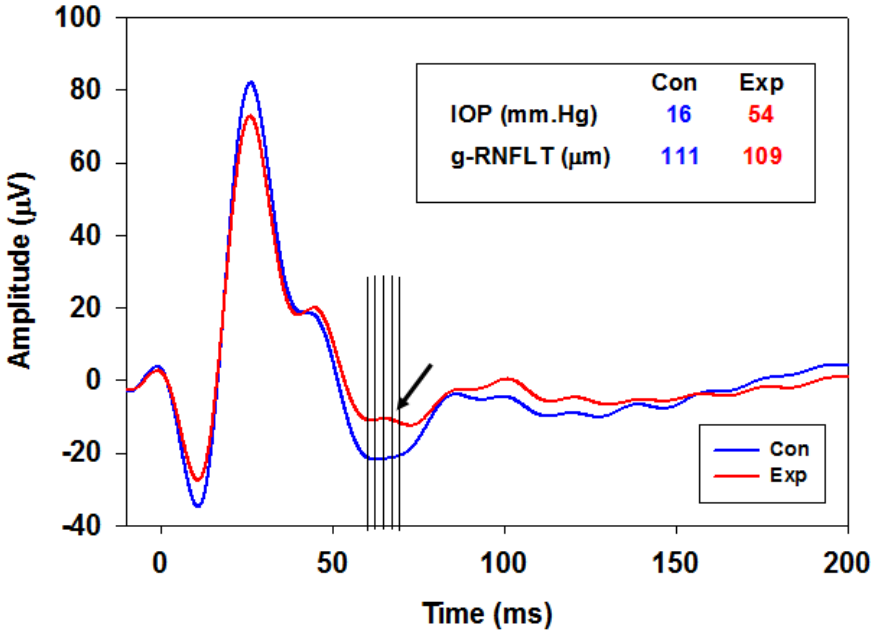

Figure 4-1: ERG traces in response to a 2.84 cd.s/ m^2 flash strength from one monkey (OHT-72) with early unilateral experimental glaucoma. *Blue line* represents Con eye and *red line* represents Exp eye. *Arrow* shows the reduction of PhNR amplitude in the Exp eye. RNFL in the Exp eye was not different from in the control eye, but there was a reduction in PhNR amplitude (see inset). PhNR amplitude was measured as a 5-point (5-ms) average within the window of the maximum trough following the b-wave *(black solid lines)*.

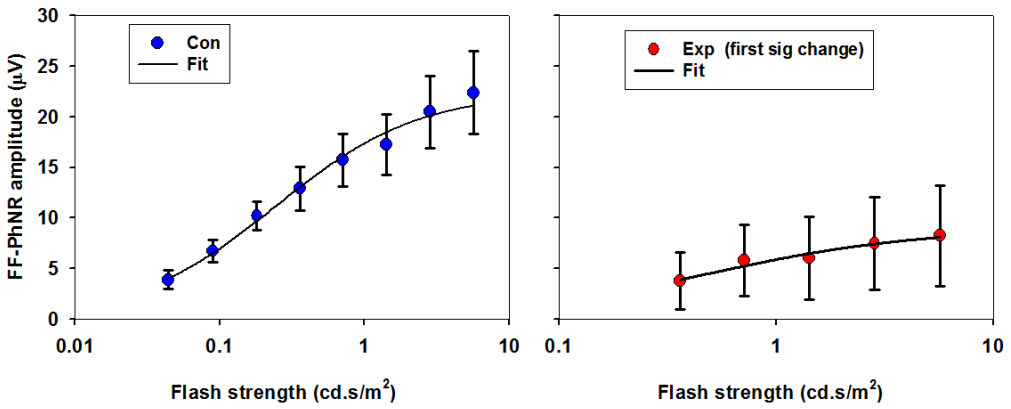

Figure 4-2: Amplitude of FF-PhNR as a function of stimulus strength (n=7). Measurements were made at the time of first significant change **(A)** Control (Con) eyes, **(B)** Experimental (Exp) glaucoma eyes in seven animals with unilateral experimental glaucoma. Error bars represent ±SE. FF-PhNR amplitudes in response to a stimulus of 2.84 cd.s/m^2 were chosen for analysis of structure-function relations.

Table 4-1: Parameters of Naka-Rushton function fits to FF-PhNR amplitudes

Parameters	Con eye (µV)	Exp eye (µV)
V_{max} (µV)	22.4 (1.3)	9.0 (2.0)
I_0 (cd.s/m^2)	0.25 (0.04)	0.5 (0.26)
n	0.9 (0.07)	0.9 (0.4)
R^2	0.99 (0.05)	0.96 (0.09)

Data presented as mean (standard error).

4.3.2 Effect of cumulative IOP on the full field PhNR amplitude

IOP was measured longitudinally in the seven monkeys with unilateral experimental glaucoma (see Table 2.1). In Figure 4-3 A, FF-PhNR amplitudes were plotted as a function of cumulative IOP in Exp eyes. FF-PhNR amplitude showed a nonlinear relationship with cumulative IOP (R^2=0.45, P<0.0001, AICc analysis) and could be described using an exponential decay function ($f=y0+a*e^{(-t*x)}$). For comparison, Figure 4-3 B shows the relationship between g-mfPhNR and cumulative IOP reported in Chapter 2. The g-mfPhNR also was fit with an exponential decay function. Interestingly, on comparing exponential fits, the value of the exponent "t" for FF-PhNR (0.0005) was larger than for g-mfPhNR (0.0002), which indicates that the changes in FF-PhNR amplitude occurred faster than changes mfPhNR amplitude. The exponential fits were supported by AICc analysis.

Non-linear, exponential, relationships between ONH parameters (MRW and ALCSD) and cumulative IOP were also reported in Chapter 2.

4.3.3 Relationship between PhNR and structural measures

Next, we analyzed the relationship between FF-PhNR amplitude and structural measures in eyes with experimental glaucoma. Figure 4-4 describes the relationship between the FF-PhNR amplitude and structural measures over all of the experimental sessions, which ranged from 4 to 8 for the seven monkeys. FF-PhNR amplitude was linearly related to both ONH measures (g-MRW, R^2=0.31, *P*<0.0001, Figure 4-4 A and ALCSD, R^2=0.34, *P*<0.0001, Figure 4-4 B). However, there was a non-linear relationship between FF-PhNR and inner retinal structures (g-RNFLT, R^2= 0.44, *P*<0.0001, Figure 4-4 C, m-GCIPLT, R^2=0.53, *P*<0.0001, Figure 4-4 D). The nonlinear relationships were fitted with an exponential growth function $f=y0+a*e^{(t*x)}$ supported by AICc analysis. The

implication of this finding is that FF-PhNR amplitude showed relatively more reduction initially compared to inner retinal structures and less reduction at later stages

A comparison of relations of global mfPhNR with structural measures (shown in Chapter 2) and FF-PhNR with structural measures (Figure 4-4), showed that both PhNR measures were linearly related to ONH measures and exponentially related to g-RNFLT. A difference was noted only for m-GCIPLT; g-mfPhNR was linearly related to m-GCIPLT while FF-PhNR was exponentially related.

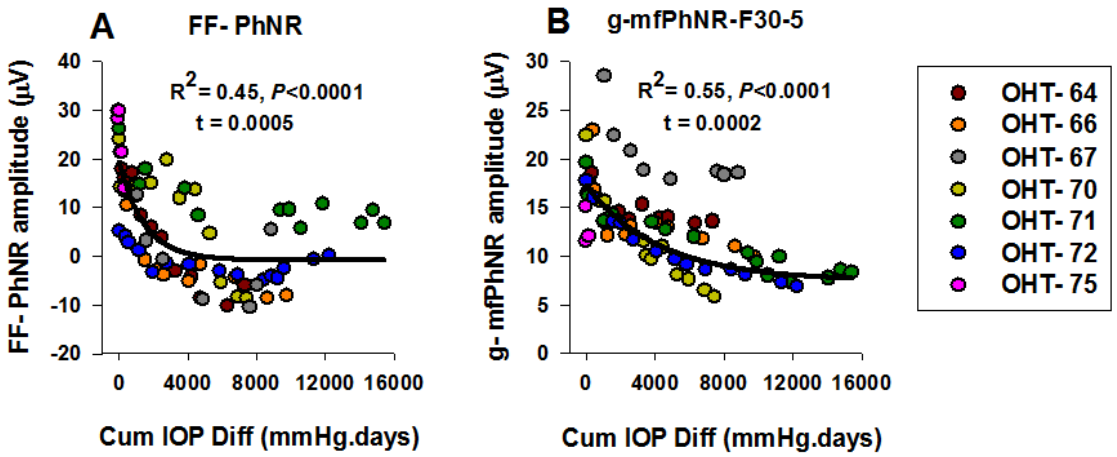

Figure 4-3: Relationship between structural and functional measures and IOP. **(A)** FF-PhNR amplitude, **(B)** global mfPhNR amplitude as a function of cumulative IOP difference. Each colored symbol represents Exp eye data of one monkey. An exponential decay function was used to describe effects of IOP insult on FF-PhNR, g-mfPhNR amplitude. *Difference in AICc; FF-PhNR= 24.2; g-mfPhNR= 2.0*

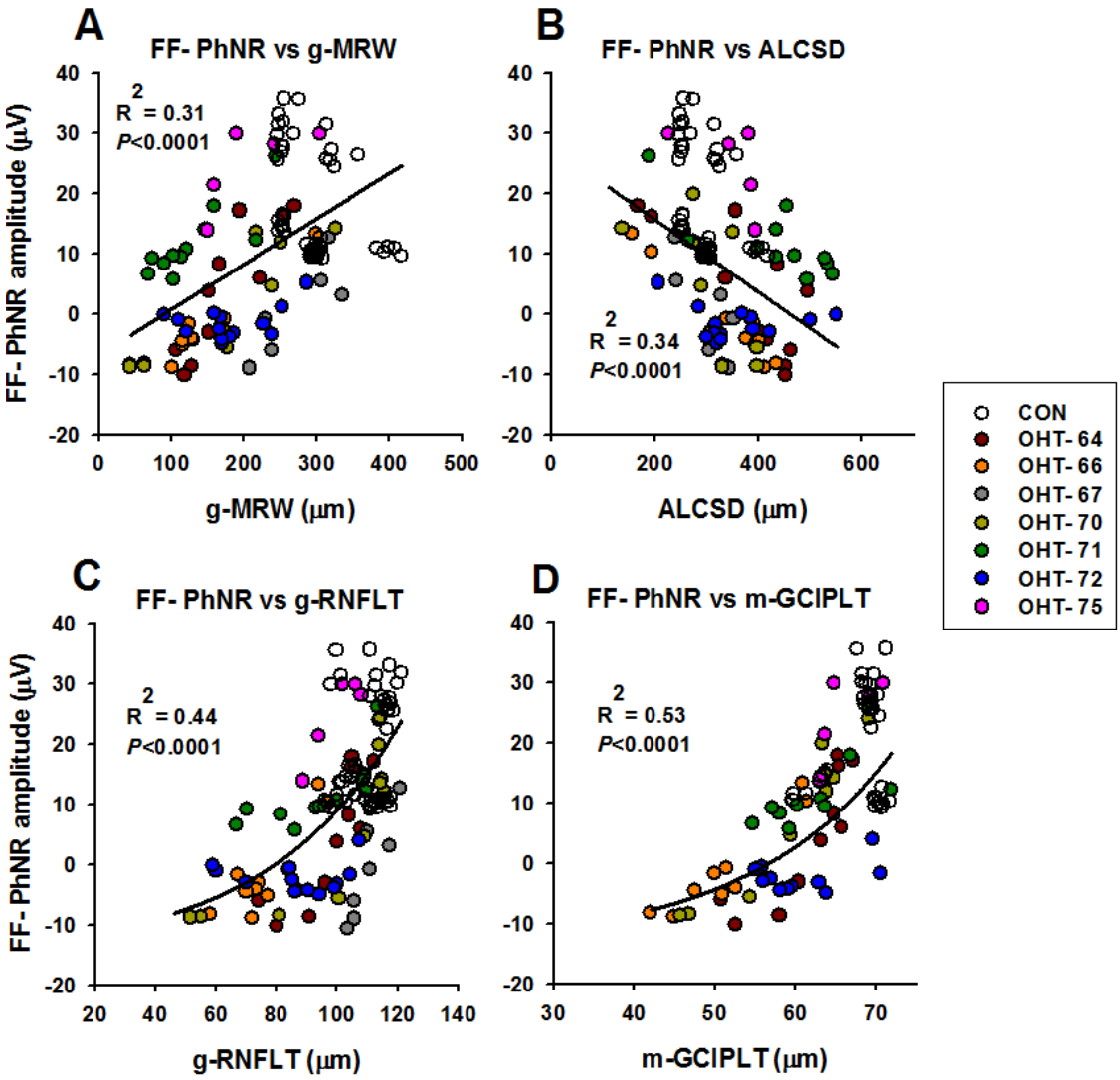

Figure 4-4: Structure-function relationship in experimental glaucoma. (A) Full field PhNR amplitude versus global MRW. **(B)** Full field PhNR amplitude versus ALCSD. **(C)** Full field PhNR amplitude versus global RNFLT. (D) Full field PhNR amplitude versus m-GCIPLT. Each colored symbol represents one time point for one monkey. *Open circles* correspond to Con eyes and *filled circles*, to Exp eyes. *Difference in AICc; g-RNFLT=1.1; m-GCIPLT= 1.5*

4.3.4 Longitudinal analysis of structural and functional measures

Plots of FF-PhNR versus cumulative IOP and the structure-function analysis showed that FF-PhNR amplitude was reduced at early stages of experimental glaucoma. To determine an approximate time of first significant change in structural and functional measures, we did a longitudinal assessment. Four monkeys (OHT-70, OHT-71, OHT-72 and OHT-73) were selected for the main analysis as described in Chapter 2. 95% CI in the Con eye was calculated for all the measures and the first significant change in the Exp eye was defined as the time point at which the amplitude of the FF-PhNR or some other parameter in the Exp eye fell outside the lower limit of the variability and subsequent points were also outside the limits. Figure 4-5 illustrates the time taken for each measures (FF-PhNR, g-mfPhNR, g-MRW, ALCSD, g-RNFLT, m-GCIPLT) to show a change in the Exp eye of one animal (OHT-71). In this monkey the FF-PhNR, g-MRW and ALCSD all changed at 42 days, followed by the g-mfPhNR, m-mfPhNR and m-GCIPLT at 84 days and finally the g-RNFLT changed at 105 days. A similar trend was noted in the other animals. Table 4-2 A shows the time points for changes in global and macular structure and function.

In Chapter 2, we reported time points for changes in local structural parameters and functional parameters for mfERG-F30-5. In the present study, we compared the time point of significant change of FF-PhNR amplitude with the time points of change of local structural and functional parameters for mfERG-F30-5, all of which are shown in Table 4-2 B. A comparison of time points for significant changes in FF-PhNR and the local s-mfPhNR shows that in three out of four monkeys, the FF-PhNR and local s-mfPhNR amplitude changed at the same (early) time and in one monkey, the change in FF-PhNR preceded the change s-mfPhNR amplitude.

Table 4-2 C shows results for analysis of responses to white flashes on a white background versus the result for red flashes on a blue background used for the analysis

throughout this report. The time of first significant change was the same in three of the four animals.

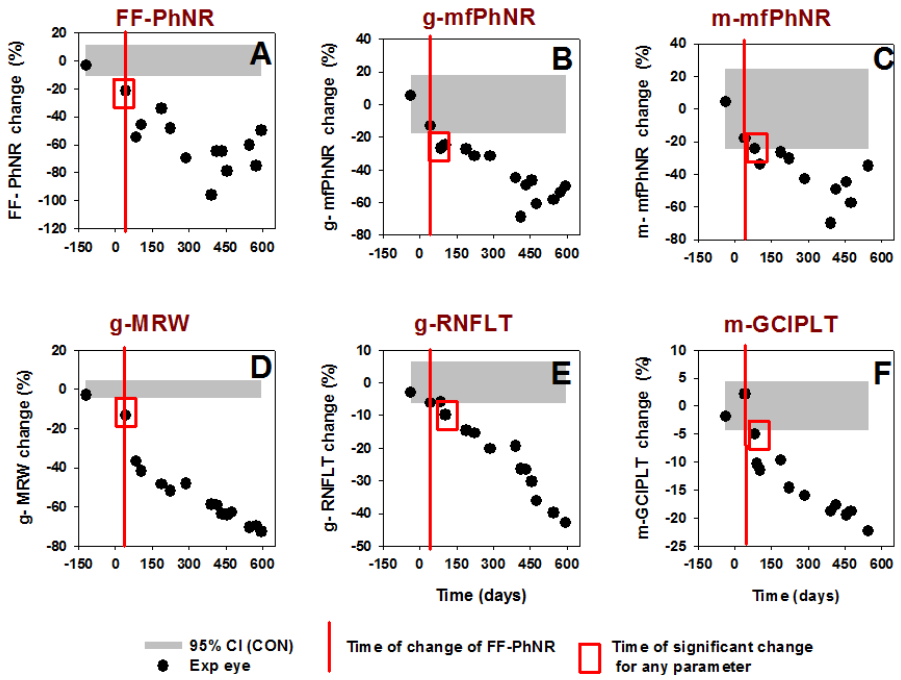

Figure 4-5: Longitudinal analysis of global structural and functional measures in experimental glaucoma (OHT-70). (A) FF-PhNR amplitude percent change, **(B)** g-mfPhNR-F30 percent change*, **(C**) m-mfPhNR-F30 percent change*, (D) Global MRW percent change*, **(E)** Global RNFLT percent change*, **(F)** m-GCIPLT percent change*. *Grey* band represents the variability for Con eye, 95% CI. *Black* symbols represent the percent change in the Exp eye from the mean of the Con eye. Time zero (0) represents the time of the first laser treatment. *Red* vertical line corresponds to the time of first significant change of g-mfPhNR- F30-5 amplitude. *Red* squares indicate the time point of first significant change of that measure. * from chapter 2

Table 4-2: Time point of first significant change in global and local structural and functional parameters

A Animal ID	Time point of the first significant change (days) in global and macular parameters						
	FF-PhNR (R/B)	g-mfPhNR-F30-5	m-mfPhNR-F30-5	m-GCIPLT	g-MRW	ALCSD	g-RNFLT
OHT-70	49	112	98	98	98	98	273
OHT-71	42	84	84	84	42	42	105
OHT-72	56	56	56	119	42	42	154
OHT-75	42	42	42	49	49	42	69

B Animal ID	Time point of the first significant change (days) in local parameters		
	s-mfPhNR-F30-5	s-RNFLT	s-MRW
OHT-70	98	182	98
OHT-71	42	84	42
OHT-72	56	56	42
OHT-75	42	49	49

C Animal ID	Time point of the first significant change (days) in the full field PhNR	
	R/B	W/W
OHT-70	49	49
OHT-71	42	84
OHT-72	56	56
OHT-75	42	42

4.3.5 Comparisons of time points for changes in structural and functional parameters

From the longitudinal analysis, it is clear that FF-PhNR and ONH measures were the earliest parameters to change. In order to compare the approximate time points of change of these measures in all four monkeys, we did a Kaplan-Meier (K-M) survival analysis with log rank test to check for significant difference. Figure 4-5 illustrates time points for changes in the various structural and functional parameters. In Chapter 2, we found that ONH parameters changed in Exp eyes prior to RNFL thinning. This is reproduced in Figure 4-6 A. Figure 4-6 B shows K-M survival curves for FF-PhNR and mfPhNR-F30-5. Although, FF-PhNR amplitude showed changes prior to g-mfPhNR in two out of four monkeys, there was not a significant difference between the two K-M curves ($\chi^2 = 2.5$, $P = 0.1$). Similarly no significant difference was found between the K-M curves for FF-PhNR versus m-mfPhNR ($\chi^2 = 2.5$, $P = 0.1$, Figure 4-6 F) or s-mfPhNR ($\chi^2 = 0.7$, $P = 0.4$, Figure 4-6 D) or ONH measures (g-MRW, $\chi^2 = 0.2$, $P = 0.6$, ALCSD, $\chi^2 = 2.5$, $P = 0.7$, Figure 4-6 A). However, the K-M curve for FF-PhNR amplitude (Figure 4-6 B) was significantly different from that of g-RNFLT ($\chi^2 = 7.5$, $P<0.05$, Figure 4-6 A) and m-GCIPLT ($\chi^2 = 4.5$, $P<0.05$, Figure 4-6 E). This suggests that, changes in the retinal function [FF-PhNR, mfPhNR (global and local)] and changes in ONH (g-MRW and ALCSD) occurred simultaneously and prior to structural changes in inner retina (g-RNFLT and m-GCIPLT).

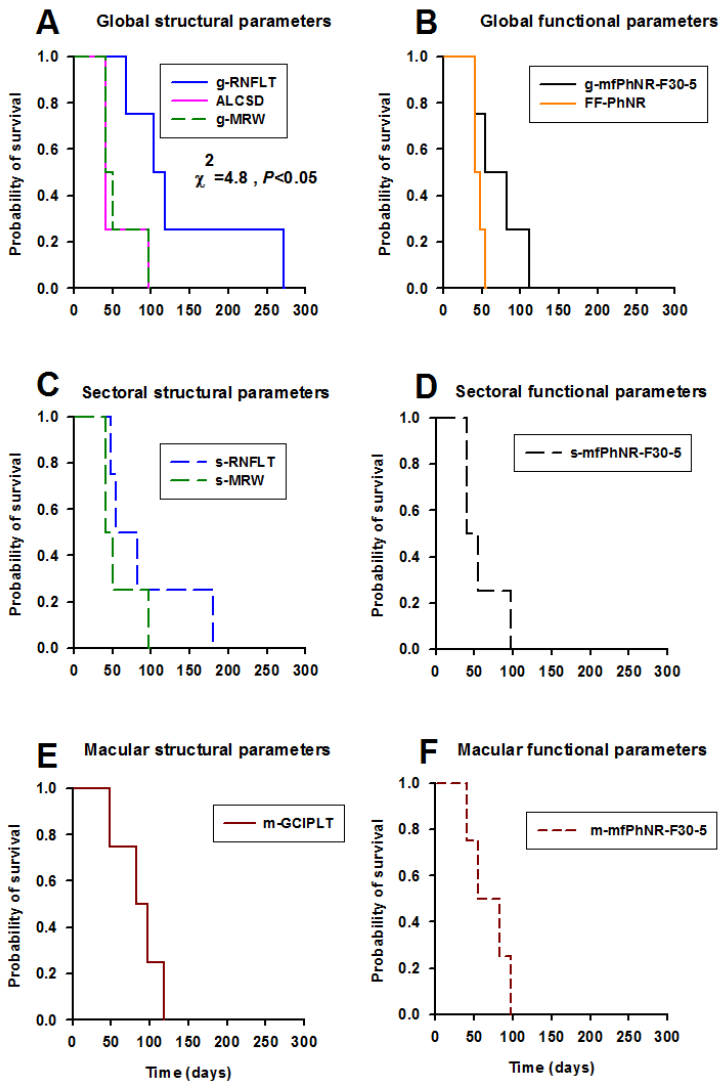

Figure 4-6: Kaplan-Meier survival analysis comparing the time points for the first significant change in the experimental glaucoma eyes. (A) Global structural parameters (g-RNFLT, g-MRW and ALCSD)*. **(B)** Global functional parameters (g-mfPhNR F30-5* and FF-PhNR). **(C)** Local structural parameters (s-RNFLT, s-MRW*). **(D)** Local functional parameters (s-mfPhNR*). **(E)** Macular structure (m-GCIPLT*). **(F)** Macular function (m-mfPhNR-F30-5*).

* From Chapter 2

4.4 Discussion

In the present study, we evaluated the relationship of full field-PhNR amplitude to cumulative IOP and structural measures (inner retina and ONH) in experimental glaucoma over time. We also compared results for FF-PhNR with results for mfPhNR-F30-5 from the same recording sessions in the same group of animals. The main findings of this study were that the FF-PhNR amplitude showed an early reduction with elevated IOP in the Exp eye and this reduction in function occurred concurrently with ONH changes but prior to changes in inner retinal structural measures, g-RNFLT and m-GCIPLT. In the relationship with cumulative IOP, we found that as cumulative IOP increased, the FF-PhNR showed relatively faster changes compared to mfPhNR-F30-5. However, we did not find any significant differences in time points for first significant change in amplitude of FF-PhNR versus the mfPhNR.

4.4.1 Full Field PhNR as an early functional biomarker

The full field PhNR has been reported to reflect the activity of RGC cells and various studies have used it to assess functional changes in glaucoma – for example (Viswanathan et al. 1999; Viswanathan et al. 2000; Drasdo et al. 2001; Viswanathan et al. 2001; Aldebasi et al. 2004; Machida et al. 2008; North et al. 2010; Machida et al. 2011). Of these studies, two showed that PhNR amplitude was reduced in ocular hypertensive subjects compared to control subjects; one using a long duration stimulus (200 ms) (Aldebasi et al. 2004) and the other using a short duration stimulus (<5 ms) (North et al. 2010). These studies highlighted the utility of the FF-PhNR in detecting early changes in inner retinal function. However, none of these studies compared changes in FF-PhNR with newer structural measures for ONH (MRW or ALCSD). Our study, in agreement with and extending these studies, found early loss of FF-PhNR amplitude that coincided with changes in ONH and preceded changes in RNFLT and m-

GCIPLT. A similar finding was reported in Chapter 2 where global mfPhNR amplitudes were reduced prior to RNFL thinning. In addition, the finding that FF-PhNR changes preceded thinning of m-GCIPL in Exp eyes is in agreement with results from Chapter 2 where, we saw a trend for mfPhNR changes to occur prior to m-GCIPLT changes (but not significant) and a previous study by Luo et al, which found that reduction of m-mfPhNR amplitude was proportionally greater than the reduction in thickness of m-GCIPL in experimental glaucoma (Luo et al. 2014). Taken together these results indicate that functional abnormalities in RGCs occur prior to the thinning of RNFL and m-GCIPLT in experimental glaucoma.

Several reasons could account for the early retinal dysfunction indicated by the PhNR. There could be early RGC morphological changes such as dendritic arbor shrinkage or synaptic degeneration prior to cell or axonal loss (Weber et al. 1998; Morgan et al. 2000; Shou et al. 2003; Weber and Harman 2005; Liu et al. 2014). On the other hand, there is evidence that apart from the RGC component in the PhNR, there is a contribution of glial currents to generation of the PhNR (Raz-Prag et al. 2010; Thompson et al. 2011) mediated by K^+ channels in Müller glia. The glial component might be affected early in experimental glaucoma. Furthermore, Niyadurupola et al demonstrated the reversibility of early losses in PhNR amplitude after IOP reduction in glaucoma patients. They also noted a delay in implicit time of the recovered PhNR amplitude and suggested that the prolonged implicit time could be due to remodeling of the glial cells (Niyadurupola et al. 2013).

4.4.2 Glial modulation in the ONH and inner retina

It is now evident that chronically elevated IOP causes conformational changes in connective tissue in the ONH that results in cupping and changes in the rim tissue (Burgoyne et al. 2005; Downs et al. 2007; Downs et al. 2008; Strouthidis et al. 2011).

The finding that retinal functional changes and structural changes in ONH occur concurrently suggests that a common mechanism may be responsible for the changes. One possibility could be that there is early glial dysfunction that affects functional and ONH measures. Two types of macroglial cells are present in the ONH; astrocytes and lamina cribrosa cells. Astrocytes provide support to axons, interface between capillaries and connective tissues, and express glial fibrillary protein (GFAP) (Hernandez et al. 2008). Lamina cribrosa cells, unlike astrocytes are negative for GFAP. Both these glial cells secrete components of the laminar extracellular matrix (ECM) (Hernandez et al. 1988) and play an important role in ECM remodeling due to IOP induced stress which results in axonal damage in glaucoma (Morgan 2000; Hernandez et al. 2008; Wallace and O'Brien 2016). Remodeling in early glaucoma might include thickening of the lamina cribrosa, cupping (Yang et al. 2007a; Yang et al. 2007b; Roberts et al. 2009) and posterior migration of the laminar insertion (Sigal et al. 2010).

Similar to glial modulation in the ONH, activated Müller glia in retina also play a role in RGC damage. Retinal Müller glia play a substantial role in spatial buffering of potassium (K^+) ions, water homeostasis and preventing retinal glutamate toxicity. Disruption of any of these functions could be detrimental to the neurons (Bringmann and Reichenbach 2001; Newman 2004; Bringmann and Wiedemann 2012). In rats with increased IOP, Müller cell activation and increased expression of GFAP was detected very early after IOP elevation (Wang et al. 2000; Kanamori et al. 2005). Therefore a dual glial modulation in ONH and in retina could be a reason for the early changes in structure and function in Exp eyes.

4.4.3 Comparison of full field ERG with focal, multifocal and pattern ERG

In this study, we found that FF- and mfPhNR had similar time points for first significant change in experimental glaucoma (Figure 4-6 B), with the FF-PhNR showing

changes prior to mfPhNR in two out of four monkeys. Previous studies compared use of full field ERG with focal ERG and PERG in glaucoma. Machida et al, showed that focal PhNR was more sensitive than full field PhNR to early and intermediate stages of glaucoma (Machida et al. 2011) although amplitudes of both full field and focal PhNR were significantly lower in early glaucoma patients than in normal subjects. One difference between that study and the current study is that we used a five point window centered within the maximum trough to measure PhNR amplitude in control and Exp eyes rather than a fixed time. This could have helped in repeatable measurement of PhNR amplitude. Besides focal PhNR, other studies using PERG have shown that PhNR and PERG had comparable diagnostic accuracies in early glaucoma patients and OHT subjects (North et al. 2010; Preiser et al. 2013).

4.4.4 Advantages and limitations of full field ERG

The advantages of the full field ERG are that it does not require proper fixation, accurate refraction or clear ocular media (Bach and Poloschek 2013). In contrast, other ERG techniques have at least one of these disadvantages. For instance, PERG and mfERG require refraction and fixation. In the present study, spectral characteristics of the stimulus could have played a role in the ability of the FF-PhNR to detect early changes in glaucoma. The red stimulus on a blue background that we used, was found previously to elicit larger PhNR amplitudes than white stimuli (Rangaswamy et al. 2007), and the mfERG stimulus that we used was white. Although, any of these factors could be a reason for the earlier time points of change for the FF-PhNR in comparison to the mfPhNR in two monkeys (Figure 4-6 B), it was interesting to note that even with the white flashes, we found that the full field PhNR showed early changes compared to the mfPhNR (Table 4-2 B and C). These observations suggest that the earlier time points noted with the full field PhNR (red and white) compared to the mfPhNR is not exclusively

due to the stimulus color differences in the two protocols. Of course. it will be important to support these findings in a larger group of subjects.

Some of the limitations of the full field PhNR are that it is not suited for accurate structure-function comparisons whereas several studies have demonstrated reliable structure-function comparisons with the mfERG measures (Rangaswamy et al. 2006; Luo et al. 2011; Luo et al. 2014). Moreover, local mfPhNR (sectoral and macular) correlated well with the local RNFL and GCIPLT changes in experimental glaucoma in the present study whereas the FF-PhNR showed a great reduction initially and quickly reached a minimum beyond which there were no further changes. This suggests that the dynamic range for the FF-PhNR is short compared to the mfPhNR and it may not be useful for tracking progression in glaucoma. Nevertheless, this study shows that the FF-PhNR can be used as a reliable screening tool to assess early loss of retinal function in glaucomatous eyes besides an added advantage of less labor-intensive recording sessions and analysis of responses compared to the mfERG.

4.5 Conclusions

In summary, in this study we found that FF-PhNR amplitude is reduced prior to thinning of RNFL and m-GCIPLT in experimental glaucoma and these changes in the FF-PhNR coincide with the changes in ONH structure (MRW and ALCSD). FF-PhNR amplitude changed as early in experimental glaucoma as any of the mfPhNR measures, local (including macula) or global. Therefore, the FF-PhNR can be a useful screening tool for detecting early loss of inner retinal function in glaucoma.

CHAPTER 5

General Discussion

5.1 Overview of the findings from the chapters in the dissertation

Glaucoma is a disease that results in structural and functional damage. Early detection of these changes is helpful for early therapeutic intervention to preserve visual function. The studies in this dissertation aimed to investigate functional changes in inner retina and changes in structure of inner retina and optic nerve head longitudinally using two objective techniques: electroretinogram (ERG) and optical coherent tomography (OCT) in a nonhuman primate (macaque monkey) model of experimental glaucoma. In this model, experimental glaucoma was induced unilaterally by elevation of intraocular pressure (IOP) in the experimental eye (Exp); the fellow eye served as a control (Con eye) (e.g. (Luo et al. 2014; Patel et al. 2014)).

Chapter 1, the Introduction, provided an overview of structural and functional changes that are known to take place in glaucoma and the various techniques used for measuring those changes. The chapter provided justification for the selection of the nonhuman primate to study glaucoma, which is because its retina and optic nerve head are similar in structure and function to those in humans. The chapter also described the major underlying mechanisms for glaucomatous damage, as they are currently understood, and accentuated the need for early detection in glaucoma.

Chapter 2 described experiments in the macaque experimental glaucoma model in which inner retinal function was assessed longitudinally using a slow sequence multifocal ERG (mfERG) protocol with 5 initial focal flashes in a 30 frame sequence (F30-5) and a stimulus display consisting of an array of 19 hexagons subtend angles of 35° X 34° on the retina. Structural changes in inner retina and optic nerve head (ONH) were measured concurrently using spectral domain optical coherence tomography (SD OCT). The F30-5 protocol was developed to increase the amplitude of the multifocal photopic negative response (mfPhNR), with the hope of improving ability to see changes in amplitude over those measured using previous other slow sequence protocols, e.g.

(Rangaswamy et al. 2006; Luo et al. 2011; Fortune et al. 2012). In the experimental (Exp) eyes, significant reductions in mfPhNR amplitude and changes in ONH parameters [minimum rim width (MRW) and anterior lamina cribrosa depth (ALCSD)] were detected at an early stage of intraocular pressure (IOP) elevation and prior to thinning of retinal nerve fiber layer (RNFL) and ganglion cell inner plexiform layer (GCIPL). There was a linear relationship between function measured globally over the entire hexagon array and ONH structural parameters, MRW and ALCSD, as the parameters changed, but a nonlinear relationship with the global RNFL. Local changes in structure and function preceded global changes, and mfPhNR amplitude showed a linear relationship with local retinal structure (s-RNFLT and temporal RNFLT) in Con and Exp eyes. These findings suggest that the mfPhNR-F30 can be used as a functional biomarker in early detection and to track changes in glaucoma.

In Chapter 3, the experiments returned to a previously used slow sequence mfERG protocol with one focal flash followed by 14 dark frames (F14) and 103 hexagons (Rangaswamy et al. 2006; Luo et al. 2014) to compare the time course of functional changes with changes in ONH structural changes in Exp eyes, which had not been done before. Additionally, the variability of mfPhNR amplitude using the F14, the F30-5 protocols, and the relative time points of changes in mfPhNR amplitude for the two protocols were compared. The reason behind this comparison was that mfPhNR amplitudes elicited using the F14 103 hexagon array were known to be small, particularly outside of the macula (Luo et al. 2014). With the F30-5 protocol, we had wanted to preserve some regional resolution, but to improve signal to noise by using more focal flashes within the integration time of the mfPhNR and a reduced number of larger hexagons Variability in the mfPhNR-F14 (CV-14.1) indeed was greater than the mfPhNR-F30-5 (CV-9.1). However, despite the larger CV, mfPhNR-F14 amplitude changes, like those for the mfPhNR-30-5 changes in Chapter 2, occurred at the same

time as the ONH structural changes and prior to the RNFL thinning. No significant change was noticed in the time points for significant reduction of mfPhNR amplitude between the two protocols.

In the final experiment described in Chapter 4, we used the more conventional light adapted full field flash ERG to assess the ability of the PhNR to detect early functional damage. The full field PhNR is known to be a useful marker for inner retinal function (Viswanathan et al. 2001). However, its capacity to detect early changes relative to structural changes has not been fully explored. In this study we found that full field PhNR (FF-PhNR), like mfPhNR from the two mfERG protocols, detected early changes in Exp eyes that occurred simultaneously with changes in ONH parameters and significantly prior to thinning of RNFL. On the other hand, no significant difference was observed between the time point for first significant change of the full field PhNR, mfPhNR-F30-5 (and hence mfPhNR-F14) and ONH measures. With the advantage of not requiring proper fixation or accurate refractive correction or a clear ocular media, the FF-PhNR remains a well-suited functional screening tool for detecting early changes in glaucoma. However, in order to do accurate structure-function comparisons the mfPhNR is a better candidate.

5.2 Origin of multifocal photopic negative response (mfPhNR)

Our findings are consistent with previous studies suggesting that the PhNR arises from spiking activity of retinal ganglion cells (or other inner retinal neurons). First, in Chapter 2, we showed that the mfPhNR was reduced in Exp eyes with elevated IOP and after administration of intravitreal tetrodotoxin (TTX). TTX blocks the voltage gated sodium channels in the inner retina (Bloomfield 1996; Stafford and Dacey 1997). Previous studies have shown that the full field PhNR (FF-PhNR) is sensitive to TTX (Viswanathan et al. 1999; Viswanathan et al. 2000) and reduced in glaucoma

(Viswanathan et al. 2001). The finding that both the mfPhNR and FF-PhNR are sensitive to TTX and IOP elevation suggests that they share a common origin in the inner retina. The major spiking neurons in inner retina are retinal ganglion cells (RGCs) albeit some amacrine cells and inner plexiform cells also generate action potentials. Secondly, the residual mfPhNR after TTX blockade suggests some non-spiking contribution to the response as well. These could be the local excitatory postsynaptic potentials in the RGCs or responses of other inner retinal neurons that cause release of potassium (K^+) ions in the extracellular space.

Thirdly, K^+ ion buffering by Müller glia (or optic nerve head astrocytes) is likely to mediate the PhNR signal. In this study, the latencies of mfPhNR and FF-PhNR were both greater than 65 ms (mfPhNR-F30-5: 70.8 ± 2.8 ms; FF-PhNR: 68.7 ± 3.6 ms) which are longer than light adapted ganglion cell responses in monkeys (Purpura et al. 1990). This slow time course of the mfPhNR and FF-PhNR suggests a glial mediation of these signals (Viswanathan et al. 1999). Previous studies have shown the contribution of K^+ buffering in the Müller glia to generation of the scotopic threshold response (STR) in cat retina (Frishman and Steinberg 1989b, a), and more recently, evidence of the glial mediation to the PhNR was demonstrated when disruption of inwardly rectifying Kir 4.1 channels Müller glia end feet resulted in reduced PhNR amplitude in rat retina (Raz-Prag et al. 2010). Similarly, in humans, mutation of Kir 4.1 channel (KCNJ10) resulted in reduced PhNR amplitudes in humans (Thompson et al. 2011).

5.3 mfOPs and mfPhNR- Effects of tetrodotoxin and experimental glaucoma

Another component of the ERG that has its origin in the inner retina is the oscillatory potentials (OPs). Various studies have shown the possible origins of OPs in the inner plexiform layer which has the processes of inner neurons (Ogden 1973) and perhaps from the amacrine cells (Wachtmeister and Dowling 1978). Other studies have

shown that membrane damage to RGC dendrites can reduce OPs (Vaegan and Millar 1994). OPs were demonstrated in the mfERG using a short slow sequence technique in humans by Wu and Sutter (Wu and Sutter 1995). Later, the slow sequence was refined by interleaving 14 dark frames after the first focal flash in the m-sequence (Rangaswamy et al. 2003; Rangaswamy et al. 2006; Zhou et al. 2007) and recordings were made of OPs in the macaque mfERG. These studies found a naso-temporal asymmetry in high frequency (fast) OPs in control eyes that was eliminated by TTX administration (Rangaswamy et al. 2003) or by experimental glaucoma (Rangaswamy et al. 2006). Subsequently, Luo et al showed a similar naso-temporal asymmetry in a low frequency component of mfERG (Luo et al. 2011). Results from our study are consistent with previous studies. Figure 5-1 shows a naso-temporal asymmetry in mfOPs of the mfERG-F30-5 protocol with temporal mfOPs larger in amplitude than nasal mfOPs in Con eyes (P<0.05, paired t-test) (Figure 5-1 A). This asymmetry was eliminated in Exp eyes (Figure 5-1 E) and after TTX (Figure 5-1 C). These results and previous findings from other investigators (Fortune et al. 2002) support the presence of an optic nerve head component (ONHC) in the mfERG OPs, the latency of which is dependent on the distance from the ONH (Sutter and Bearse 1999). When the local retinal component and ONHC of the mfERG are aligned perfectly in phase, larger amplitude OPs are seen in temporal retina while a slight phase misalignment results in the reduction of the amplitude of the OPs in nasal retina (Bearse et al. 2000). In glaucoma and with intravitreal TTX, this naso-temporal asymmetry was reduced primarily by attenuation of temporal mfOPs.

In contrast to mfOPs, we did not see a naso-temporal asymmetry in mfPhNR amplitudes for control eyes (P=0.55, paired t-test, Figure 5-1 B). This result differs from findings in focal ERG studies where focal macular PhNR was larger in superior and nasal macula compared to inferior and temporal regions. The focal studies used a 15°

diameter hemi circular red stimulus on a blue background bisecting the fovea, whereas we used white hexagons that did not have distinct separation in the center. Differences in stimulus characteristics (red stimulus on blue background elicits bigger PhNR response (Rangaswamy et al. 2007) and the testing region could have contributed to the discrepancies. In the current study, the mfPhNR response from the center hexagon was distinctively larger than nasal or temporal responses ($P<0.05$, paired t-test) (Figure 5-1 B). After TTX injection and in experimental glaucoma there was a uniform reduction in mfPhNR amplitude (Figure 5-1 D and Figure 5-1 F).

Changes in the amplitude of temporal mfOPs with increases in cumulative IOP showed an exponential decline in amplitude. On comparing exponential fits to the mfPhNR (Figure 2-5 A) and the mfOPs (Figure 2-5 B) amplitude versus cumulative IOP data, it's interesting to note that the exponential decay curve looks slightly shallower for mfPhNR than for the temp mfOPs. The reason for this could be that the dynamic range of mfPhNR is shorter compared to mfOPs and that mfPhNR has a floor effect (i.e.it saturated beyond about a cum IOP difference of 8000) whereas the temp mfOPs amplitude was still declining. In the longitudinal analysis, we found that s-mfPhNR amplitude was reduced prior to temp mfOPs in 3 out of 4 monkeys. Although this was not statistically significant, there is a possibility that the s-mfPhNR is more sensitive to the initial IOP insult and could be used to study early glaucomatous damage and the less sensitive temporal mfOPs can be used to study progression (Rangaswamy et al. 2006). A similar result was reported in a rat model of experimental glaucoma where OPs showed continuous decline while other ERG parameters such as STR did not (Bayer et al. 2001).

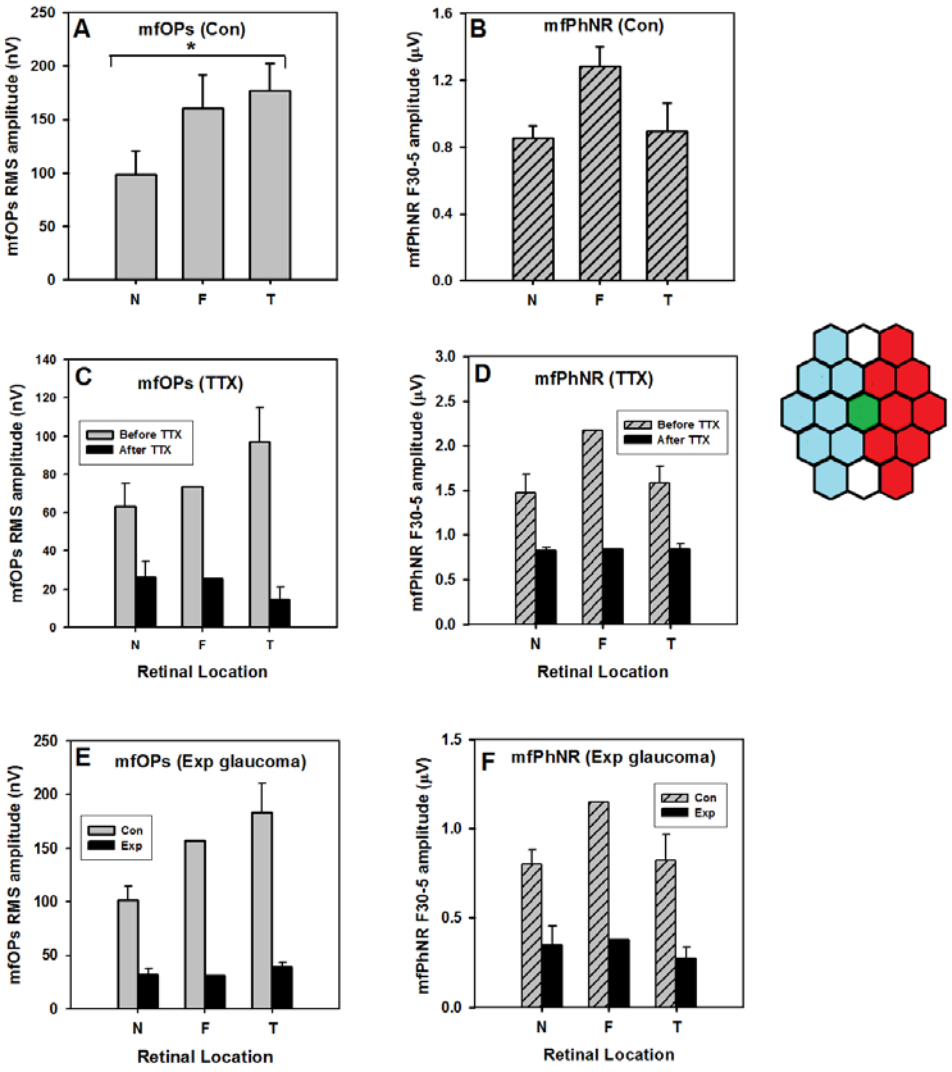

Figure 5-1: Nasal temporal asymmetry (A) Comparison of the average RMS mfOPs for the chevrons in the control eyes (*gray bars)* of all experimental glaucoma monkeys (n=7). **(B)** Comparison of the average mfPhNR for the chevrons in the control eyes (*gray striped bars)* of all monkeys (n=7). mfOPs and mfPhNRs in control eyes were averaged from all experimental sessions (ranging from 4 to 8) in seven monkeys. Average mfOPs and mfPhNR amplitudes were calculated by dividing the summed amplitude over all hexagons in the region (N, F, or T) by the number of hexagons in that region **(C)** Comparison of average RMS mfOPs before (*gray bars)* and after TTX

(*black bars)* in one monkey. **(D)** Comparison of average mfPhNR amplitude before (*gray striped bars)* and after TTX (*black bars)* in one monkey. **(E)** Comparison of average RMS mfOPs in the Con (*gray bars)* and Exp eye (*black bars)* of one monkey (OHT-70) in the last experimental session. **(F)** Comparison of average mfPhNR amplitude in the Con (*gray striped bars)* and Exp eye (*black bars)* of one monkey (OHT-70) in the last experimental session. Error bars represent ± SD. Inset shows the grouping of the hexagons. Asterisks represent significant difference for paired t-test, $P<0.05$.

5.4 Early changes in mfPhNR, FF-PhNR and ONH in experimental glaucoma prior to RNFL thinning

One of the important findings of this dissertation was that mfPhNRs from both mfERG protocols (F30-5 and F14) and full field PhNR showed significant reductions in amplitude in Exp eyes at the same early time that ONH measures were first altered. In addition, these changes were all noted prior to RNFL thinning and more specifically FF-PhNR changes occurred significantly earlier than g-RNFL and m-GCIPL thinning. Figure 5-2 compares longitudinal changes in all structural and functional measures for one monkey (A) and the average in a subset of four monkeys (B). On average, we found that the FF-PhNR changed at 47 ± 7 days whereas the g-RNFLT took the longest time to change 150 ± 80 days. No significant differences were found in the time points for mfPhNR, FF-PhNR and ONH measures. Several studies in nonhuman primates (Strouthidis et al. 2010; He et al. 2014; Patel et al. 2014; Ivers et al. 2015) and humans (Chauhan et al. 2013; Furlanetto et al. 2013; Patel et al. 2014) have found that ONH parameters such as MRW and ALCSD are more sensitive to early changes in glaucoma than RNFLT. Other studies have reported early inner retinal functional changes prior to RNFL thinning (Fortune et al. 2012; He et al. 2014). Our study is the first to show that functional changes in the inner retina as reflected by mfPhNR and FF-PhNR and structural changes in the ONH changes occur concurrently. Fortune et al reported that only the high frequency component (HFC) and not the mfPhNR (or N2 wave) showed early changes in experimental glaucoma (Fortune et al. 2012). However, they used a filter setting between 10 and 300 Hz to capture the signals. In our study, the filter was between 1 and 300 Hz that allowed us to measure mfPhNR signals (which are relatively slow) more effectively. Therefore, the present mfERG settings and analysis of mfPhNR could be reason for the differences in the two studies.

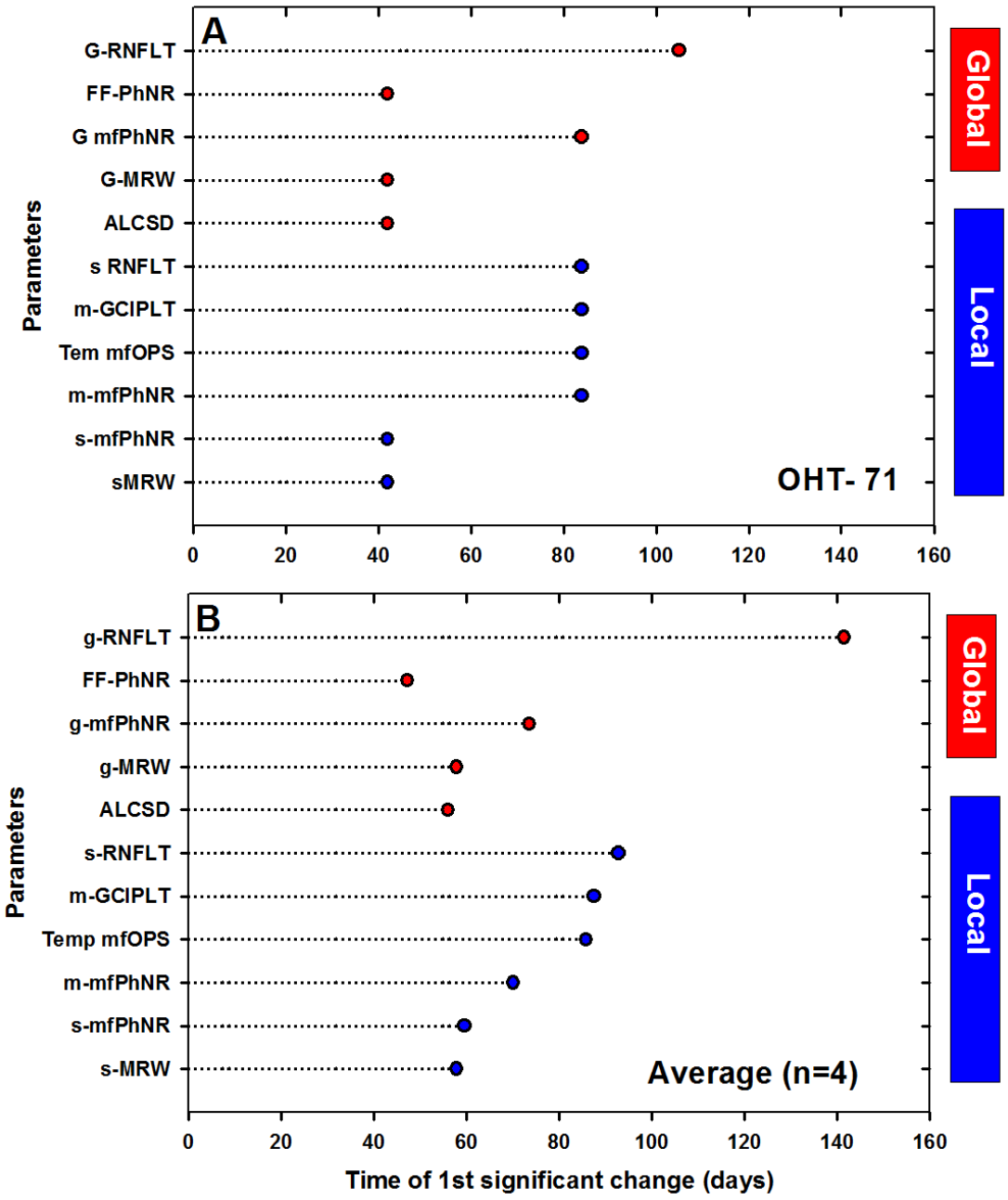

Figure 5-2: Relative time points of significant change in the structural and functional parameters. (A) In one monkey (OHT- 71), **(B)** Average of time points in four monkeys.

5.5 Is there a common perspective for the early changes in inner retinal function and ONH?

Several investigators have reported significant early changes in RGC morphology, synaptic degeneration and RGC arbor shrinkage prior to cell death in macaques and rodents (Morgan et al. 2000; Fu et al. 2009), cell shrinkage in the larger RGCs in cats (Shou et al. 2003). (Weber et al. 1998) noted very early changes in the RGC dendrites (parasol cells) prior to axonal thinning and cell shrinkage in a macaque model of experimental glaucoma. The observed morphological changes in dendritic architecture of RGCs in macaques were associated with reduced visual function (responses to drifting and counter phased gratings) (Weber and Harman 2005).

Apart from early neuronal changes there are also non-neuronal causes, specifically via the glial cells for the glaucomatous damage (Carter-Dawson et al. 1998; Wang et al. 2000; Kanamori et al. 2005). For instance, in glaucoma, glutamate toxicity is one among many factors contributing to RGC death (David et al. 1988). Müller cells play an important role in clearing the glutamate released by the neurons (Riepe and Norenburg 1977). A significant disruption in retinal glutamate uptake and disruption of the glutamine/glutamate cycle was demonstrated in rats with elevated IOP (Moreno et al. 2005). Another study reported reduction in PhNR and pSTR with increased expression of GFAP and heme oxygenase 1(HO1) at a very early stage of elevated pressure with no significant reduction in RGCs (Chrysostomou and Crowston 2013). The above findings imply that the causes for RGC damage could be either direct or could be indirect (glial mediated).

Early changes seen in the ONH are a result of conformational changes due to stress caused by increased IOP (Burgoyne et al. 2005; Downs et al. 2008). One of the consequences of this stress, is the deformation of the laminar tissue, and remodeling of the connective tissue and extracellular matrix (ECM) (Hernandez 1992; Pena et al. 1998;

Bellezza et al. 2003; Downs et al. 2007; Yang et al. 2007a; Yang et al. 2011). Like the Müller glia in the retina, astrocytes and lamina cribrosa cells are the predominant macroglial cells in ONH. Both of these glial cells secrete the components for the laminar extracellular matrix (ECM) (Hernandez et al. 1988) and play an important role in ECM remodeling due to IOP induced stress and resulting in axonal damage in glaucoma (Morgan 2000; Hernandez et al. 2008; Wallace and O'Brien 2016). Activated astrocytes secrete matrix metalloproteinases (MMPs) and degrade the ECM (Hernandez 2000; Agapova et al. 2003). In support of this glial hypothesis, many investigators have suggested that in glaucoma, early changes in the minimum rim width (MRW) could be non-neuronal and changes in the RNFL that occur later could relate to axonal loss (Strouthidis et al. 2011; Chauhan et al. 2013). More evidence from Fortune et al, indicated that the reduction in the RNFL correlated well with the axonal loss compared to the MRW in experimental glaucoma although MRW changes were observed prior to RNFL thinning (Fortune et al. 2016).

Apart from the macroglia, activated microglial cells in retina and ONH also play a crucial role in glaucomatous damage (Neufeld 1999; Yuan and Neufeld 2001). Reactive microglia was found as early as 3 months of age in the DBA/2J mouse model of glaucoma (Bosco et al. 2011) and recent studies reported slowing of RGC death by inhibiting microglial activity in mouse model of glaucoma (Nakazawa et al. 2006; Bosco et al. 2008).

Taken together, these findings suggest that there is early glial cell activation in response to the IOP stress and this could occur at two levels; at the level of retina and in the ONH. Further investigations in this hypothesis could help in designing better therapeutic care for glaucoma.

5.6 ERG as an early functional biomarker in glaucoma diagnosis

Standard automated perimetry (SAP) is the primary functional test used clinically to measure visual sensitivity in glaucoma. However, substantial reduction of RGCs is necessary to obtain a statistically significant change in visual sensitivity (Quigley et al. 1989; Harwerth et al. 1999a; Kerrigan-Baumrind et al. 2000). Furthermore, since SAP is a behavioral test, the outcomes can be confounded by the patient's compliance and reliability indices. Therefore, an objective functional test could provide useful information about the state and the integrity of the RGCs in glaucoma.

The results of this dissertation indicate that the mfPhNR (F30 and F14) (Figure 2-11 and Figure 3-11) and the FF-PhNR (Figure 4-5) were all sensitive to early changes in glaucoma prior to thinning of the RNFL. Multifocal ERG has an advantage over the full field ERG in providing data on local changes in function for comparison with the local structure assessed using OCT. This was shown in Chapter 2 and Chapter 3 where we used a topographic map to compare corresponding regions in the structure (m-GCIPLT and s-RNFL) and function (m-mfPhNR, s-mfPhNR, s-mfOPs). Furthermore, we also showed that the amplitudes of the s-mfPhNR and s-mfOPs correlated well with the measures of corresponding structures (Figure 2-7; Figure 3-8) in the Exp eyes. One caveat in this study was that we did not find any significant difference between the time points of change for the global, macular or sectoral measures of mfPhNR although two of four monkeys showed early changes in the s-mfPhNR and 1 monkey showed change in the m-mfPhNR prior to g-mfPhNR. Other investigators have showed that retinal function in the central region of a multifocal array was more affected in glaucoma compared to in the surrounding regions (Kaneko et al. 2015). A possible reason could be that we used an experimental model of glaucoma in which the IOP was elevated to as high as 50 mmHg in Exp eyes for short durations, which could have resulted in an overall functional reduction. The duration and extent of IOP elevation in human

glaucoma patients are different from the experimental conditions, which could have resulted in more regional variations in inner retinal functional loss in glaucoma patients. It should be noted that, the Kaneko study filtered out signals less than 10 Hz, which means that mfPhNRs in less central regions were very small even in normal eyes.

Full field ERG records the mass response of the entire retina. Previous studies have showed the efficacy of the PhNR in detecting functional changes in glaucoma (Viswanathan et al. 2001; Machida et al. 2008; North et al. 2010; Huang et al. 2012). The finding that reduction of FF-PhNR in the Exp eyes occurred prior to macular GCIPLT and global RNFL changes suggests a huge potential for the ERG as an important screening tool for early diagnosis. In fact, changes in the FF-PhNR occurred as early as ONH changes (MRW, ALCSD). With the advantage of less compliant recording conditions (does not require accurate refractive correction and fixation), and less labor-intensive analysis, the FF-PhNR could be the front-runner for a reliable screening tool in glaucoma. Additionally the finding that the mfPhNR correlates better with the local RNFL changes than with global changes over time suggests that the mfPhNR can be used to track and monitor changes in early to moderate glaucoma.

Some limitations in these studies include the small sample size: seven monkeys. There was variability in the time course of pathological changes with a subset of monkeys showing early changes in a similar timeframe, and another group in which changes were more delayed. Additionally, the peak IOP increase achieved in these monkeys was very high (50 mm Hg) in a short duration. This is in contrast to the controlled pressures over years in most human glaucoma patients. Although, we reduced the IOP during experimental sessions to prevent the acute effects, other effects due to the high elevation cannot be ruled out. Therefore, more investigations with a larger sample size, and perhaps lower elevations in pressure in the future could yield a better interpretation of results. Nevertheless, the findings from these experiments

indicate the potential application of the ERG in early diagnosis of glaucoma. The time lag between the measures (ERG versus RNFLT) opens the door for potential therapeutic intervention to preserve the RGC structural integrity and restore the function.

5.7 Conclusion

The experiments in this dissertation showed that the mfPhNR and the FF-PhNR were sensitive to IOP-related stress in glaucoma. Changes in the functional parameters occurred concurrently with ONH structural changes but prior to thinning of the RNFL and m-GCIPL in a nonhuman model of experimental glaucoma.

References

Agapova OA, Kaufman PL, Lucarelli MJ, Gabelt BT, Hernandez MR. 2003. Differential expression of matrix metalloproteinases in monkey eyes with experimental glaucoma or optic nerve transection. Brain research 967:132-143.

Aihara M, Lindsey JD, Weinreb RN. 2003. Ocular hypertension in mice with a targeted type i collagen mutation. Investigative ophthalmology & visual science 44:1581-1585.

Akashi A, Kanamori A, Nakamura M, Fujihara M, Yamada Y, Negi A. 2013. Comparative assessment for the ability of cirrus, rtvue, and 3d-oct to diagnose glaucoma. Investigative ophthalmology & visual science 54:4478-4484.

Aldebasi YH, Drasdo N, Morgan JE, North RV. 2004. S-cone, l + m-cone, and pattern, electroretinograms in ocular hypertension and glaucoma. Vision research 44:2749-2756.

Anctil JL, Anderson DR. 1984. Early foveal involvement and generalized depression of the visual field in glaucoma. Archives of ophthalmology 102:363-370.

Anderson DR, Hendrickson A. 1974. Effect of intraocular pressure on rapid axoplasmic transport in monkey optic nerve. Investigative ophthalmology 13:771-783.

Anderson DR. 1996. Glaucoma, capillaries and pericytes. 1. Blood flow regulation. Ophthalmologica Journal international d'ophtalmologie International journal of ophthalmology Zeitschrift fur Augenheilkunde 210:257-262.

Anderson MG, Smith RS, Hawes NL, Zabaleta A, Chang B, Wiggs JL, et al. 2002. Mutations in genes encoding melanosomal proteins cause pigmentary glaucoma in dba/2j mice. Nature genetics 30:81-85.

Arintawati P, Sone T, Akita T, Tanaka J, Kiuchi Y. 2013. The applicability of ganglion cell complex parameters determined from sd-oct images to detect glaucomatous eyes. Journal of glaucoma 22:713-718.

Bach M, Hoffmann MB. 2008. Update on the pattern electroretinogram in glaucoma. Optometry and vision science : official publication of the American Academy of Optometry 85:386-395.

Bach M, Poloschek CM. 2013. Electrophysiology and glaucoma: Current status and future challenges. Cell and tissue research 353:287-296.

Baptiste DC, Powell KJ, Jollimore CA, Hamilton C, LeVatte TL, Archibald ML, et al. 2005. Effects of minocycline and tetracycline on retinal ganglion cell survival after axotomy. Neuroscience 134:575-582.

Bayer AU, Danias J, Brodie S, Maag KP, Chen B, Shen F, et al. 2001. Electroretinographic abnormalities in a rat glaucoma model with chronic elevated intraocular pressure. Experimental eye research 72:667-677.

Bearse MA, Jr., Sutter EE. 1996. Imaging localized retinal dysfunction with the multifocal electroretinogram. Journal of the Optical Society of America A, Optics, image science, and vision 13:634-640.

Bearse MA, Jr., Shimada Y, Sutter EE. 2000. Distribution of oscillatory components in the central retina. Documenta ophthalmologica Advances in ophthalmology 100:185-205.

Bellezza AJ, Hart RT, Burgoyne CF. 2000. The optic nerve head as a biomechanical structure: Initial finite element modeling. Investigative ophthalmology & visual science 41:2991-3000.

Bellezza AJ, Rintalan CJ, Thompson HW, Downs JC, Hart RT, Burgoyne CF. 2003. Deformation of the lamina cribrosa and anterior scleral canal wall in early experimental glaucoma. Investigative ophthalmology & visual science 44:623-637.

Bloomfield SA. 1996. Effect of spike blockade on the receptive-field size of amacrine and ganglion cells in the rabbit retina. Journal of neurophysiology 75:1878-1893.

Bonomi L, Perfetti S, Noya E, Bellucci R, Tomazzoli L. 1978. Experimental corticosteroid ocular hypertension in the rabbit. Albrecht von Graefes Archiv fur klinische und experimentelle Ophthalmologie Albrecht von Graefe's archive for clinical and experimental ophthalmology 209:73-82.

Bosco A, Inman DM, Steele MR, Wu G, Soto I, Marsh-Armstrong N, et al. 2008. Reduced retina microglial activation and improved optic nerve integrity with minocycline treatment in the dba/2j mouse model of glaucoma. Investigative ophthalmology & visual science 49:1437-1446.

Bosco A, Steele MR, Vetter ML. 2011. Early microglia activation in a mouse model of chronic glaucoma. The Journal of comparative neurology 519:599-620.

Bowman CL, Kimelberg HK, Frangakis MV, Berwald-Netter Y, Edwards C. 1984. Astrocytes in primary culture have chemically activated sodium channels. The Journal of neuroscience : the official journal of the Society for Neuroscience 4:1527-1534.

Bringmann A, Reichenbach A. 2001. Role of muller cells in retinal degenerations. Frontiers in bioscience : a journal and virtual library 6:E72-92.

Bringmann A, Pannicke T, Grosche J, Francke M, Wiedemann P, Skatchkov SN, et al. 2006. Muller cells in the healthy and diseased retina. Progress in retinal and eye research 25:397-424.

Bringmann A, Wiedemann P. 2012. Muller glial cells in retinal disease. Ophthalmologica Journal international d'ophtalmologie International journal of ophthalmology Zeitschrift fur Augenheilkunde 227:1-19.

Buckingham BP, Inman DM, Lambert W, Oglesby E, Calkins DJ, Steele MR, et al. 2008. Progressive ganglion cell degeneration precedes neuronal loss in a mouse model of glaucoma. The Journal of neuroscience : the official journal of the Society for Neuroscience 28:2735-2744.

Burgoyne CF, Varma R, Quigley HA, Vitale S, Pease ME, Lenane PL. 1994. Global and regional detection of induced optic disc change by digitized image analysis. Archives of ophthalmology 112:261-268.

Burgoyne CF, Quigley HA, Thompson HW, Vitale S, Varma R. 1995. Early changes in optic disc compliance and surface position in experimental glaucoma. Ophthalmology 102:1800-1809.

Burgoyne CF, Downs JC, Bellezza AJ, Hart RT. 2004. Three-dimensional reconstruction of normal and early glaucoma monkey optic nerve head connective tissues. Investigative ophthalmology & visual science 45:4388-4399.

Burgoyne CF, Downs JC, Bellezza AJ, Suh JK, Hart RT. 2005. The optic nerve head as a biomechanical structure: A new paradigm for understanding the role of iop-related stress and strain in the pathophysiology of glaucomatous optic nerve head damage. Progress in retinal and eye research 24:39-73.

Burnham KP, Anderson DR. 2004. Multimodel inference understanding aic and bic in model selection. Sociological methods & research 33:261-304.

Carter-Dawson L, Shen F, Harwerth RS, Smith EL, 3rd, Crawford ML, Chuang A. 1998. Glutamine immunoreactivity in muller cells of monkey eyes with experimental glaucoma. Experimental eye research 66:537-545.

Chang B, Smith RS, Hawes NL, Anderson MG, Zabaleta A, Savinova O, et al. 1999. Interacting loci cause severe iris atrophy and glaucoma in dba/2j mice. Nature genetics 21:405-409.

Chauhan BC. 2008. Endothelin and its potential role in glaucoma. Canadian journal of ophthalmology Journal canadien d'ophtalmologie 43:356-360.

Chauhan BC, O'Leary N, Almobarak FA, Reis AS, Yang H, Sharpe GP, et al. 2013. Enhanced detection of open-angle glaucoma with an anatomically accurate optical coherence tomography-derived neuroretinal rim parameter. Ophthalmology 120:535-543.

Chrysostomou V, Crowston JG. 2013. The photopic negative response of the mouse electroretinogram: Reduction by acute elevation of intraocular pressure. Investigative ophthalmology & visual science 54:4691-4697.

Colotto A, Falsini B, Salgarello T, Iarossi G, Galan ME, Scullica L. 2000. Photopic negative response of the human erg: Losses associated with glaucomatous damage. Investigative ophthalmology & visual science 41:2205-2211.

Crawford Downs J, Roberts MD, Sigal IA. 2011. Glaucomatous cupping of the lamina cribrosa: A review of the evidence for active progressive remodeling as a mechanism. Experimental eye research 93:133-140.

Cull G, Burgoyne CF, Fortune B, Wang L. 2013. Longitudinal hemodynamic changes within the optic nerve head in experimental glaucoma. Investigative ophthalmology & visual science 54:4271-4277.

Cull GA, Reynaud J, Wang L, Cioffi GA, Burgoyne CF, Fortune B. 2012. Relationship between orbital optic nerve axon counts and retinal nerve fiber layer thickness measured

by spectral domain optical coherence tomography. Investigative ophthalmology & visual science 53:7766-7773.

Curcio CA, Allen KA. 1990. Topography of ganglion cells in human retina. The Journal of comparative neurology 300:5-25.

David P, Lusky M, Teichberg VI. 1988. Involvement of excitatory neurotransmitters in the damage produced in chick embryo retinas by anoxia and extracellular high potassium. Experimental eye research 46:657-662.

Downs JC, Yang H, Girkin C, Sakata L, Bellezza A, Thompson H, et al. 2007. Three-dimensional histomorphometry of the normal and early glaucomatous monkey optic nerve head: Neural canal and subarachnoid space architecture. Investigative ophthalmology & visual science 48:3195-3208.

Downs JC, Roberts MD, Burgoyne CF. 2008. Mechanical environment of the optic nerve head in glaucoma. Optometry and vision science : official publication of the American Academy of Optometry 85:425-435.

Drasdo N, Aldebasi YH, Chiti Z, Mortlock KE, Morgan JE, North RV. 2001. The s-cone phnr and pattern erg in primary open angle glaucoma. Investigative ophthalmology & visual science 42:1266-1272.

Drasdo N, Millican CL, Katholi CR, Curcio CA. 2007. The length of henle fibers in the human retina and a model of ganglion receptive field density in the visual field. Vision research 47:2901-2911.

Fahy ET, Chrysostomou V, Crowston JG. 2016. Mini-review: Impaired axonal transport and glaucoma. Current eye research 41:273-283.

Fechtner RD, Weinreb RN. 1994. Mechanisms of optic nerve damage in primary open angle glaucoma. Survey of ophthalmology 39:23-42.

Fortune B, Bearse MA, Jr., Cioffi GA, Johnson CA. 2002. Selective loss of an oscillatory component from temporal retinal multifocal erg responses in glaucoma. Investigative ophthalmology & visual science 43:2638-2647.

Fortune B, Wang L, Bui BV, Cull G, Dong J, Cioffi GA. 2003. Local ganglion cell contributions to the macaque electroretinogram revealed by experimental nerve fiber layer bundle defect. Investigative ophthalmology & visual science 44:4567-4579.

Fortune B, Bui BV, Morrison JC, Johnson EC, Dong J, Cepurna WO, et al. 2004. Selective ganglion cell functional loss in rats with experimental glaucoma. Investigative ophthalmology & visual science 45:1854-1862.

Fortune B, Burgoyne CF, Cull GA, Reynaud J, Wang L. 2012. Structural and functional abnormalities of retinal ganglion cells measured in vivo at the onset of optic nerve head surface change in experimental glaucoma. Investigative ophthalmology & visual science 53:3939-3950.

Fortune B, Burgoyne CF, Cull G, Reynaud J, Wang L. 2013a. Onset and progression of peripapillary retinal nerve fiber layer (rnfl) retardance changes occur earlier than rnfl thickness changes in experimental glaucoma. Investigative ophthalmology & visual science 54:5653-5661.

Fortune B, Reynaud J, Wang L, Burgoyne CF. 2013b. Does optic nerve head surface topography change prior to loss of retinal nerve fiber layer thickness: A test of the site of injury hypothesis in experimental glaucoma. PloS one 8:e77831.

Fortune B, Cull G, Reynaud J, Wang L, Burgoyne CF. 2015. Relating retinal ganglion cell function and retinal nerve fiber layer (rnfl) retardance to progressive loss of rnfl thickness and optic nerve axons in experimental glaucoma. Investigative ophthalmology & visual science 56:3936-3944.

Fortune B, Hardin C, Reynaud J, Cull G, Yang H, Wang L, et al. 2016. Comparing optic nerve head rim width, rim area, and peripapillary retinal nerve fiber layer thickness to axon count in experimental glaucoma. Investigative ophthalmology & visual science 57:OCT404-412.

Francoz M, Fenolland JR, Giraud JM, El Chehab H, Sendon D, May F, et al. 2014. Reproducibility of macular ganglion cell-inner plexiform layer thickness measurement with cirrus hd-oct in normal, hypertensive and glaucomatous eyes. The British journal of ophthalmology 98:322-328.

Frishman LJ, Steinberg RH. 1989a. Intraretinal analysis of the threshold dark-adapted erg of cat retina. Journal of neurophysiology 61:1221-1232.

Frishman LJ, Steinberg RH. 1989b. Light-evoked increases in [k+]o in proximal portion of the dark-adapted cat retina. Journal of neurophysiology 61:1233-1243.

Frishman LJ, Shen FF, Du L, Robson JG, Harwerth RS, Smith EL, 3rd, et al. 1996. The scotopic electroretinogram of macaque after retinal ganglion cell loss from experimental glaucoma. Investigative ophthalmology & visual science 37:125-141.

Frishman LJ, Saszik S, Harwerth RS, Viswanathan S, Li Y, Smith EL, 3rd, et al. 2000. Effects of experimental glaucoma in macaques on the multifocal erg. Multifocal erg in laser-induced glaucoma. Documenta ophthalmologica Advances in ophthalmology 100:231-251.

Fu QL, Li X, Shi J, Xu G, Wen W, Lee DH, et al. 2009. Synaptic degeneration of retinal ganglion cells in a rat ocular hypertension glaucoma model. Cellular and molecular neurobiology 29:575-581.

Fujikawa K, Iwata T, Inoue K, Akahori M, Kadotani H, Fukaya M, et al. 2010. Vav2 and vav3 as candidate disease genes for spontaneous glaucoma in mice and humans. PloS one 5:e9050.

Fulton AB, Rushton WA. 1978. The human rod erg: Correlation with psychophysical responses in light and dark adaptation. Vision research 18:793-800.

Furlanetto RL, Park SC, Damle UJ, Sieminski SF, Kung Y, Siegal N, et al. 2013. Posterior displacement of the lamina cribrosa in glaucoma: In vivo interindividual and intereye comparisons. Investigative ophthalmology & visual science 54:4836-4842.

Gaasterland D, Kupfer C. 1974. Experimental glaucoma in the rhesus monkey. Investigative ophthalmology 13:455-457.

Galassi F, Sodi A, Ucci F, Renieri G, Pieri B, Baccini M. 2003. Ocular hemodynamics and glaucoma prognosis: A color doppler imaging study. Archives of ophthalmology 121:1711-1715.

Garas A, Vargha P, Hollo G. 2011. Diagnostic accuracy of nerve fibre layer, macular thickness and optic disc measurements made with the rtvue-100 optical coherence tomograph to detect glaucoma. Eye 25:57-65.

Gardiner SK, Fortune B, Wang L, Downs JC, Burgoyne CF. 2012. Intraocular pressure magnitude and variability as predictors of rates of structural change in non-human primate experimental glaucoma. Experimental eye research 103:1-8.

Gardiner SK, Ren R, Yang H, Fortune B, Burgoyne CF, Demirel S. 2014. A method to estimate the amount of neuroretinal rim tissue in glaucoma: Comparison with current methods for measuring rim area. American journal of ophthalmology 157:540-549 e541-542.

Gardiner SK, Fortune B, Demirel S. 2016. Localized changes in retinal nerve fiber layer thickness as a predictor of localized functional change in glaucoma. American journal of ophthalmology.

Garway-Heath DF, Poinoosawmy D, Fitzke FW, Hitchings RA. 2000. Mapping the visual field to the optic disc in normal tension glaucoma eyes. Ophthalmology 107:1809-1815.

Garway-Heath DF, Holder GE, Fitzke FW, Hitchings RA. 2002. Relationship between electrophysiological, psychophysical, and anatomical measurements in glaucoma. Investigative ophthalmology & visual science 43:2213-2220.

Gelatt KN, Gum GG, Gwin RM, Bromberg NM, Merideth RE, Samuelson DA. 1981. Primary open angle glaucoma: Inherited primary open angle glaucoma in the beagle. The American journal of pathology 102:292-295.

Gordon MO, Beiser JA, Brandt JD, Heuer DK, Higginbotham EJ, Johnson CA, et al. 2002. The ocular hypertension treatment study: Baseline factors that predict the onset of primary open-angle glaucoma. Archives of ophthalmology 120:714-720; discussion 829-730.

Gotoh Y, Machida S, Tazawa Y. 2004. Selective loss of the photopic negative response in patients with optic nerve atrophy. Archives of ophthalmology 122:341-346.

Griffin JW, Watson DF. 1988. Axonal transport in neurological disease. Annals of neurology 23:3-13.

Grillo LM, Wang DL, Ramachandran R, Ehrlich AC, De Moraes CG, Ritch R, et al. 2016. The 24-2 visual field test misses central macular damage confirmed by the 10-2 visual field test and optical coherence tomography. Translational vision science & technology 5:15.

Grunwald JE, Riva CE, Stone RA, Keates EU, Petrig BL. 1984. Retinal autoregulation in open-angle glaucoma. Ophthalmology 91:1690-1694.

Hampson EC, Smith RI, Bernays ME. 2002. Primary glaucoma in burmese cats. Australian veterinary journal 80:672-680.

Hare WA, WoldeMussie E, Lai RK, Ton H, Ruiz G, Chun T, et al. 2004. Efficacy and safety of memantine treatment for reduction of changes associated with experimental glaucoma in monkey, i: Functional measures. Investigative ophthalmology & visual science 45:2625-2639.

Harwerth RS, Smith EL, 3rd, DeSantis L. 1993. Behavioral perimetry in monkeys. Investigative ophthalmology & visual science 34:31-40.

Harwerth RS, Carter-Dawson L, Shen F, Smith EL, 3rd, Crawford ML. 1999a. Ganglion cell losses underlying visual field defects from experimental glaucoma. Investigative ophthalmology & visual science 40:2242-2250.

Harwerth RS, Smith EL, 3rd, Chandler M. 1999b. Progressive visual field defects from experimental glaucoma: Measurements with white and colored stimuli. Optometry and vision science : official publication of the American Academy of Optometry 76:558-570.

Harwerth RS, Carter-Dawson L, Smith EL, 3rd, Barnes G, Holt WF, Crawford ML. 2004. Neural losses correlated with visual losses in clinical perimetry. Investigative ophthalmology & visual science 45:3152-3160.

Harwerth RS, Vilupuru AS, Rangaswamy NV, Smith EL, 3rd. 2007. The relationship between nerve fiber layer and perimetry measurements. Investigative ophthalmology & visual science 48:763-773.

Harwerth RS, Wheat JL, Fredette MJ, Anderson DR. 2010. Linking structure and function in glaucoma. Progress in retinal and eye research 29:249-271.

Hayreh SS. 2001a. Blood flow in the optic nerve head and factors that may influence it. Progress in retinal and eye research 20:595-624.

Hayreh SS. 2001b. The blood supply of the optic nerve head and the evaluation of it - myth and reality. Progress in retinal and eye research 20:563-593.

He L, Yang H, Gardiner SK, Williams G, Hardin C, Strouthidis NG, et al. 2014. Longitudinal detection of optic nerve head changes by spectral domain optical coherence tomography in early experimental glaucoma. Investigative ophthalmology & visual science 55:574-586.

Heijl A, Lundqvist L. 1984. The frequency distribution of earliest glaucomatous visual field defects documented by automatic perimetry. Acta ophthalmologica 62:658-664.

Hernandez MR, Igoe F, Neufeld AH. 1988. Cell culture of the human lamina cribrosa. Investigative ophthalmology & visual science 29:78-89.

Hernandez MR. 1992. Ultrastructural immunocytochemical analysis of elastin in the human lamina cribrosa. Changes in elastic fibers in primary open-angle glaucoma. Investigative ophthalmology & visual science 33:2891-2903.

Hernandez MR, Ye H, Roy S. 1994. Collagen type iv gene expression in human optic nerve heads with primary open angle glaucoma. Experimental eye research 59:41-51.

Hernandez MR, Pena JD. 1997. The optic nerve head in glaucomatous optic neuropathy. Archives of ophthalmology 115:389-395.

Hernandez MR. 2000. The optic nerve head in glaucoma: Role of astrocytes in tissue remodeling. Progress in retinal and eye research 19:297-321.

Hernandez MR, Miao H, Lukas T. 2008. Astrocytes in glaucomatous optic neuropathy. Progress in brain research 173:353-373.

Hood DC, Seiple W, Holopigian K, Greenstein V. 1997. A comparison of the components of the multifocal and full-field ergs. Visual neuroscience 14:533-544.

Hood DC, Frishman LJ, Viswanathan S, Robson JG, Ahmed J. 1999. Evidence for a ganglion cell contribution to the primate electroretinogram (erg): Effects of ttx on the multifocal erg in macaque. Visual neuroscience 16:411-416.

Hood DC. 2007. Relating retinal nerve fiber thickness to behavioral sensitivity in patients with glaucoma: Application of a linear model. Journal of the Optical Society of America A, Optics, image science, and vision 24:1426-1430.

Hood DC, Anderson SC, Wall M, Kardon RH. 2007. Structure versus function in glaucoma: An application of a linear model. Investigative ophthalmology & visual science 48:3662-3668.

Hood DC, Raza AS. 2011. Method for comparing visual field defects to local rnfl and rgc damage seen on frequency domain oct in patients with glaucoma. Biomedical optics express 2:1097-1105.

Hood DC, Raza AS, de Moraes CG, Odel JG, Greenstein VC, Liebmann JM, et al. 2011. Initial arcuate defects within the central 10 degrees in glaucoma. Investigative ophthalmology & visual science 52:940-946.

Hood DC, Raza AS, de Moraes CG, Liebmann JM, Ritch R. 2013. Glaucomatous damage of the macula. Progress in retinal and eye research 32:1-21.

Hoyt WF, Newman NM. 1972. The earliest observable defect in glaucoma? Lancet 1:692-693.

Huang L, Shen X, Fan N, He J. 2012. Clinical application of photopic negative response of the flash electroretinogram in primary open-angle glaucoma. Eye science 27:113-118.

Ishikawa H, Stein DM, Wollstein G, Beaton S, Fujimoto JG, Schuman JS. 2005. Macular segmentation with optical coherence tomography. Investigative ophthalmology & visual science 46:2012-2017.

Ivers KM, Li C, Patel N, Sredar N, Luo X, Queener H, et al. 2011. Reproducibility of measuring lamina cribrosa pore geometry in human and nonhuman primates with in vivo adaptive optics imaging. Investigative ophthalmology & visual science 52:5473-5480.

Ivers KM, Sredar N, Patel NB, Rajagopalan L, Queener HM, Twa MD, et al. 2015. In vivo changes in lamina cribrosa microarchitecture and optic nerve head structure in early experimental glaucoma. PloS one 10:e0134223.

Jia Y, Wei E, Wang X, Zhang X, Morrison JC, Parikh M, et al. 2014. Optical coherence tomography angiography of optic disc perfusion in glaucoma. Ophthalmology 121:1322-1332.

Johnson CA. 1996. Standardizing the measurement of visual fields for clinical research: Guidelines from the eye care technology forum. Ophthalmology 103:186-189.

Johnson EC, Morrison JC, Farrell S, Deppmeier L, Moore CG, McGinty MR. 1996. The effect of chronically elevated intraocular pressure on the rat optic nerve head extracellular matrix. Experimental eye research 62:663-674.

Johnson MA, Drum BA, Quigley HA, Sanchez RM, Dunkelberger GR. 1989. Pattern-evoked potentials and optic nerve fiber loss in monocular laser-induced glaucoma. Investigative ophthalmology & visual science 30:897-907.

Jonas JB, Fernandez MC, Sturmer J. 1993. Pattern of glaucomatous neuroretinal rim loss. Ophthalmology 100:63-68.

Jung HH, Sung MS, Heo H, Park SW. 2014. Macular inner plexiform and retinal nerve fiber layer thickness in glaucoma. Optometry and vision science : official publication of the American Academy of Optometry 91:1320-1327.

Kanamori A, Nakamura M, Nakanishi Y, Yamada Y, Negi A. 2005. Long-term glial reactivity in rat retinas ipsilateral and contralateral to experimental glaucoma. Experimental eye research 81:48-56.

Kaneko M, Machida S, Hoshi Y, Kurosaka D. 2015. Alterations of photopic negative response of multifocal electroretinogram in patients with glaucoma. Current eye research 40:77-86.

Kass MA, Heuer DK, Higginbotham EJ, Johnson CA, Keltner JL, Miller JP, et al. 2002. The ocular hypertension treatment study: A randomized trial determines that topical ocular hypotensive medication delays or prevents the onset of primary open-angle glaucoma. Archives of ophthalmology 120:701-713; discussion 829-730.

Kerrigan-Baumrind LA, Quigley HA, Pease ME, Kerrigan DF, Mitchell RS. 2000. Number of ganglion cells in glaucoma eyes compared with threshold visual field tests in the same persons. Investigative ophthalmology & visual science 41:741-748.

Kim DH, Kim HS, Ahn MD, Chun MH. 2004. Ganglion cell death in rat retina by persistent intraocular pressure elevation. Korean journal of ophthalmology : KJO 18:15-22.

Kim KE, Park KH, Yoo BW, Jeoung JW, Kim DM, Kim HC. 2014. Topographic localization of macular retinal ganglion cell loss associated with localized peripapillary retinal nerve fiber layer defect. Investigative ophthalmology & visual science 55:3501-3508.

Kondo M, Kurimoto Y, Sakai T, Koyasu T, Miyata K, Ueno S, et al. 2008. Recording focal macular photopic negative response (phnr) from monkeys. Investigative ophthalmology & visual science 49:3544-3550.

Kurimoto Y, Kondo M, Ueno S, Sakai T, Machida S, Terasaki H. 2009. Asymmetry of focal macular photopic negative responses (phnrs) in monkeys. Experimental eye research 88:92-98.

Lebrun-Julien F, Morquette B, Douillette A, Saragovi HU, Di Polo A. 2009. Inhibition of p75(ntr) in glia potentiates trka-mediated survival of injured retinal ganglion cells. Molecular and cellular neurosciences 40:410-420.

Libby RT, Anderson MG, Pang IH, Robinson ZH, Savinova OV, Cosma IM, et al. 2005. Inherited glaucoma in dba/2j mice: Pertinent disease features for studying the neurodegeneration. Visual neuroscience 22:637-648.

Liu L, Jia Y, Takusagawa HL, Pechauer AD, Edmunds B, Lombardi L, et al. 2015. Optical coherence tomography angiography of the peripapillary retina in glaucoma. JAMA ophthalmology 133:1045-1052.

Liu M, Guo L, Salt TE, Cordeiro MF. 2014. Dendritic changes in rat visual pathway associated with experimental ocular hypertension. Current eye research 39:953-963.

Luo X, Frishman LJ. 2011. Retinal pathway origins of the pattern electroretinogram (perg). Investigative ophthalmology & visual science 52:8571-8584.

Luo X, Patel NB, Harwerth RS, Frishman LJ. 2011. Loss of the low-frequency component of the global-flash multifocal electroretinogram in primate eyes with experimental glaucoma. Investigative ophthalmology & visual science 52:3792-3804.

Luo X, Patel N, Rajagopalan LP, Harwerth RS, Frishman LJ. 2014. Relation between macular retinal ganglion cell/inner plexiform layer thickness and multifocal

electroretinogram measures in experimental glaucoma. Investigative ophthalmology & visual science.

Machida S, Gotoh Y, Toba Y, Ohtaki A, Kaneko M, Kurosaka D. 2008. Correlation between photopic negative response and retinal nerve fiber layer thickness and optic disc topography in glaucomatous eyes. Investigative ophthalmology & visual science 49:2201-2207.

Machida S, Tamada K, Oikawa T, Yokoyama D, Kaneko M, Kurosaka D. 2010. Sensitivity and specificity of photopic negative response of focal electoretinogram to detect glaucomatous eyes. The British journal of ophthalmology 94:202-208.

Machida S, Tamada K, Oikawa T, Gotoh Y, Nishimura T, Kaneko M, et al. 2011. Comparison of photopic negative response of full-field and focal electroretinograms in detecting glaucomatous eyes. Journal of ophthalmology 2011.

Mafei L, Fiorentini A. 1981. Electroretinographic responses to alternating gratings before and after section of the optic nerve. Science 211:953-955.

Magistretti PJ. 2006. Neuron-glia metabolic coupling and plasticity. The Journal of experimental biology 209:2304-2311.

Marx MS, Podos SM, Bodis-Wollner I, Howard-Williams JR, Siegel MJ, Teitelbaum CS, et al. 1986. Flash and pattern electroretinograms in normal and laser-induced glaucomatous primate eyes. Investigative ophthalmology & visual science 27:378-386.

Marx MS, Podos SM, Bodis-Wollner I, Lee PY, Wang RF, Severin C. 1988. Signs of early damage in glaucomatous monkey eyes: Low spatial frequency losses in the pattern erg and vep. Experimental eye research 46:173-184.

Minckler DS, Bunt AH, Johanson GW. 1977. Orthograde and retrograde axoplasmic transport during acute ocular hypertension in the monkey. Investigative ophthalmology & visual science 16:426-441.

Miyake Y, Yanagida K, Kondo T, Yagasaki K. 1981. [simultaneous recording of local erg and ver under direct fundus observation with infrared television fundus camera (author's transl)]. Nippon Ganka Gakkai zasshi 85:1521-1533.

Moreno MC, Sande P, Marcos HA, de Zavalia N, Keller Sarmiento MI, Rosenstein RE. 2005. Effect of glaucoma on the retinal glutamate/glutamine cycle activity. FASEB journal : official publication of the Federation of American Societies for Experimental Biology 19:1161-1162.

Morgan JE. 2000. Optic nerve head structure in glaucoma: Astrocytes as mediators of axonal damage. Eye 14 (Pt 3B):437-444.

Morgan JE, Uchida H, Caprioli J. 2000. Retinal ganglion cell death in experimental glaucoma. The British journal of ophthalmology 84:303-310.

Morgan JE. 2004. Circulation and axonal transport in the optic nerve. Eye 18:1089-1095.

Morgan JE, Datta AV, Erichsen JT, Albon J, Boulton ME. 2006. Retinal ganglion cell remodelling in experimental glaucoma. Advances in experimental medicine and biology 572:397-402.

Morrison JC, Dorman-Pease ME, Dunkelberger GR, Quigley HA. 1990. Optic nerve head extracellular matrix in primary optic atrophy and experimental glaucoma. Archives of ophthalmology 108:1020-1024.

Morrison JC, Moore CG, Deppmeier LM, Gold BG, Meshul CK, Johnson EC. 1997. A rat model of chronic pressure-induced optic nerve damage. Experimental eye research 64:85-96.

Mwanza JC, Durbin MK, Budenz DL, Sayyad FE, Chang RT, Neelakantan A, et al. 2012. Glaucoma diagnostic accuracy of ganglion cell-inner plexiform layer thickness: Comparison with nerve fiber layer and optic nerve head. Ophthalmology 119:1151-1158.

Na JH, Kook MS, Lee Y, Baek S. 2012. Structure-function relationship of the macular visual field sensitivity and the ganglion cell complex thickness in glaucoma. Investigative ophthalmology & visual science 53:5044-5051.

Nakamura H, Hangai M, Mori S, Hirose F, Yoshimura N. 2011. Hemispherical focal macular photopic negative response and macular inner retinal thickness in open-angle glaucoma. American journal of ophthalmology 151:494-506 e491.

Nakazawa T, Nakazawa C, Matsubara A, Noda K, Hisatomi T, She H, et al. 2006. Tumor necrosis factor-alpha mediates oligodendrocyte death and delayed retinal ganglion cell loss in a mouse model of glaucoma. The Journal of neuroscience : the official journal of the Society for Neuroscience 26:12633-12641.

Neufeld AH, Hernandez MR, Gonzalez M. 1997. Nitric oxide synthase in the human glaucomatous optic nerve head. Archives of ophthalmology 115:497-503.

Neufeld AH. 1999. Microglia in the optic nerve head and the region of parapapillary chorioretinal atrophy in glaucoma. Archives of ophthalmology 117:1050-1056.

Newman EA. 2004. A dialogue between glia and neurons in the retina: Modulation of neuronal excitability. Neuron glia biology 1:245-252.

Nicholas SP, Werner EB. 1980. Location of early glaucomatous visual field defects. Canadian journal of ophthalmology Journal canadien d'ophtalmologie 15:131-133.

Niyadurupola N, Luu CD, Nguyen DQ, Geddes K, Tan GX, Wong CC, et al. 2013. Intraocular pressure lowering is associated with an increase in the photopic negative

response (phnr) amplitude in glaucoma and ocular hypertensive eyes. Investigative ophthalmology & visual science 54:1913-1919.

North RV, Jones AL, Drasdo N, Wild JM, Morgan JE. 2010. Electrophysiological evidence of early functional damage in glaucoma and ocular hypertension. Investigative ophthalmology & visual science 51:1216-1222.

O'Brien C, Butt Z, Ludlam C, Detkova P. 1997. Activation of the coagulation cascade in untreated primary open-angle glaucoma. Ophthalmology 104:725-729; discussion 729-730.

Obara M, Szeliga M, Albrecht J. 2008. Regulation of ph in the mammalian central nervous system under normal and pathological conditions: Facts and hypotheses. Neurochemistry international 52:905-919.

Ogden TE. 1973. The oscillatory waves of the primate electroretinogram. Vision research 13:1059-1074.

Patel NB, Luo X, Wheat JL, Harwerth RS. 2011. Retinal nerve fiber layer assessment: Area versus thickness measurements from elliptical scans centered on the optic nerve. Investigative ophthalmology & visual science 52:2477-2489.

Patel NB, Sullivan-Mee M, Harwerth RS. 2014. The relationship between retinal nerve fiber layer thickness and optic nerve head neuroretinal rim tissue in glaucoma. Investigative ophthalmology & visual science 55:6802-6816.

Pederson JE, Gaasterland DE. 1984. Laser-induced primate glaucoma. I. Progression of cupping. Archives of ophthalmology 102:1689-1692.

Pena JD, Netland PA, Vidal I, Dorr DA, Rasky A, Hernandez MR. 1998. Elastosis of the lamina cribrosa in glaucomatous optic neuropathy. Experimental eye research 67:517-524.

Pickett JE, Terry SA, O'Connor PS, O'Hara M. 1985. Early loss of central visual acuity in glaucoma. Ophthalmology 92:891-896.

Pillunat LE, Stodtmeister R, Wilmanns I, Christ T. 1986. [a test of pressure tolerance of the optic nerve head in ocular hypertension]. Klinische Monatsblatter fur Augenheilkunde 188:39-44.

Pillunat LE, Stodtmeister R, Wilmanns I. 1987. Pressure compliance of the optic nerve head in low tension glaucoma. The British journal of ophthalmology 71:181-187.

Preiser D, Lagreze WA, Bach M, Poloschek CM. 2013. Photopic negative response versus pattern electroretinogram in early glaucoma. Investigative ophthalmology & visual science 54:1182-1191.

Purpura K, Tranchina D, Kaplan E, Shapley RM. 1990. Light adaptation in the primate retina: Analysis of changes in gain and dynamics of monkey retinal ganglion cells. Visual neuroscience 4:75-93.

Quigley HA, Anderson DR. 1977. Distribution of axonal transport blockade by acute intraocular pressure elevation in the primate optic nerve head. Investigative ophthalmology & visual science 16:640-644.

Quigley HA, Green WR. 1979. The histology of human glaucoma cupping and optic nerve damage: Clinicopathologic correlation in 21 eyes. Ophthalmology 86:1803-1830.

Quigley HA, Addicks EM. 1980a. Chronic experimental glaucoma in primates. Ii. Effect of extended intraocular pressure elevation on optic nerve head and axonal transport. Investigative ophthalmology & visual science 19:137-152.

Quigley HA, Addicks EM. 1980b. Chronic experimental glaucoma in primates. I. Production of elevated intraocular pressure by anterior chamber injection of autologous ghost red blood cells. Investigative ophthalmology & visual science 19:126-136.

Quigley HA, Addicks EM, Green WR, Maumenee AE. 1981. Optic nerve damage in human glaucoma. Ii. The site of injury and susceptibility to damage. Archives of ophthalmology 99:635-649.

Quigley HA. 1982. Glaucoma's optic nerve damage: Changing clinical perspectives. Annals of ophthalmology 14:611-612.

Quigley HA, Addicks EM, Green WR. 1982. Optic nerve damage in human glaucoma. Iii. Quantitative correlation of nerve fiber loss and visual field defect in glaucoma, ischemic neuropathy, papilledema, and toxic neuropathy. Archives of ophthalmology 100:135-146.

Quigley HA, Hohman RM. 1983. Laser energy levels for trabecular meshwork damage in the primate eye. Investigative ophthalmology & visual science 24:1305-1307.

Quigley HA, Dunkelberger GR, Green WR. 1988. Chronic human glaucoma causing selectively greater loss of large optic nerve fibers. Ophthalmology 95:357-363.

Quigley HA, Dunkelberger GR, Green WR. 1989. Retinal ganglion cell atrophy correlated with automated perimetry in human eyes with glaucoma. American journal of ophthalmology 107:453-464.

Quigley HA. 2005. Glaucoma: Macrocosm to microcosm the friedenwald lecture. Investigative ophthalmology & visual science 46:2662-2670.

Quigley HA, Broman AT. 2006. The number of people with glaucoma worldwide in 2010 and 2020. The British journal of ophthalmology 90:262-267.

Rangaswamy NV, Hood DC, Frishman LJ. 2003. Regional variations in local contributions to the primate photopic flash erg: Revealed using the slow-sequence mferg. Investigative ophthalmology & visual science 44:3233-3247.

Rangaswamy NV, Zhou W, Harwerth RS, Frishman LJ. 2006. Effect of experimental glaucoma in primates on oscillatory potentials of the slow-sequence mferg. Investigative ophthalmology & visual science 47:753-767.

Rangaswamy NV, Shirato S, Kaneko M, Digby BI, Robson JG, Frishman LJ. 2007. Effects of spectral characteristics of ganzfeld stimuli on the photopic negative response (phnr) of the erg. Investigative ophthalmology & visual science 48:4818-4828.

Raz-Prag D, Grimes WN, Fariss RN, Vijayasarathy C, Campos MM, Bush RA, et al. 2010. Probing potassium channel function in vivo by intracellular delivery of antibodies in a rat model of retinal neurodegeneration. Proceedings of the National Academy of Sciences of the United States of America 107:12710-12715.

Raza AS, Cho J, de Moraes CG, Wang M, Zhang X, Kardon RH, et al. 2011. Retinal ganglion cell layer thickness and local visual field sensitivity in glaucoma. Archives of ophthalmology 129:1529-1536.

Ren L, Danias J. 2010. A role for complement in glaucoma? Advances in experimental medicine and biology 703:95-104.

Riepe RE, Norenburg MD. 1977. Muller cell localisation of glutamine synthetase in rat retina. Nature 268:654-655.

Roberts MD, Grau V, Grimm J, Reynaud J, Bellezza AJ, Burgoyne CF, et al. 2009. Remodeling of the connective tissue microarchitecture of the lamina cribrosa in early experimental glaucoma. Investigative ophthalmology & visual science 50:681-690.

Rosen AM, Stevens B. 2010. The role of the classical complement cascade in synapse loss during development and glaucoma. Advances in experimental medicine and biology 703:75-93.

Ruiz-Ederra J, Garcia M, Hernandez M, Urcola H, Hernandez-Barbachano E, Araiz J, et al. 2005. The pig eye as a novel model of glaucoma. Experimental eye research 81:561-569.

Saleh M, Nagaraju M, Porciatti V. 2007. Longitudinal evaluation of retinal ganglion cell function and iop in the dba/2j mouse model of glaucoma. Investigative ophthalmology & visual science 48:4564-4572.

Schulze A, Lamparter J, Pfeiffer N, Berisha F, Schmidtmann I, Hoffmann EM. 2011. Diagnostic ability of retinal ganglion cell complex, retinal nerve fiber layer, and optic nerve head measurements by fourier-domain optical coherence tomography. Graefe's archive for clinical and experimental ophthalmology = Albrecht von Graefes Archiv fur klinische und experimentelle Ophthalmologie 249:1039-1045.

Schuman JS, Hee MR, Arya AV, Pedut-Kloizman T, Puliafito CA, Fujimoto JG, et al. 1995a. Optical coherence tomography: A new tool for glaucoma diagnosis. Current opinion in ophthalmology 6:89-95.

Schuman JS, Hee MR, Puliafito CA, Wong C, Pedut-Kloizman T, Lin CP, et al. 1995b. Quantification of nerve fiber layer thickness in normal and glaucomatous eyes using optical coherence tomography. Archives of ophthalmology 113:586-596.

Sehi M, Grewal DS, Goodkin ML, Greenfield DS. 2010. Reversal of retinal ganglion cell dysfunction after surgical reduction of intraocular pressure. Ophthalmology 117:2329-2336.

Senatorov V, Malyukova I, Fariss R, Wawrousek EF, Swaminathan S, Sharan SK, et al. 2006. Expression of mutated mouse myocilin induces open-angle glaucoma in transgenic mice. The Journal of neuroscience : the official journal of the Society for Neuroscience 26:11903-11914.

Shou T, Liu J, Wang W, Zhou Y, Zhao K. 2003. Differential dendritic shrinkage of alpha and beta retinal ganglion cells in cats with chronic glaucoma. Investigative ophthalmology & visual science 44:3005-3010.

Sigal IA, Flanagan JG, Tertinegg I, Ethier CR. 2010. 3d morphometry of the human optic nerve head. Experimental eye research 90:70-80.

Sommer A, Katz J, Quigley HA, Miller NR, Robin AL, Richter RC, et al. 1991. Clinically detectable nerve fiber atrophy precedes the onset of glaucomatous field loss. Archives of ophthalmology 109:77-83.

Sredar N, Ivers KM, Queener HM, Zouridakis G, Porter J. 2013. 3d modeling to characterize lamina cribrosa surface and pore geometries using in vivo images from normal and glaucomatous eyes. Biomedical optics express 4:1153-1165.

Stafford DK, Dacey DM. 1997. Physiology of the a1 amacrine: A spiking, axon-bearing interneuron of the macaque monkey retina. Visual neuroscience 14:507-522.

Stevens B, Allen NJ, Vazquez LE, Howell GR, Christopherson KS, Nouri N, et al. 2007. The classical complement cascade mediates cns synapse elimination. Cell 131:1164-1178.

Strouthidis NG, Grimm J, Williams GA, Cull GA, Wilson DJ, Burgoyne CF. 2010. A comparison of optic nerve head morphology viewed by spectral domain optical coherence tomography and by serial histology. Investigative ophthalmology & visual science 51:1464-1474.

Strouthidis NG, Fortune B, Yang H, Sigal IA, Burgoyne CF. 2011. Longitudinal change detected by spectral domain optical coherence tomography in the optic nerve head and peripapillary retina in experimental glaucoma. Investigative ophthalmology & visual science 52:1206-1219.

Strouthidis NG, Girard MJ. 2013. Altering the way the optic nerve head responds to intraocular pressure-a potential approach to glaucoma therapy. Current opinion in pharmacology 13:83-89.

Sutter EE. 1991. The fast m-transform - a fast computation of cross-correlations with binary m-sequences. Siam J Comput 20:686-694.

Sutter EE, Tran D. 1992. The field topography of erg components in man--i. The photopic luminance response. Vision research 32:433-446.

Sutter EE, Bearse MA, Jr. 1999. The optic nerve head component of the human erg. Vision research 39:419-436.

Tait MJ, Saadoun S, Bell BA, Papadopoulos MC. 2008. Water movements in the brain: Role of aquaporins. Trends in neurosciences 31:37-43.

Tamada K, Machida S, Yokoyama D, Kurosaka D. 2009. Photopic negative response of full-field and focal macular electroretinograms in patients with optic nerve atrophy. Japanese journal of ophthalmology 53:608-614.

Tamada K, Machida S, Oikawa T, Miyamoto H, Nishimura T, Kurosaka D. 2010. Correlation between photopic negative response of focal electroretinograms and local loss of retinal neurons in glaucoma. Current eye research 35:155-164.

Tan O, Chopra V, Lu AT, Schuman JS, Ishikawa H, Wollstein G, et al. 2009. Detection of macular ganglion cell loss in glaucoma by fourier-domain optical coherence tomography. Ophthalmology 116:2305-2314 e2301-2302.

Tezel G, Hernandez MR, Wax MB. 2001. In vitro evaluation of reactive astrocyte migration, a component of tissue remodeling in glaucomatous optic nerve head. Glia 34:178-189.

Tham YC, Li X, Wong TY, Quigley HA, Aung T, Cheng CY. 2014. Global prevalence of glaucoma and projections of glaucoma burden through 2040: A systematic review and meta-analysis. Ophthalmology 121:2081-2090.

Thompson DA, Feather S, Stanescu HC, Freudenthal B, Zdebik AA, Warth R, et al. 2011. Altered electroretinograms in patients with kcnj10 mutations and east syndrome. The Journal of physiology 589:1681-1689.

Townsend KA, Wollstein G, Schuman JS. 2009. Imaging of the retinal nerve fibre layer for glaucoma. The British journal of ophthalmology 93:139-143.

Traynis I, De Moraes CG, Raza AS, Liebmann JM, Ritch R, Hood DC. 2014. Prevalence and nature of early glaucomatous defects in the central 10 degrees of the visual field. JAMA ophthalmology 132:291-297.

Vaegan, Millar TJ. 1994. Effect of kainic acid and nmda on the pattern electroretinogram, the scotopic threshold response, the oscillatory potentials and the electroretinogram in the urethane anaesthetized cat. Vision research 34:1111-1125.

Varela HJ, Hernandez MR. 1997. Astrocyte responses in human optic nerve head with primary open-angle glaucoma. Journal of glaucoma 6:303-313.

Ventura LM, Porciatti V. 2005. Restoration of retinal ganglion cell function in early glaucoma after intraocular pressure reduction: A pilot study. Ophthalmology 112:20-27.

Ventura LM, Porciatti V, Ishida K, Feuer WJ, Parrish RK, 2nd. 2005. Pattern electroretinogram abnormality and glaucoma. Ophthalmology 112:10-19.

Vilupuru AS, Rangaswamy NV, Frishman LJ, Smith EL, 3rd, Harwerth RS, Roorda A. 2007. Adaptive optics scanning laser ophthalmoscopy for in vivo imaging of lamina cribrosa. Journal of the Optical Society of America A, Optics, image science, and vision 24:1417-1425.

Viswanathan S, Frishman LJ, Robson JG, Harwerth RS, Smith EL, 3rd. 1999. The photopic negative response of the macaque electroretinogram: Reduction by experimental glaucoma. Investigative ophthalmology & visual science 40:1124-1136.

Viswanathan S, Frishman LJ, Robson JG. 2000. The uniform field and pattern erg in macaques with experimental glaucoma: Removal of spiking activity. Investigative ophthalmology & visual science 41:2797-2810.

Viswanathan S, Frishman LJ, Robson JG, Walters JW. 2001. The photopic negative response of the flash electroretinogram in primary open angle glaucoma. Investigative ophthalmology & visual science 42:514-522.

Vizzeri G, Balasubramanian M, Bowd C, Weinreb RN, Medeiros FA, Zangwill LM. 2009. Spectral domain-optical coherence tomography to detect localized retinal nerve fiber layer defects in glaucomatous eyes. Optics express 17:4004-4018.

Wachtmeister L, Dowling JE. 1978. The oscillatory potentials of the mudpuppy retina. Investigative ophthalmology & visual science 17:1176-1188.

Wallace DM, O'Brien CJ. 2016. The role of lamina cribrosa cells in optic nerve head fibrosis in glaucoma. Experimental eye research 142:102-109.

Wang J, Cheng H, Hu YS, Tang RA, Frishman LJ. 2012. The photopic negative response of the flash electroretinogram in multiple sclerosis. Investigative ophthalmology & visual science 53:1315-1323.

Wang L, Cioffi GA, Cull G, Dong J, Fortune B. 2002. Immunohistologic evidence for retinal glial cell changes in human glaucoma. Investigative ophthalmology & visual science 43:1088-1094.

Wang L, Dong J, Cull G, Fortune B, Cioffi GA. 2003. Varicosities of intraretinal ganglion cell axons in human and nonhuman primates. Investigative ophthalmology & visual science 44:2-9.

Wang X, Tay SS, Ng YK. 2000. An immunohistochemical study of neuronal and glial cell reactions in retinae of rats with experimental glaucoma. Experimental brain research 132:476-484.

Weber AJ, Kaufman PL, Hubbard WC. 1998. Morphology of single ganglion cells in the glaucomatous primate retina. Investigative ophthalmology & visual science 39:2304-2320.

Weber AJ, Zelenak D. 2001. Experimental glaucoma in the primate induced by latex microspheres. Journal of neuroscience methods 111:39-48.

Weber AJ, Harman CD. 2005. Structure-function relations of parasol cells in the normal and glaucomatous primate retina. Investigative ophthalmology & visual science 46:3197-3207.

Weber AJ, Harman CD. 2008. Bdnf preserves the dendritic morphology of alpha and beta ganglion cells in the cat retina after optic nerve injury. Investigative ophthalmology & visual science 49:2456-2463.

Weber AJ, Harman CD, Viswanathan S. 2008. Effects of optic nerve injury, glaucoma, and neuroprotection on the survival, structure, and function of ganglion cells in the mammalian retina. The Journal of physiology 586:4393-4400.

Wheat JL, Rangaswamy NV, Harwerth RS. 2012. Correlating rnfl thickness by oct with perimetric sensitivity in glaucoma patients. Journal of glaucoma 21:95-101.

Wollstein G, Schuman JS, Price LL, Aydin A, Stark PC, Hertzmark E, et al. 2005. Optical coherence tomography longitudinal evaluation of retinal nerve fiber layer thickness in glaucoma. Archives of ophthalmology 123:464-470.

Wu S, Sutter EE. 1995. A topographic study of oscillatory potentials in man. Visual neuroscience 12:1013-1025.

Yamazaki Y, Drance SM. 1997. The relationship between progression of visual field defects and retrobulbar circulation in patients with glaucoma. American journal of ophthalmology 124:287-295.

Yan X, Tezel G, Wax MB, Edward DP. 2000. Matrix metalloproteinases and tumor necrosis factor alpha in glaucomatous optic nerve head. Archives of ophthalmology 118:666-673.

Yang H, Downs JC, Bellezza A, Thompson H, Burgoyne CF. 2007a. 3-d histomorphometry of the normal and early glaucomatous monkey optic nerve head: Prelaminar neural tissues and cupping. Investigative ophthalmology & visual science 48:5068-5084.

Yang H, Downs JC, Girkin C, Sakata L, Bellezza A, Thompson H, et al. 2007b. 3-d histomorphometry of the normal and early glaucomatous monkey optic nerve head: Lamina cribrosa and peripapillary scleral position and thickness. Investigative ophthalmology & visual science 48:4597-4607.

Yang H, Thompson H, Roberts MD, Sigal IA, Downs JC, Burgoyne CF. 2011. Deformation of the early glaucomatous monkey optic nerve head connective tissue after acute iop elevation in 3-d histomorphometric reconstructions. Investigative ophthalmology & visual science 52:345-363.

Yuan L, Neufeld AH. 2001. Activated microglia in the human glaucomatous optic nerve head. Journal of neuroscience research 64:523-532.

Zangwill LM, Bowd C. 2006. Retinal nerve fiber layer analysis in the diagnosis of glaucoma. Current opinion in ophthalmology 17:120-131.

Zhou W, Rangaswamy N, Ktonas P, Frishman LJ. 2007. Oscillatory potentials of the slow-sequence multifocal erg in primates extracted using the matching pursuit method. Vision research 47:2021-2036.

Zhou Y, Grinchuk O, Tomarev SI. 2008. Transgenic mice expressing the tyr437his mutant of human myocilin protein develop glaucoma. Investigative ophthalmology & visual science 49:1932-1939.